SYNTHESIS OF ACTIVATED CARBONS FROM COFFEE GROUND RESIDUES AND THEIR APPLICATION AS CATALYSTS FOR ETHANOL DEHYDROGENATION

Miss Jeerati Ob-eye

จุฬาลงกรณ์มหาวิทยาลัย
CHULALONGKORN UNIVERSITY

A Dissertation Submitted in Partial Fulfillment of the Requirements
for the Degree of Doctor of Engineering in Chemical Engineering
Department of Chemical Engineering
Faculty of Engineering
Chulalongkorn University
Academic Year 2018
Copyright of Chulalongkorn University

การสังเคราะห์ถ่านกัมมันต์จากกากกาแฟบดและการประยุกต์ใช้เป็นตัวเร่งปฏิกิริยาสำหรับเอทานอลดีไฮโดรจิเนชัน

น.ส.จีรติ อบอาย

จุฬาลงกรณ์มหาวิทยาลัย
Chulalongkorn University

วิทยานิพนธ์นี้เป็นส่วนหนึ่งของการศึกษาตามหลักสูตรปริญญาวิศวกรรมศาสตรดุษฎีบัณฑิต
สาขาวิชาวิศวกรรมเคมี ภาควิชาวิศวกรรมเคมี
คณะวิศวกรรมศาสตร์ จุฬาลงกรณ์มหาวิทยาลัย
ปีการศึกษา 2561

ลิขสิทธิ์ของจุฬาลงกรณ์มหาวิทยาลัย

Thesis Title	SYNTHESIS OF ACTIVATED CARBONS FROM COFFEE GROUND RESIDUES AND THEIR APPLICATION AS CATALYSTS FOR ETHANOL DEHYDROGENATION
By	Miss Jeerati Ob-eye
Field of Study	Chemical Engineering
Thesis Advisor	Professor Bunjerd Jongsomjit, Ph.D.

Accepted by the Faculty of Engineering, Chulalongkorn University in Partial Fulfillment of the Requirement for the Doctor of Engineering

..... Dean of the Faculty of Engineering
(Associate Professor Supot Teachavorasinskun, D.Eng.)

DISSERTATION COMMITTEE

..... Chairman
(Assistant Professor Sasiradee Jantasee, D.Eng.)

..... Thesis Advisor
(Professor Bunjerd Jongsomjit, Ph.D.)

..... Examiner
(Professor Muenduen Phisalaphong, Ph.D.)

..... Examiner
(Chutimon Satirapipathkul, D.Eng.)

..... Examiner
(Assistant Professor Suphot Phatanasri, D.Eng.)

จุฬาลงกรณ์มหาวิทยาลัย
CHULALONGKORN UNIVERSITY

จีรติ อบอาย : การสังเคราะห์ถ่านกัมมันต์จากกากกาแฟบดและการประยุกต์ใช้เป็นตัวเร่งปฏิกิริยาสำหรับเอทานอลดีไฮโดรจิเนชัน. (SYNTHESIS OF ACTIVATED CARBONS FROM COFFEE GROUND RESIDUES AND THEIR APPLICATION AS CATALYSTS FOR ETHANOL DEHYDROGENATION) อ.ที่ปรึกษาหลัก : ศ. ดร. บรรเจิด จงสมจิตร

งานวิจัยนี้มุ่งเน้นถึงการศึกษาคุณลักษณะและสมบัติการเร่งปฏิกิริยาของถ่านกัมมันต์จากกากกาแฟและโลหะโคบอลต์ (Co) บนตัวรองรับถ่านกัมมันต์จากกากกาแฟ และตัวเร่งปฏิกิริยาโลหะต่างชนิดกัน [ซีเรียม (Ce), โคบอลต์ (Co), ทองแดง (Cu) และ นิกเกิล (Ni)] บนตัวรองรับถ่านกัมมันต์เชิงพาณิชย์ ซึ่งจะถูกวิเคราะห์และมีความสัมพันธ์เกี่ยวข้องกัน โดยงานวิจัยนี้แบ่งการศึกษาออกเป็น 3 ส่วน เมื่อพิจารณาถึงการศึกษาในส่วนแรก คือ การสังเคราะห์ตัวเร่งปฏิกิริยาถ่านกัมมันต์จากกากกาแฟด้วยขั้นตอนการกระตุ้นทางกายภาพที่แตกต่างกัน พบว่าการกระตุ้นทางกายภาพด้วยแก๊สคาร์บอนไดออกไซด์เป็นเวลา 4 ชั่วโมง ทำให้ได้ตัวเร่งปฏิกิริยาที่มีคุณสมบัติในการเร่งปฏิกิริยาเอทานอลดีไฮโดรจิเนชันเป็นอะซีทัลดีไฮด์ได้ว่องไวที่สุด การศึกษาในส่วนที่สองตัวเร่งปฏิกิริยาถ่านกัมมันต์ที่มีคุณสมบัติดีที่สุดจากการศึกษาในส่วนแรกถูกนำมาปรับปรุงด้วยโลหะโคบอลต์ (Co) ในปริมาณที่แตกต่างกัน จากการทดลองพบว่า การปรับปรุงด้วยโลหะโคบอลต์ 4% โดยน้ำหนัก ทำให้ได้ตัวเร่งปฏิกิริยาที่มีความว่องไวเพิ่มมากขึ้น งานวิจัยส่วนที่สาม นำโลหะ4 ชนิด ได้แก่ ซีเรียม, โคบอลต์, ทองแดง และ นิกเกิล ปริมาณ 10% โดยน้ำหนักมาปรับปรุงถ่านกัมมันต์เชิงพาณิช์ พบว่า โลหะทองแดง (Cu) สามารถพัฒนาตัวเร่งปฏิกิริยาถ่านกัมมันต์เชิงพาณิชย์สำหรับปฏิกิริยาดีไฮโดรจิเนชันของเอทานอลไปเป็นอะซีทัลดีไฮด์ได้ดีที่สุด

CHULALONGKORN UNIVERSITY

สาขาวิชา	วิศวกรรมเคมี	ลายมือชื่อนิสิต .....
ปีการศึกษา	2561	ลายมือชื่อ อ.ที่ปรึกษาหลัก .....

5771434421 : MAJOR CHEMICAL ENGINEERING

KEYWORD: coffee ground residue, activated carbon, catalyst, ethanol dehydrogenation, acetaldehyde

Jeerati Ob-eye : SYNTHESIS OF ACTIVATED CARBONS FROM COFFEE GROUND RESIDUES AND THEIR APPLICATION AS CATALYSTS FOR ETHANOL DEHYDROGENATION. Advisor: Prof. Bunjerd Jongsomjit, Ph.D.

In this present study, characteristics and catalytic properties of activated carbon derived from coffee ground residue, cobalt metal (Co) supported-activated carbon and various metals (Ce, Co, Cu and Ni) supported-commercial activated carbon were determined and characterized. This study was divided into three parts. Regarding to the first part, the synthesis of activated carbon catalysts derived from coffee ground residues with different methods of physical activation was investigated. The results showed that the catalyst with physically activated by CO_2 for 4 hours, exhibited the best catalytic activity of ethanol dehydrogenation to acetaldehyde. In the second part, the best catalyst from the first part, was improved by various cobalt metal loading. It was found that 4 wt% of cobalt loading enhanced the activity of catalyst. In the third part, four metals such as Ce, Co, Cu and Ni with 10 wt% loading to improve the commercial activated carbons were investigated. The results showed that Cu was the most suitable metal for commercial activated carbon support in ethanol dehydrogenation to acetaldehyde.

จุฬาลงกรณ์มหาวิทยาลัย
Chulalongkorn University

Field of Study:	Chemical Engineering	Student's Signature .....
Academic Year:	2018	Advisor's Signature .....

ACKNOWLEDGEMENTS

Completion of this doctoral dissertation was possible with the support of several people. At the outset, I would like to express my sincere gratitude to my advisor Prof. Dr. Bunjerd Jongsomjit for the continuous support of my Ph.D. study and related research, for his patience, motivation, and immense knowledge. As my supervisor, he has constantly forced me to remain focused on achieving my goal. His observations and comments helped me to establish the overall direction of the research and to move forward with investigation in depth. I could not have imagined having a better advisor and mentor for my Ph.D study.

Besides my advisor, I would like to thank the rest of my thesis committee: Asst. Prof. Dr. Sasiradee Jantasee, as a chairman, prof. Dr. Muenduen Phisalaphong, Dr. Chutimon Satirapipathkul and Asst. Prof. Dr. Suphot Phatanasri as the members of the thesis committee for their valuable guidance and revision of my thesis.

I gratefully acknowledge the funding sources that made my Ph.D. work possible. I would like to thank the Grant for International Research Integration: Chula Research Scholar, Ratchadaphiseksomphot Endowment Fund and Grant for Research: Government Budget, Chulalongkorn University (2018) for providing scholarships to pursue doctoral studies.

Finally, I would like to thank my family for all their love and encouragement. For my father and mother who supported me in my pursuits. They are the most important people in my world and I dedicate this dissertation to them.

Jeerati Ob-eye

จุฬาลงกรณ์มหาวิทยาลัย
Chulalongkorn University

TABLE OF CONTENTS

Page

ABSTRACT (THAI) iii

ABSTRACT (ENGLISH) iv

ACKNOWLEDGEMENTS v

TABLE OF CONTENTS vi

LIST OF TABLES x

LIST OF FIGURES xii

CHAPTER I INTRODUCTION 1

1.1 General introduction 1

1.2 Research objectives 5

1.3 Research scopes 5

1.4 Research methodology 6

CHAPTER II THEORY 9

2.1 Activated carbon 9

2.2 Cobalt 13

2.3 Cobalt(II, III) Oxides 16

2.4 Acetaldehyde 17

2.4.1 Acetaldehyde production 18

2.4.2 Acetaldehyde applications and market trend 20

2.5 Ethanol conversion 23

CHAPTER III LITERATURE REVIEW 25

3.1 Activated carbon from other precursors 25

จุฬาลงกรณ์มหาวิทยาลัย
Chulalongkorn University

3.2 Activated carbon from coffee residues 26

3.3 Co catalyst 27

3.4 Dehydrogenation reaction of ethanol 31

3.5 Co/AC catalysts 33

CHAPTER IV EXPERIMENTAL 37

4.1 Preparation of activated carbon derived coffee residue 37

4.1.1 Chemicals and reagents 37

4.1.2 Experimental procedure 37

4.1.3 The nomenclature of samples 37

4.2 Preparation of activated carbon supported cobalt catalyst 38

4.2.1 Chemicals and regents 38

4.2.2 Experimental procedure 38

4.2.3 The nomenclature of samples 38

4.3 Preparation of various metals supported-commercial activated carbon catalysts 38

4.3.1 Chemicals and regents 38

4.3.2 Experimental procedure 38

4.3.3 The nomenclature of samples 39

4.4 Catalyst characterization 39

4.4.1 Nitrogen adsorption-desorption isotherm 39

4.4.2 X-ray diffraction (XRD) 39

4.4.3 Thermal Gravimetric analysis (TGA) 39

4.4.4 Fourier transforms infrared spectroscopy (FT-IR) 39

จุฬาลงกรณ์มหาวิทยาลัย
Chulalongkorn University

4.4.5 Scanning Electron Microscopy (SEM) and Energy dispersive X-ray spectroscopy (EDX) 40

4.4.6 CO_2 temperature programed adsorption TPD 40

4.4.7 NH_3 temperature programed adsorption TPD 40

4.4.8 Transmission electron microscopy (TEM) 41

4.4.9 Inductively coupled plasma mass spectrometer (ICP) 41

4.4.10 Temperature-programmed reduction (H_2-TPR) 41

4.5 Measurement of catalytic activity with ethanol dehydrogenation 41

4.5.1 Chemicals and reagents 41

4.5.2 Instrument and apparatus 42

4.5.3 Ethanol dehydrogenation reaction procedure 43

CHAPTER V RESULTS AND DISCUSSIONS 44

5.1 Characteristics of activated carbons prepared by different physical activation and catalytic activity for ethanol dehydrogenation. 44

5.1.1 Characteristics of synthesized-activated carbons 44

5.1.2 Dehydrogenation of ethanol of synthesized-activated carbons 56

5.2 Characteristics and catalytic activity of cobalt metal supported on synthesized activated carbon for ethanol dehydrogenation. 62

5.2.1 Catalyst Characterization 62

5.2.2 Catalyst Testing 71

5.3 Characteristics and catalytic activity of various metal supported on commercial activated carbon for ethanol dehydrogenation. 74

5.3.1 Catalysts Characterization 74

5.3.2 Catalyst Testing 81

CHAPTER VI CONCLUSION AND RECOMMENDATIONS 86

6.1 Conclusion 86

6.2 Recommendations 87

REFERENCES 88

APENDIX A CALCULATION FOR CATALYST PREPARATION 98

APPENDIX B THE AMOUNT OF METAL AND THE TEMPERATURE OF REDUCTION OF CATALYSTS 100

APPENDIX C CALIBRATION CURVES 102

APPENDIX D CALCULATION OF REACTANT CONVERSION, PRODUCT SELECTIVITY AND PRODUCT YIELD 105

VITA 106

จุฬาลงกรณ์มหาวิทยาลัย
CHULALONGKORN UNIVERSITY

LIST OF TABLES

Page

Table 1 Physical properties of cobalt. 15

Table 2 Physical properties of acetaldehyde. 18

Table 3 Comparisons of the characteristics of porosity of other literature data for other precursors under optimum condition. 25

Table 3 Comparisons of the characteristics of porosity of other literature data for other precursors under optimum condition (continued). 26

Table 4 Operating conditions for gas chromatographs. 43

Table 5 Pore characteristics for activated carbons. 46

Table 6 Total acidity and total basicity of activated carbons. 48

Table 7 Functional group of activated carbons [87, 89-91]. 53

Table 8. Ethanol conversion and acetaldehyde yield for all catalysts. 59

Table 9 Comparison of carbon catalysts for ethanol dehydrogenation and their catalytic ability. 61

Table 10 Surface areas and pore characteristics for Co/C catalysts. 62

Table 11 Metal content of the carbon-supported Co catalysts. 65

Table 12 Total acidity and total basicity of carbon-supported Co catalysts. 67

Table 13 Functional group of activated carbons [87-90]. 69

Table 14 Ethanol conversion and acetaldehyde yield for activated carbon-supported Co catalysts. 73

Table 15 Surface areas and pore characteristics for activated carbon catalysts. 74

Table 16 Metal contents of the different commercial activated carbon catalysts. 76

Table 17 Total acidity and total basicity of catalysts. 77

จุฬาลงกรณ์มหาวิทยาลัย
Chulalongkorn University

Table 18 Comparison of metal on commercial activated carbon for ethanol dehydrogenation and their catalytic ability. 85

Table 19 Metal content of the different commercial activated carbon catalysts..... 100

Table 20 The retention time of the each component in the chromatogram. 102

จุฬาลงกรณ์มหาวิทยาลัย
CHULALONGKORN UNIVERSITY

LIST OF FIGURES

Page

Figure 1 Coffee ground residue. 1

Figure 2 Production of acetaldehyde summary all over the world between 1990 and 2003. 19

Figure 3 World consumption of acetaldehyde in year 2012. 22

Figure 4 The global acetaldehyde market trends, drivers and projections. 23

Figure 5 Proposed mechanism of dehydrogenation reaction [48]. 24

Figure 6 Ethanol conversion to acetaldehyde and ethyl acetate. [rewrite from Gallo et al., [38]] 31

Figure 7 Flow diagram of catalytic dehydrogenation reaction of ethanol. 44

Figure 8 Adsorption-desorption isotherm at -196°C of activated carbons at different activation conditions. 47

Figure 9. NH_3-TPD profiles of activated carbons.. 48

Figure 10 CO_2-TPD profiles of activated carbons. 49

Figure 11 XRD patterns of activated carbons and coffee residue. 50

Figure 12 Scanning electron micrographs of activated carbons. 50

Figure 13 FTIR spectra of activated carbons. 52

Figure 14 Thermal analysis of fresh activated carbons and spent AC-D catalyst. 56

Figure 15 Ethanol conversion and acetaldehyde yield of activated carbon catalysts for ethanol dehydrogenation. 58

Figure 16 Mechanism of ethanol to acetaldehyde by Lewis acid and Lewis base sites on activated carbon catalyst. 58

Figure 17 Stability test for AC-D catalyst at reaction temperature of 400°C. 60

จุฬาลงกรณ์มหาวิทยาลัย
CHULALONGKORN UNIVERSITY

Figure 18 Scanning electron micrographs of spent AC-D catalyst after ethanol dehydrogenation. 60

Figure 19 Adsorption-desorption isotherm at -196°C of activated carbon-supported Co catalysts. 63

Figure 20 SEM images of activated carbon-supported Co catalysts. 64

Figure 21 EDX of activated carbon-supported Co catalysts. 65

Figure 22 TEM images of activated carbon-supported Co catalysts. 66

Figure 23 (a) NH_3-TPD profiles and (b) CO_2-TPD profiles. 67

Figure 24 X-ray diffraction patterns of cobalt catalysts. Legend: (□) graphite; (●) Co_3O_4 68

Figure 25 A typical FTIR spectrum of Co/C catalyst. 68

Figure 26 Thermal analysis of all catalysts. 70

Figure 27 Ethanol conversion of activated carbon-supported Co catalysts. 72

Figure 28 Acetaldehyde yield of activated carbon-supported Co catalysts. 72

Figure 29 Adsorption-desorption isotherm at -196°C of catalysts. 75

Figure 30 TEM images of activated carbon supported-metal catalysts. 76

Figure 31 NH_3-TPD profiles of catalysts. 78

Figure 32 CO_2-TPD profiles of catalysts. 79

Figure 33 X-ray diffraction patterns of catalysts. 80

Figure 34 Ethanol conversion of catalysts. 81

Figure 35 Selectivity of acetaldehyde of catalysts. 81

Figure 36 Selectivity of ethylene of catalysts. 82

Figure 37 A proposed mechanism for dehydrogenation reaction of ethanol on Cu/ACC catalyst. 84

Figure 38 Stability test of Cu/ACC catalyst at 350 °C. 84

จุฬาลงกรณ์มหาวิทยาลัย
Chulalongkorn University

Figure 39 TPR profiles of activated carbon-supported metal catalysts. 101

Figure 40 The calibration curve of ethanol. 103

Figure 41 The calibration curve of ethylene. 103

Figure 42 The calibration curve of diethyl ether. 104

Figure 43 The calibration curve of acetaldehyde. 104

จุฬาลงกรณ์มหาวิทยาลัย
CHULALONGKORN UNIVERSITY

CHAPTER I

INTRODUCTION

1.1 General introduction

The coffee grounds, which are the residues of the soluble coffee industry, are normally discarded, resold or reused as body scrub, facial mask, fertilizer or odor-eliminator. However, the coffee grounds can be used as a source to produce activated carbon that can increase its value. This is a very interesting topic. Thus, in the first part in this research focuses on using coffee ground residue to obtain the activated carbons that will be further applied as a catalyst support.

Figure 1 Coffee ground residue.

จุฬาลงกรณ์มหาวิทยาลัย
Chulalongkorn University

In fact, activated carbons are the most widely used absorbents because of their excellent absorption capability for inorganic pollutants [1] the removal of heavy metal from waste water [2], as a catalyst or a catalyst support in the catalytic process [3, 4] and etc. So, the activated carbon has an important role in many industries. The properties of activated carbons depend on the activation process and the nature of the source materials. Moreover, in both physical and chemical activation processes, knowledge of different variables is very important in developing the porosity of the carbons such as surface area, pore volumes, and porosity [1, 5].

In principle, the methods to prepare activated carbons can be divided into two categories; physical activation and chemical activation. In the physical activation, a raw material is first carbonized and the carbonized material is secondary activated by steam, carbon dioxide, air or their mixture. There are two steps: carbonization step and activation step. In the chemical activation, a raw material is impregnated with an activation agent and an impregnated material is heat-treated under inert atmosphere. The carbonization step and activation step are carried out simultaneously in the chemical activation process. However, sometime the methods for preparing an activated carbon is modified (such as chemical activation followed by physical activation to improve characteristics of activated carbon such as surface area and pore volume [5, 6]. The carbonization step and the activation step simultaneously progress in chemical activation. This method occurs at lower temperature than that of physical methods. Therefore, it improves the pore development in the carbon structure. The type of chemical agent is selected as a function of the characteristics of the desired activated carbon. C. Almansa et al. [7] reported that $ZnCl_2$ gave both wide micropores and low mesopores. Chemical activation with $ZnCl_2$ has been studied by several researchers [6-8] using different preparation conditions. These producing bulk chemicals from renewable biomass instead of depleting fossil resource is of great importance to sustainable goals of the chemical industry.

จุฬาลงกรณ์มหาวิทยาลัย
CHULALONGKORN UNIVERSITY

Ethanol can be used as fuel and fuel additive, but it is also very assuring as a platform for the production of value-added chemicals, which are attractive growing concern in the last decade. It can be used as a renewable feedstock for both drop-in chemicals, such as ethylene, propylene, diethyl ether and 1,3-butadiene, as well as the production of oxygenated chemicals, such as 1-butanol, ethyl acetate, acetic acid, acetaldehyde and ketone, because the process is relative simple, non-corrosive, green technology, less toxic and always needs only one feedstock of ethanol. Dehydrogenation and dehydration of alcohol, which are catalyzed by carbon material

have not been frequently studied. Even in ethanol, it is converted to acetaldehyde and ethylene associated with dehydrogenation and dehydration reactions, respectively. Both of the products deserve interest particularly with an acetaldehyde, which is one of important raw materials in production of chemicals (e.g. acetic acid, acetic anhydride, ethyl acetate, pyridine, vinyl acetate). These chemicals are used for manufacturing plastic, construction materials, fire retardant paints and explosives [9, 10]. Acetaldehyde is the one of attractive chemicals that is an ethanol-derived product, which is one of the most important aldehydes produced and consumed globally for different industrial applications. The market for acetaldehyde is primarily expected to be driven by the downstream markets that use the compound as a key raw material [11]. Acetic acid, acetic anhydride, n-butanol, and 2-ethylhexanol are the major products derived from acetaldehyde. The commercial production processes of acetaldehyde include dehydrogenation and oxidation of ethanol, the hydration of acetylene, the partial oxidation of hydrocarbons, and direct oxidation of ethylene. With the ever-growing of the world output of bioethanol, the production of acetaldehyde via oxidative dehydrogenation has been gradually considered a feasible process [12]. The properties of catalysts, which is used to catalyze in ethanol reaction, have a great influence to the pathway mechanism project to the desire products. For example, ethanol can be dehydrated into ethylene, diethyl ether using solid acid catalysts. In addition, oxygenated chemicals such as acetaldehyde and ketones can be produced from ethanol by dehydrogenation reaction with basic catalysts.

Direct dehydrogenation of ethanol to acetaldehyde has gained great attention because it is an economical and environmentally friendly alternative to conventional commercial processes [13-15]. In previous studies, the catalytic activities of catalysts, such as ZrO_2 [13, 14], SiO_2 [13], Al_2O_3 [15, 16], ZSM-5 [16], SBA-15 [17], and MCM-41 [18], with high acidities for ethanol reaction have been studied. Although these catalysts showed high activities for ethanol dehydrogenation, low selectivity to

acetaldehyde was observed. These results indicated that catalysts with acidities that were too high were not suitable for the dehydrogenation of ethanol to acetaldehyde. It appeared that different metals doped on support may be suitable for good surface basicities for ethanol dehydrogenation. Many pieces of research on the reaction of alcohols using heterogeneous catalysts have focused principally on highly active noble metals, such as platinum [19] and gold [20-22]. Therefore, more lasting solutions based on cheap, harmless, and stable metals to replace noble metals would be appealing. In this regard, the application of catalysts based on relatively inexpensive metals, including manganese [20], nickel [20, 23, 24], cobalt [23], copper [13, 14, 24-26], vanadium [27, 28], silver [22, 29, 30], and iron [31], are being increasingly explored for dehydrogenation under ambient conditions. Moreover, a few studies have used activated carbon for ethanol dehydrogenation [31-34]. In contrast, these catalysts have very high selectivity to acetaldehyde.

In this study, the coffee ground residues were used to produce activated carbons using different physical activation. Then, the activated carbons obtained were modified as and used as catalysts for dehydration and/or dehydrogenation of ethanol. On the other words, the main goal of this study, is to produce a catalyst from biomass as renewable resource. Then, utilize it in a selected catalytic process in order to obtain more value added products (i.e. from ethanol to ethylene or acetaldehyde). As a result, a cleaner technology will be developed.

จุฬาลงกรณ์มหาวิทยาลัย
CHULALONGKORN UNIVERSITY

1.2 Research objectives

1. To investigate characteristics of activated carbons derived from coffee ground residues.
2. To investigate characteristics of cobalt metal modification of synthesized activated carbon catalysts.
3. To investigate characteristics of various metal (Ce, Co, Cu and Ni) modification of commercial activated carbon catalysts.
4. To investigate catalytic properties and of all activated carbons, that is used as catalyst in ethanol dehydrogenation.

1.3 Research scopes

- Synthesis of the activated carbons from coffee ground residues.
- Preparation of the activated carbons supported cobalt catalysts via incipient wetness impregnation method.
- Preparation of various metals supported-commercial activated carbon catalysts via incipient wetness impregnation method.
- Characterization of the activated carbons with several techniques; XRD, N_2 physisorption, NH_3-TPD, CO_2-TPD, TPR, SEM-EDX, TEM and TGA.
- Investigation of the catalytic activity all of activated carbon catalysts for ethanol dehydrogenation in temperature range of 250-400°C.

จุฬาลงกรณ์มหาวิทยาลัย
Chulalongkorn University

1.4 Research methodology

Part 1 : Preparation activated carbon from coffee ground residues. Investigation of the catalytic activity and stability of activated carbon catalysts.

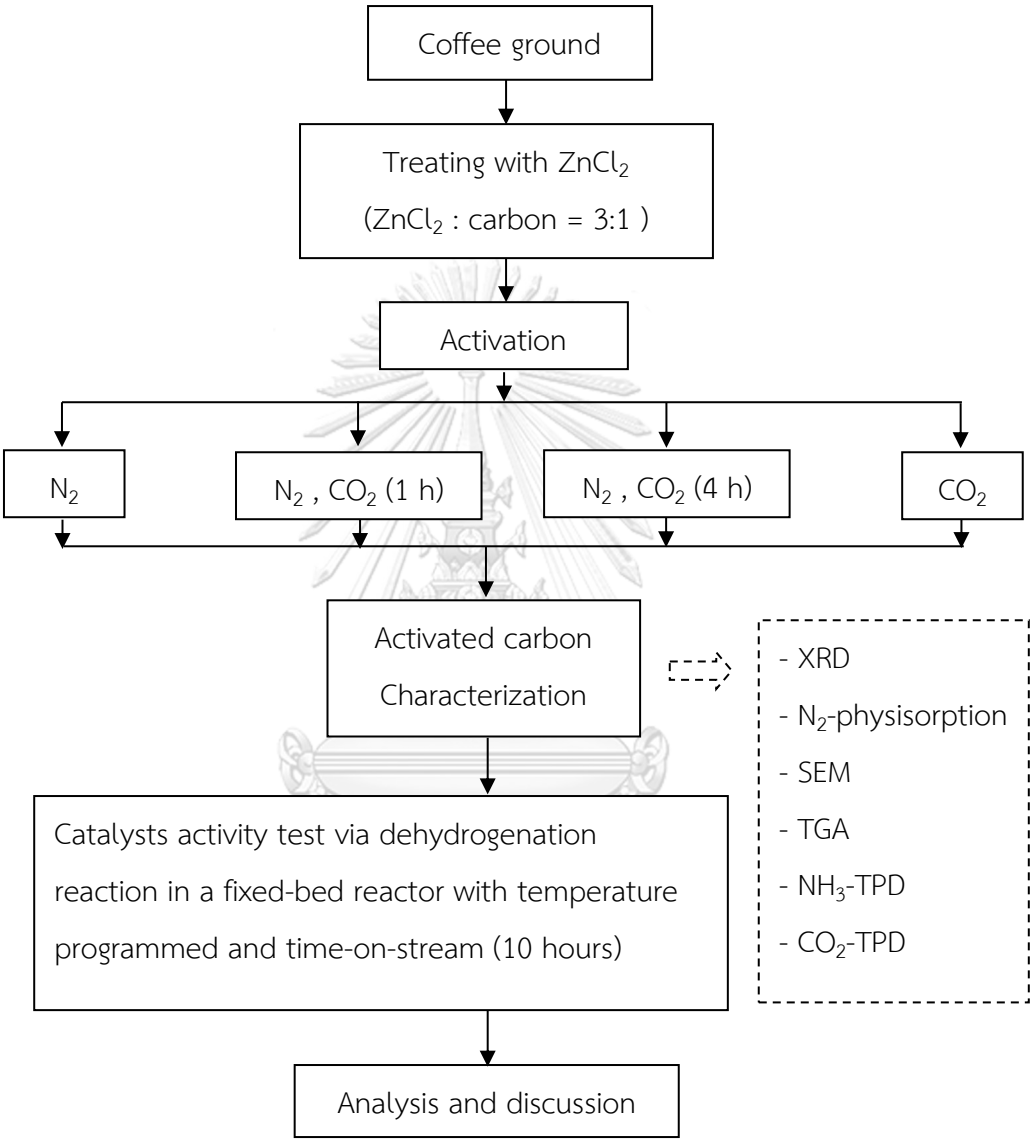

Part 2 : Investigation of the catalytic activity and stability of cobalt doped on the best activated carbon from part 1 for ethanol dehydrogenation

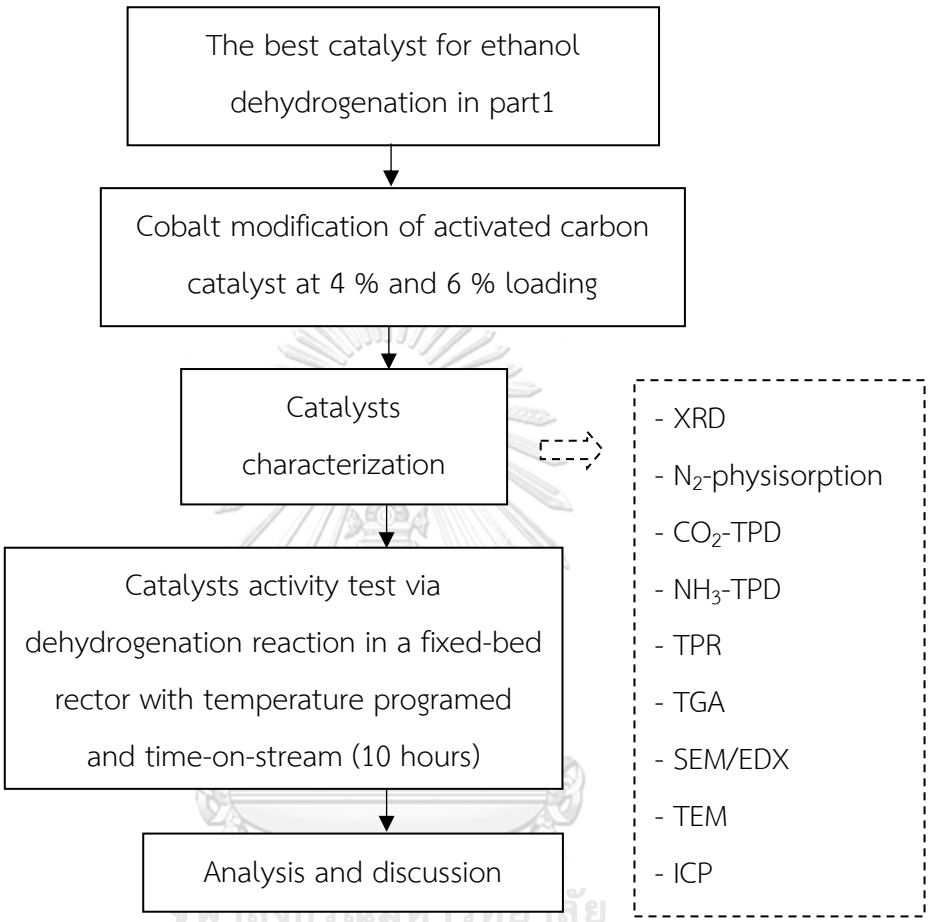

CHULALONGKORN UNIVERSITY

Part 3 : Investigation of the catalytic activity and stability of various metals supported-commercial activated carbon catalysts for ethanol dehydrogenation

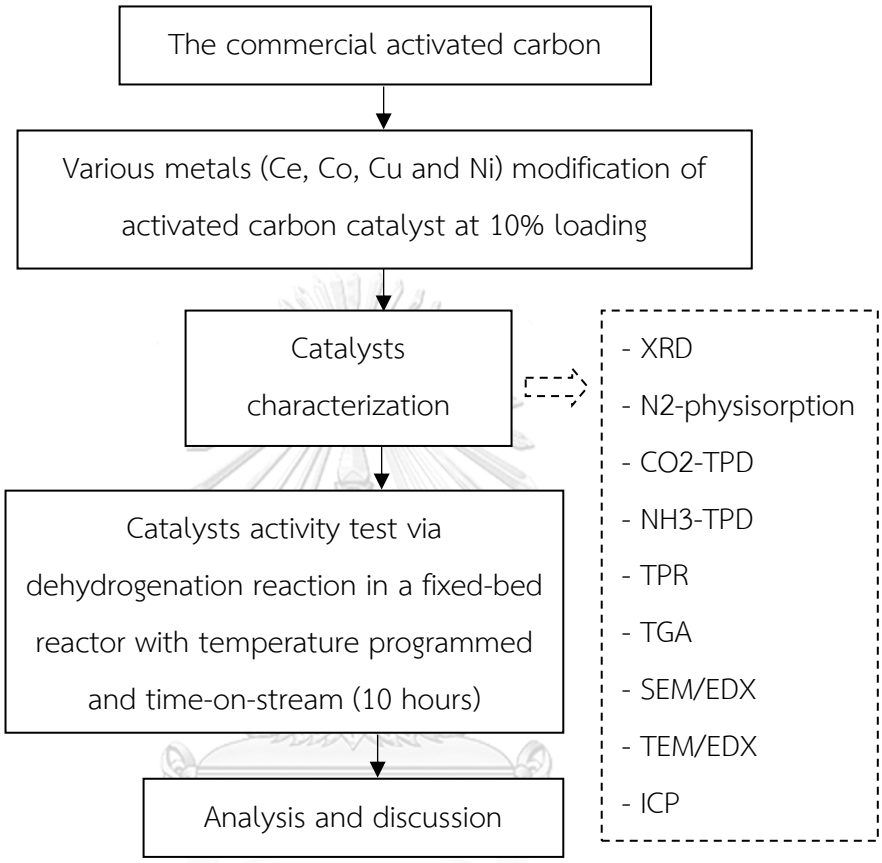

จุฬาลงกรณ์มหาวิทยาลัย
CHULALONGKORN UNIVERSITY

CHAPTER II

THEORY

2.1 Activated carbon

Activated carbon, also called activated charcoal or activated coal is a form of carbon that has been processed to make it extremely porous, and thus to have a very large surface area available for adsorption or chemical reactions. The word activated in the name is sometimes replaced with active. Due to its high degree of microporosity, just 1 gram of activated carbon has a surface area in excess of 500 m^2. Sufficient activation for useful applications may come solely from the high surface area, though further chemical treatment often enhances the absorbing properties of the material.

Activated carbon is carbon produced from carbonaceous source materials like coconut shells, peat, wood, coir, lignite, coal and petroleum pitch. It can be produced by one of the following processes: physical activation, chemical activation or combine of physical and chemical activation to obtain a desired activated carbon.

Physical activation : The precursor is developed into activated carbons using gases. This is generally done by using one or a combination of the following processes:

- *Carbonization* : Material with carbon content is pyrolyzed at temperatures in the range 600–900 °C, in absence of air (usually in inert atmosphere with gases like argon or nitrogen).
- *Activation/Oxidation* : Raw material or carbonised material is exposed to oxidizing atmospheres by the gasifying agent(carbon dioxide, oxygen, or steam) at temperatures above 250 °C, usually in the temperature range of 600–1200 °C. These agents extract carbon atoms from the structure of the porous carbon according to the following equations.

จุฬาลงกรณ์มหาวิทยาลัย
CHULALONGKORN UNIVERSITY

For the C-CO_2 reaction the mechanism is postulated to be :

$$C + CO_2 \leftrightarrow CO + C(O)$$

In which a surface oxygen complex [C(O)] is initially formed, subsequently becoming stable under the reaction conditions and acting as a retardant by blocking reaction sites:

$$C(O) \leftrightarrow C\text{-}O$$

It may, however, decompose leaving the surface as CO,

$$C(O) \longrightarrow CO$$

Involving the use of steam (water vapor), hydrogen is similarly chemisorbed on the carbon surface, where C(H) describes hydrogen chemisorbed on a carbon surface :

$$C + H_2O \leftrightarrow CO + H_2$$

$$2C + H_2 \longrightarrow 2C(H)$$

Summarizing, the activation reactions result in (a) the opening of porosity which, originally, was not accessible to an adsorbate; (b) the enhancement of micropore volumes and (c) widening of micropores into the mesopore range.

Chemical activation : Prior to carbonization, the raw material is impregnated with certain chemicals. The chemical is typically an acid, strong base, or a salt (phosphoric acid, potassium hydroxide, sodium hydroxide, zinc chloride, respectively). Then, the raw material is carbonized at lower temperatures (450–900 °C). It is believed that the carbonization / activation step proceeds simultaneously with the chemical activation. This technique can be problematic in some cases, for example, zinc trace residues may remain in the end product. However, chemical activation is preferred over physical activation owing to the lower temperatures and shorter time needed for activating material.

Effects of impregnations (chemical activation) :

For activation with $ZnCl_2$, (a) the volume of micropores developed is similar to the volume of zinc chloride introduced into the particle, and the microporosity is uniform and (b) zinc chloride acts at temperatures < 500°C.

For activation with H_3PO_4 , (a) the volume of micropores developed during activation is similar to the volume of the acid used in the impregnation of the precursor, the heterogeneity of the microporosity being constant in all carbons and (b) phosphoric acid acts at temperatures < 450°C leading to highly activated carbon.

For activation with KOH , (a) the reactant acts after the pyrolysis of the precursor, at temperatures above 700°C ; (b) the development of porosity relates to the extent of impregnation by the KOH ; (c) initially, narrow microporosity is formed followed by the wider microporosity at the expense of the narrow microporosity ; (d) activation can proceed without disintegration to form powder and (e) high ratios of KOH to carbon result in the disintegration of the carbon granules to powder.

A principal conclusion is that chemical activation produces similar or higher porosity than does physical activation. There are two advantages to the use of chemical activation methods namely (a) higher yields, 27-47 wt% compared with 6 wt% for physical activation and (b) the surfaces of the activated fibers prepared by chemical activation are less damaged.

จุฬาลงกรณ์มหาวิทยาลัย
CHULALONGKORN UNIVERSITY

Under an electron microscope, the high surface-area structures of activated carbon are revealed. Individual particles are intensely convoluted and display various kinds of porosity; there may be many areas where flat surfaces of graphite-like material run parallel to each other.

Activated carbons are complex products which are difficult to classify on the basis of their behaviour, surface characteristics and preparation methods. However, some broad classification is made for general purpose based on their physical characteristics.

Powdered activated carbon (PAC) : Traditionally, active carbons are made in particular form as powders or fine granules less than 1.0 mm in size with an average diameter between .15 and .25 mm. Thus they present a large surface to volume ratio with a small diffusion distance. PAC is made up of crushed or ground carbon particles, 95–100% of which will pass through a designated mesh sieve or sieve. Granular activated carbon is defined as the activated carbon being retained on a 50-mesh sieve (0.297 mm) and PAC material as finer material. PAC is not commonly used in a dedicated vessel, owing to the high head loss that would occur. PAC is generally added directly to other process units, such as raw water intakes, rapid mix basins, clarifiers, and gravity filters.

Granular activated carbon (GAC): Granular activated carbon has a relatively larger particle size compared to powdered activated carbon and consequently, presents a smaller external surface. Diffusion of the adsorbate is thus an important factor. These carbons are therefore preferred for all adsorption of gases and vapors as their rate of diffusion are faster. Granulated carbons are used for water treatment, deodorization and separation of components of flow system. GAC can be either in the granular form or extruded. GAC is designated by sizes such as 8×20, 20×40, or 8×30 for liquid phase applications and 4×6, 4×8 or 4×10 for vapor phase applications. A 20×40 carbon is made of particles that will pass through a U.S. Standard Mesh Size No. 20 sieve (0.84 mm) (generally specified as 85% passing) but be retained on a U.S. Standard Mesh Size No. 40 sieve (0.42 mm) (generally specified as 95% retained). The most popular aqueous phase carbons are the 12×40 and 8×30 sizes because they have a good balance of size, surface area, and head loss characteristics.

Extruded activated carbon (EAC): Extruded activated carbon combines powdered activated carbon with a binder, which are fused together and extruded into a cylindrical shaped activated carbon block with diameters from 0.8 to 130 mm. These

จุฬาลงกรณ์มหาวิทยาลัย
CHULALONGKORN UNIVERSITY

are mainly used for gas phase applications because of their low pressure drop, high mechanical strength and low dust content.

Impregnated carbon: Porous carbons containing several types of inorganic impregnate such as iodine, silver, cations such as Al, Mn, Zn, Fe, Li, Ca have also been prepared for specific application in air pollution control especially in museums and galleries. Due to antimicrobial/antiseptic properties, silver loaded activated carbon is used as an adsorbent for purification of domestic water. Drinking water can be obtained from natural water by treating the natural water with a mixture of activated carbon and $Al(OH)_3$, a flocculating agent. Impregnated carbons are also used for the adsorption of H_2S and thiols. Adsorption rates for H_2S as high as 50% by weight have been reported.

Polymer coated carbon : This is a process by which a porous carbon can be coated with a biocompatible polymer to give a smooth and permeable coat without blocking the pores. The resulting carbon is useful for hemoperfusion. Hemoperfusion is a treatment technique in which large volumes of the patient's blood are passed over an adsorbent substance in order to remove toxic substances from the blood.

Other : Activated carbon is also available in special forms such as cloths and fibres. The "carbon cloth" for instance is used in personnel protection for the military.

จุฬาลงกรณ์มหาวิทยาลัย
CHULALONGKORN UNIVERSITY

2.2 Cobalt

Cobalt, a transition series metallic element having atomic number 27, is similar to silver in appearance. Cobalt and cobalt compounds have expended from use colorants in glasses and ground coat fits for pottery to drying agents in paints and lacquers, animal and human nutrients, electroplating materials, and high temperature alloys, hard facing alloys, and high speed tools, and magnetic alloys, alloys used for prosthetics, and used in radiology. Cobalt is also as a catalyst for hydrocarbon refining from crude oil for the synthesis of heating fuel.

The electronic structure of cobalt is [Ar]$3d^7 4s^2$. At room temperature the crystalline structure of the α (or ε) form, is close-packed hexagonal (cph) and lattice parameters are a = 0.2501 nm and c = 0.4066 nm. Above approximately 417°C, a face-centered cubic (fcc) allotrope, the γ (or β) form, having a lattice parameter a = 0.3554 nm, becomes the stable crystalline form. The scale formed on unalloyed cobalt during exposure to air or oxygen at high temperature is double-layered. In the range of 300 to 900°C, the scale consists of a thin layer of mixed cobalt oxide, Co_3O_4, on the outside and cobalt (II) oxide, CoO, layer next to metal. Cobalt (III) oxide, Co_2O_3, may be formed at temperatures below 300°C. Above 900°C, Co_3O_4 decomposes and both layers, although of different appearance, are composed of CoO only. Scales formed below 600°C and above 750°C appear to be stable to cracking on cooling, whereas those produced at 600-750°C crack and flake off the surface.

Cobalt forms numerous compounds and complexes of industrial importance. Cobalt, atomic weight 58.933, is one of the first transition series of Group 9 (VIIIB). There are thirteen know isotope, but only three are significant: ^{59}Co is the only stable and naturally occurring isotope; ^{60}Co has a half-life of 5.3 years and is a common source of γ-source for Mossbauer spectroscopy. Cobalt exists in the +2 or +3 valance states for the major of its compounds and complexes. A multitude of complexes of the cobalt (III) ion exists, but few stable simple salt are known. Octahedral stereochemistry is the most common for cobalt (II) ion as well as for cobalt (III). Cobalt (II) forms numerous simple compounds and complexes, most of which are octahedral or tetrahedral in nature; cobalt (II) forms more tetrahedral complex than other transition-metal ions. Because of the small stability difference between octahedral and tetrahedral complexes of cobalt (II), both can be found equilibrium for a number of complexes. Typically, octahedral cobalt (II) salts and complexes are pink to brownish red; most of the tetrahedral Co (II) species are blue.

Table 1 Physical properties of cobalt.

Property	Value
atomic number	27
atomic weight	58.93
transformation temperature, °C	417
heat of transformation, J/g[a]	251
melting point, °C	1493
latent heat of fusion, ΔH_{fus} J/g[a]	395
boiling point, , °C	3100
latent heat of vaporization at bp, ΔH_{vap} kJ/g[a]	6276
specific heat, J/(g·°C)[a]	
15-100°C	0.442
molten metal	0.560
coefficient of thermalexpansion, $°C^{-1}$	
cph at room temperature	12.5
fcc at 417 °C	14.2
thermal conductivity at 25 °C, W/(m·K)	69.16
thermal neutron absorption, Bohr atom	34.8
resistivity, at 20 °C[b], $10^{-8}\Omega\cdot m$	6.24
Curie temperature, °C	1121
saturation induction, $4\pi I_s$, T[c]	1.870
permeability, μ	
initial	68
max	245
residual induction, T[c]	0.490
coercive force, A/m	708
Young's modulus, Gpac	211

จุฬาลงกรณ์มหาวิทยาลัย
CHULALONGKORN UNIVERSITY

Table 1 Physical properties of cobalt (continued).

Property		Value	
Poisson's ratio		0.32	
Hardness[f], diamond pyramid, of %Co		99.9	99.98[e]
At 20 °C		225	253
At 300 °C		141	145
At 600 °C		62	43
At 900 °C		22	17
strength of 99.99 %cobalt, MPa[g]	as cast	annealed	sintered
tensile	237	588	679
tensile yield	138	193	302
compressive	841	808	
compressive yield	291	387	

[a] To convert J to cal, divided by 4.184.

[b] conductivity = 27.6 % of International Annealed Copper Standard.

[c] To convert T to gauss, multiply by 10^4.

[d] To convert GPa to psi , multiply by 145,000.

[e] Zone refined.

[f] Vickers, [g] To convert MPa to psi , multiply by 145.

จุฬาลงกรณ์มหาวิทยาลัย
CHULALONGKORN UNIVERSITY

2.3 Cobalt(II, III) Oxides

Cobalt has three well-know oxides: Cobalt (II) oxide, CoO, is an olive green, cubic crystalline material. Cobalt (II) oxide is the final product formed when the carbonate or the other oxides are calcined to a sufficiently high temperature, preferably in a neutral or slightly reducing atmosphere. Pure cobalt (II) oxide is a difficult substance to prepare, since it readily takes up oxygen even at room temperature to re-form a higher oxide. Above about 850°C, cobalt (II) oxide form is the stable oxide. The product of commerce is usually dark gray and contains 77-78 wt% cobalt. Cobalt (II) oxide is soluble in water, ammonia solution, and organic

solvents, but dissolves in strong mineral acids. It is used in glass decorating and coloring and is a precursor for the production of cobalt chemical.

Cobalt (III) oxide, Co_2O_3, is form when cobalt compounds are heated at a low temperature in the presence of an excess of air. Some authorities told that cobalt (III) oxide exists only in the hydrate form. The lower hydrate may be made as a black power by oxidizing neutral cobalt solutions with substances like sodium hypochlorite. Co_2O_3 or $Co_2O_3.H_2O$ is completely converted to Co_3O_4 at temperatures above 265°C. Co_3O_4 will absorb oxygen in a sufficient quantity to correspond to the higher oxide Co_2O_3.

Cobalt oxide, Co_3O_4, is formed when cobalt compounds, such as the carbonate or the hydrated sesquioxide, are heated in air at temperatures above approximately 265°C and not exceeding 800°C.

2.4 Acetaldehyde

Acetaldehyde, the formula CH_3CHO, is a colorless liquid or gas with a characteristic fruity odor. Acetaldehyde is a mobile, light molecular weight, low boiling point, flammable substance. Especially, a highly reactive properties, acetaldehyde is often used the most one organic compound, as an intermediate of downstream products and even if a solvent. However, when reaction temperature is higher than 420°C, acetaldehyde decomposes into methane and carbon monoxide. Acetaldehyde is not importance only in chemical industry, but it also has a large influence in the living thing. It is a mediator in the metabolism of plant and animal organisms that produced by the partial oxidation of ethanol by the liver enzyme called alcohol dehydrogenase. Large amounts of acetaldehyde interfere the biological processes. In alcoholic fermentation, as an intermediate in small amounts of all alcoholic beverage, such as beer, wine, and spirits. Though it also presents in plant juices, essential oils, roasted coffee, and tobacco smoke [35]. Other physical properties [35, 36] are listed below in **Table 2**.

Table 2 Physical properties of acetaldehyde.

Other names	**acetic aldehyde and ethyl aldehyde**
Molecular weight	44.054
Boiling point at 101.3 kPa	20.16°C
Melting point	-123.5°C
Solubility	slightly soluble in chloroform completely miscible with water, benzene, diethyl ether and ethanol
Vapor pressure	98 kPa at 20°C
Relative vapor density	1.52 (air = 1)
Reactivity	polymerizes violently in the presence of trace amounts of metals or acids; can react violently with acid anhydrides, alcohols, ketones, phenols, ammonia, hydrocyanic acid, hydrogen sulfide, halogens, phosphorus, isocyanates, strong alkalis and amines

About the safety information, this flammable compound from Gas Data Book [37] shows the lower and upper explosive limits of 3.3 to 19.0 % by volume, so we should operate below or above this range to avoid an explosion or fire. Flash point -20°C and ignition temperature 140°C.

2.4.1 Acetaldehyde production

Acetaldehyde is typically derived from petroleum and natural gas. In the case of chemical reaction production, the first time of discovery acetaldehyde occurred in 1774 by Carl Wilhelm Scheele during the reaction of black manganese dioxide and sulfuric acid with alcohol and then investigated by Antoine François, comte de Fourcroy and Louis Nicolas Vauquelin in 1800, Johann Wolfgang Dobereiner between

1821 and 1832. Finally, in 1835 Liebig who prepared pure acetaldehyde from the oxidation of ethanol by chromic acid, designated this product "aldehyde". Later that the name was altered to "acetaldehyde", a shortness of the full-word of “aldehyde dehydrogenatus”[35].

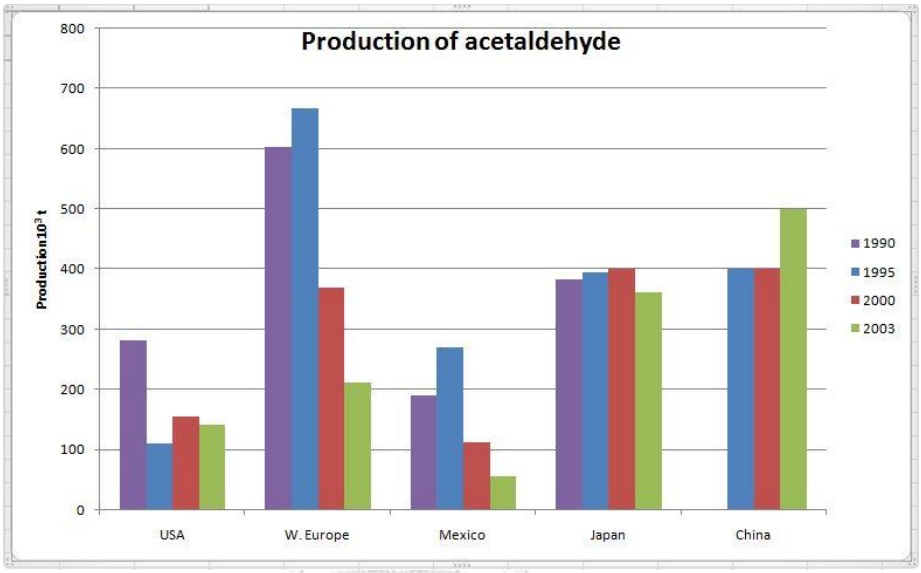

Figure 2 Production of acetaldehyde summary all over the world between 1990 and 2003.

Before 1962, ethanol and acetylene were the major sources of acetaldehyde. Since then, ethylene is the dominant feedstock because of the lower cost. In 2003, global acetaldehyde production was about 1 million tones [11]. The commercial production processes include: dehydrogenation and oxidation of ethanol [13, 38-40], the hydration of acetylene [41], the partial oxidation of hydrocarbons, and direct oxidation of ethylene [35] (also known as Wacker-Hoechst process). There are equation reactions shown below.

Dehydrogenation of ethanol: $CH_3CH_2OH \longrightarrow CH_3CHO + H_2$

Oxidation of ethanol: $CH_3CH_2OH + {}^1/_2\, O_2 \longrightarrow CH_3CHO + H_2O$

Hydration of acetylene: $C_2H_2 + H_2O \longrightarrow CH_3CHO$

Partial oxidation of ethane: $3\, C_2H_6 + O_2 \longrightarrow 2\, CH_3CHO + 3\, H_2$

Wacker-Hoechst process: $2\ C_2H_4 + O_2 \longrightarrow 2\ CH_3CHO$

This industrial route was dominant prior to the Wacker process. It is estimated that in 1976, more than 82% of the world's 2.3 megaton per year plant capacity use last one reaction [42]. However, the drawback of Wacker-Hoechst process is the formation of polymerization and condensation products of acetaldehyde. Moreover, it is costly and environmentally problematic, because the catalyst is methylated to give methylmercury during the process.

2.4.2 Acetaldehyde applications and market trend

Acetaldehyde has industrial importance for long times ago. The first commercial usage, occurred between 1914 and 1918, was the production of acetone by acetic acid in Germany (Wacker-Chemie and Hoechst) and in Canada (Shawinigan). The main part applications are using as a starting material in the production of chemical commodities such as acetic acid, acetic anhydride, ethyl acetate, cellulose acetate, vinyl acetate resins, butyl aldehyde, crotonaldehyde, peracetic acid, pentaerythritol, terephthalic acid, and synthetic pyridine derivatives [35]. In addition, acetaldehyde is not only used as an intermediate for the chemicals like describing previous, but also became downstream itself include: as a solvent in the rubber production, in the silvering of mirrors, in leather tanning, as a denaturant for alcohol, as an additive in fuel mixture, as a hardener for gelatin fibers, as a preservative for fruit and fish, as a synthetic flavoring agent, and in the manufacture of cosmetics, pharmaceutical, plastics, paper, glue and casein products [35, 42, 43].

From Chemical economics handbook (CEH) [44] informed in April 2013 that in the last few years, worldwide acetaldehyde's demand has also continuously decreased because of end-use markets and the effects of the economic downturn on these acetaldehyde-derived products. The dearth of demand caused by acetic acid manufacturing, the main product of acetaldehyde industry, shift to more effective technological and lower-cost methanol carbonylation process and even if the minor

effect of the plasticizer alcohols industry that completely switched from n-butyraldehyde based on acetaldehyde to the worthwhile process; oxonation of propylene.

However, CEH data in series of china report, in 2012, [45] acetic acid facilities based on acetaldehyde still remain continue to operate mainly in Asia and South America. China is the largest consumer of acetaldehyde in the world, accounting most half of global consumption. Their consumption is heavily weighted toward of acetic acid. Western Europe is the second-largest consumer, accounting for 20% of consumption. The US acetaldehyde market will also rise only minimally, at 1–2% per year during 2012–2018. In contrast, Japan could be the brightest spot for acetaldehyde consumption in the next five years and this hinges upon the on-purpose production of butadiene from acetaldehyde. The supply of butadiene has been volatile in Japan and the rest of Asia because of the limited availability of naphtha feedstock. Typically, butadiene and other C_4 hydrocarbons are coproduced when naphtha is used as a feedstock for ethylene manufacture. However, the increased production of natural gas from shale gas, particularly in the United States, has caused many ethylene crackers to switch feedstock from naphtha to ethane, which yields lower volumes of co-product butadiene and other C_4 hydrocarbons. This has spurred the revival of on-purpose production for butadiene and Japan certainly has enough sources of acetaldehyde to support such a project. This new end use should provide a much-needed boost to an otherwise flat acetaldehyde market. The following pie chart in **Figure 3** shows worldwide consumption of acetaldehyde that describe previously.

จุฬาลงกรณ์มหาวิทยาลัย
CHULALONGKORN UNIVERSITY

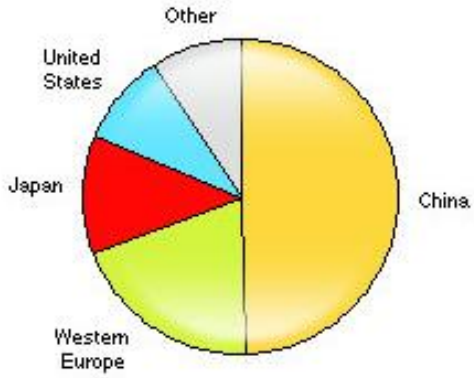

Figure 3 World consumption of acetaldehyde in year 2012.

Other uses such as pyridines and pentaerythritol will grow faster than acetic acid, but the volumes are not large enough to offset the decline in acetic acid. Synthetic pyridine derivatives, peracetic acid, pentaerythritol, and acetate esters accounted for 40% of acetaldehyde demand of 2012 global acetaldehyde consumption [45]. Pyridine and derivatives are important raw materials in agricultural chemicals. Pentaerythritol and acetate esters are both used widely in surface coatings. The other acetaldehyde applications accounted for the remaining global consumption of acetaldehyde in 2012 includes 1,3-butylene glycol, crotonaldehyde and glyoxal, along with some smaller-volume derivatives.

In 2015, Global Industry Analysts Inc. (GIA) [46] reported about the market trend for acetaldehyde by the year 2022. The demand of acetaldehyde is projected to exceed 1.4 million tons, forced by the rising use as a platform molecule in the production of various organic compounds for wide ranges application including construction, paints and coating, food preservatives, pharmaceuticals and cosmetics, flavoring agent, and food additives in dairy products. Asia-pacific represents the largest region consumption. While a closure of acetic acid based acetaldehyde productions in various parts of the world, China still produced continuously by the same process until recently. Japan represents the large-volume market registering a compound annual growth rate of 3.2% over the forecast period that driven by the commercial scale of

butadiene production from acetaldehyde [44, 47]. These data from CEH and GIA summarize in the same way of acetaldehyde future trend. **Figure 4** [46] summarizes the global acetaldehyde market trends, drivers and projections from GIA.

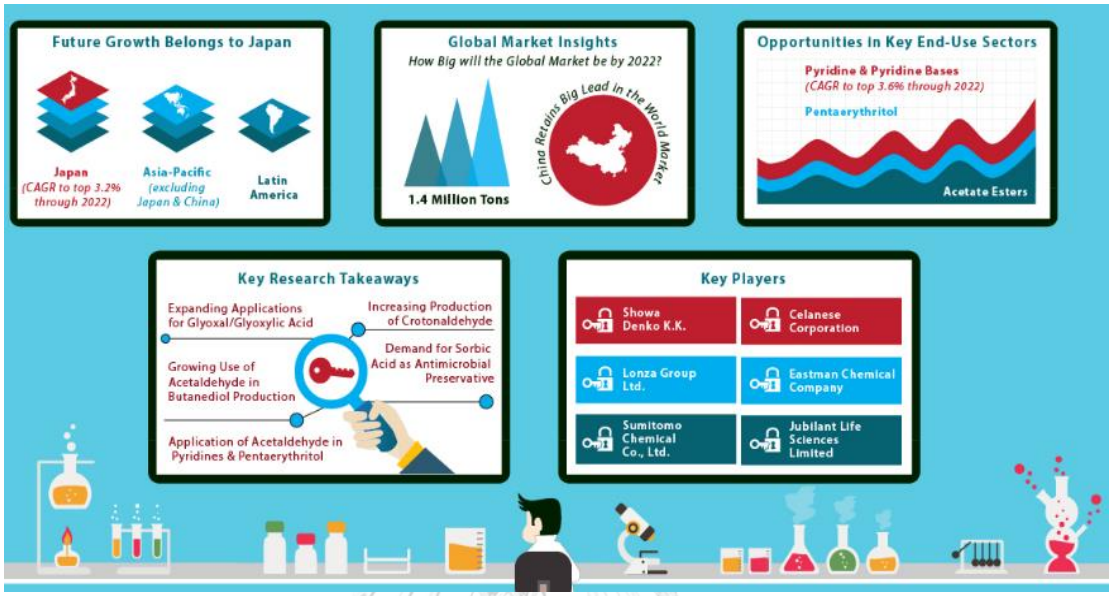

Figure 4 The global acetaldehyde market trends, drivers and projections.

2.5 Ethanol conversion

Dehydrogenation reaction of alcohol

The definition of dehydrogenation is the reaction that mechanism go by removing a hydrogen from the molecule. It is an endothermic reaction. Dehydrogenation reaction can be converse low molecular weight alkenes (such as ethane and propene) to the corresponding alkane, converse primary alcohol to aldehyde and ketone. During dehydrogenation, nucleophile addition of basic catalysts cause hydrogen removing from the alcohol reactant. Often, primary alcohols can be converted into aldehydes by hydrogen acceptors in the absence of oxygen. **Figure 5** summarizes the dehydrogenation of a primary alcohol, secondary alcohol, or amine results in an aldehyde, ketone, or imine, respectively from picture left to right.

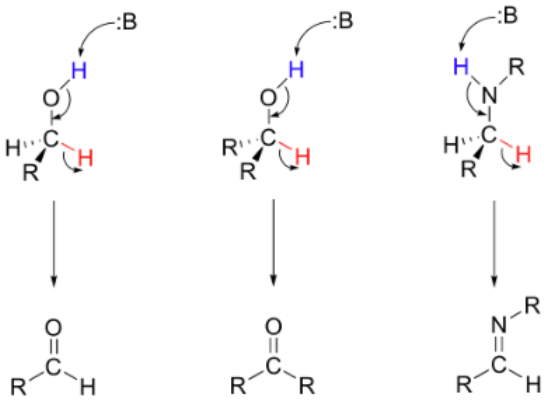

Figure 5 Proposed mechanism of dehydrogenation reaction [48].

The products yields will be various by the different kind of catalysts and external conditions such as temperature, pressure, retention time, etc. In case of our interesting section of ethanol dehydrogenation, the dehydrogenation of ethanol can be produce acetaldehyde and hydrogen byproduct and subsequently to ethyl acetate. The first work was reported in 1886, at 260°C.

$$CH_3CH_2OH\ (l) \longrightarrow CH_3CHO\ (l) + H_2\ (g) \quad ; \Delta H = +82.5\ kJ/mole$$

Catalytic dehydrogenation of ethanol ever used the catalysts such as iron [49], copper [13, 22, 40, 49], or oxide of zinc, nickel, or cobalt [38, 50, 51]. In later patents, zinc and chromium catalysts [52], oxides of rare earth metals, and mixtures of copper and chromium oxides have been published.

จุฬาลงกรณ์มหาวิทยาลัย
CHULALONGKORN UNIVERSITY

CHAPTER III

LITERATURE REVIEW

3.1 Activated carbon from other precursors

As is well known, the activated carbon prepared from different precursors or prepared by different activation process, will have different textural characteristics that are shown in **Table 3**. Furthermore, it was usually applied as potential adsorbents for the purification of gases [8, 53], for the removal of organic pollutants from water [1], and etc.

Table 3 Comparisons of the characteristics of porosity of other literature data for other precursors under optimum condition.

References	Precursor	Activation method	S_{BET} (m^2/g)	V_{tot} (cm^3/g)	V_{micro} (cm^3/g)
Guo et al.,2002	Rice husk	Chemical(KOH)	more than 3,000	1.9	-
Wei et al.,2006	Coconut shell	Physical(Air)	more than 700	-	-
Azevedo et al.,2007	Coconut shell	Chemical activation with $ZnCl_2$ followed by physical activation	2,114	1.307	1.142
Li et al.,2008	Coconut shell	Physical(stream)	1,926	1.26	0.931
Kalderis et al.,2008	Rice husk	Chemical($ZnCl_2$)	750	0.38	-
Basta et al.,2009	Rice straw	Chemical(KOH)	1,917	0.94	-

จุฬาลงกรณ์มหาวิทยาลัย
CHULALONGKORN UNIVERSITY

Table 4 Comparisons of the characteristics of porosity of other literature data for other precursors under optimum condition (continued).

References	Precursor	Activation method	S_{BET} (m^2/g)	V_{tot} (cm^3/g)	V_{micro} (cm^3/g)
Guo et al.,2009	Coconut shell	Physical(CO_2)	1,700	1.135	0.882
Liou and Wu, 2009	Rice husk	Chemical($ZnCl_2$)	2,434	1.344	
Boudrahem F et al., 2009.	Coffee residue	Chemical ($ZnCl_2$)	890		0.772
Boudrahem F et al., 2011.	Coffee residue	Chemical ($ZnCl_2$)	889	0.765	0.418
		(H_3PO_4)	1003	0.618	0.423
Benjapol et al., 2013.	Deoil rice bran residue	Chemical (H_3PO_4, $ZnCl_2$)	1404	0.74	0.63
Maraisa et al., 2013.	Coffee husk	Chemical ($ZnCl_2$) Physical (N_2)	1450		
Kanokwan et al., 2015	Coffee residue	Chemical ($ZnCl_2$) Physical (CO_2)	1218	1.02	
Hamza et al., 2017.	Coffee grounds	Chemical (KOH)	1778		

จุฬาลงกรณ์มหาวิทยาลัย
Chulalongkorn University

3.2 Activated carbon from coffee residues

There have reported that few researchers used coffee ground residue as precursor for activated carbons. Boudrahem F et al., 2009 [54] reported the preparation of activated carbons from coffee residue by using chemical activation with $ZnCl_2$ that resulted in a BET surface area of 890 m^2/g and a micropore volume of 0.772 cm^3/g.Then, Boudrahem F et al., 2011 [55] studied the preparation of activated carbon from coffee residue again, found that using chemical activation with $ZnCl_2$ and H_3PO_4 that resulted in a BET surface area of 889 and 1003 m^2/g respectively. Then, Maraisa et al., 2013 [56] prepared activated carbons from coffee husk by using chemical

activation with $ZnCl_2$ and physical activation with N_2 that resulted in a BET surface area of 1450 m^2/g. Moreover, Kanokwan et al., 2015 [57] preparation of activated carbons from coffee residue by using chemical activation with $ZnCl_2$ and physical activation with CO_2 found that these is a BET surface area of 1218 m^2/g.

These results indicated that coffee residue could be an economically promising material. Meanwhile, Hamza et al., 2017 [58] prepared activated carbons from coffee grounds by using chemical activation (KOH) as activation method that resulted in a BET surface area of 1778 m^2/g.

3.3 Co catalyst

In many years later, cobalt is the metal which was proposed by many reactions. Many studies usually used cobalt catalysts for synthesis of hydrocarbons in Fisher – Tropsch process [59-61]. Furthermore, in few years later, cobalt catalysts was used in ethanol reaction. Cyril Gaudillere et al., 2017 [62] investigated steam reforming of ethanol reaction over 3 mol% Y_2O_3 doped ZrO_2 monolith infiltrated with cobalt as catalysts. Monoliths were fabricated by implementing the freeze-casting technique in order to obtain hierarchical, vertical and highly ordered porous microstructure resulting in very low pressure drop, high surface area and accessibility to active sites. Catalytic monoliths were firstly loaded with 3 wt% of Co. Catalytic activity of Co-containing monolith was compared with the catalytic activity of a powdered material with the same chemical composition than the catalytic monolith. The results show a clear improvement all over the temperature range of the ethanol conversion and H_2 yield and a decrease of the by-products contents when using a freeze-cast monolith support. The incorporation of La enabled a strong decrease in coke deposition over the activated monolith. Finally, the beneficial effect of the implementation of freeze-cast monolith in comparison with the not structured fixed-bed configuration is explained by the difference of packing since and improved fluid dynamics at similar GHSV, the former one promotes in a higher proportion the Water Gas Shift Reaction

จุฬาลงกรณ์มหาวิทยาลัย
CHULALONGKORN UNIVERSITY

(WGSR) further in the monolith length. While K. Jiratova et al., 2017 [63] studied oxidation of ethanol and N_2O decomposition on cobalt oxides supported over ceria–zirconia coated cordierite monoliths as catalysts. Interaction of Co_3O_4 with ceria–zirconia washcoat led to formation of Co_3O_4 particles with slightly worse structure ordering resulting in better reducibility than that observed for the commercial Co_3O_4 catalyst. In oxidation of ethanol, activity of the Co_3O_4-containing monoliths was comparable with that of pelletized cobalt oxide catalyst with nearly 7 times higher content of active components. However, conversions of N_2O over the monolith catalysts were lower. Nonetheless, incorporation of Co_3O_4 onto ZrO_2–CeO_2 washcoat increased rate of both catalytic reactions. Furthermore, K. Jiratova et al., 2017 [64] studied ethanol oxidation and N_2O decomposition on cobalt oxide catalysts on titania–ceria supports. Supports with various molar ratio of CeO_2/TiO_2 were prepared by the sol–gel method and cobalt components were introduced by impregnation and subsequent calcination. It was found that the ethanol conversion at 200°C is proportional to the $CeO_2/(CeO_2+TiO_2)$ molar ratio in the supports, and temperature T_{50} of ethanol oxidation is proportional to the amount of components reducible in the temperature of 20–500°C. A comparison of specific catalytic activities in both ethanol oxidation and N_2O decomposition proved a lower rate of N_2O decomposition than that of oxidation of ethanol (approximately 25 times). The findings confirmed the great importance of the supports surface areas on specific activity of cobalt catalysts in both reactions. The obtained results showed that ceria is the best support of cobalt oxides for both deep ethanol oxidation and N_2O decomposition when reaction rates are related to unit amount of active component in the catalysts.

Moreover, Guofeng Zhao et al., 2016 [65] studied reaction-induced self-assembly of $CoO@Cu_2O$ nanocomposites In-Situ onto SiC-foam for gas-phase oxidation of bioethanol to acetaldehyde. CoO (50-100 nm) partially covered with Cu_2O (~ 10 nm), is engineered from nano to macro scales in one step for high-throughput gas-

phase aerobic oxidation of bioethanol to acetaldehyde. Such special CoO@Cu_2O nanostructure shows much higher activity/selectivity than other binary metal-oxide assemblies such as CuO_x&CoO nanomixture and inverse Cu_2O@CoO nanostructure. The catalyst is facilely but exclusively obtainable by in-situ reaction-induced transformation of their nitrates supported on SiC-foam into CoO@Cu_2O nanostructure in the reaction stream, which generates 95% conversion with 98% selectivity under mild conditions and is stable for at least 150 h for a feed of 20 vol% ethanol at a high EtOH weight hourly space velocity of 8.5 h^{-1}. Abundant Cu_2O-CoO interface and high stability of the CoO@Cu_2O nanostructure is in nature responsible for the high activity/selectivity and promising reaction stability in this reaction.

Alexandru Popa et al., 2017 [66] investigated catalytic properties from ethanol reactions of cobalt salts of Keggin type heteropolyacids supported on mesoporous silica in different concentrations (20–40 wt%CoHPM) of active phase. The main products obtained on acid (dehydration) catalytic centres were ethylene and diethyl ether, besides acetaldehyde which was obtained on redox (dehydrogenation) catalytic centres. It is found that silica – supported catalysts, seem to be more active than bulk CoHPM catalyst in dehydration and dehydrogenation reactions. The higher values of dehydration and reaction products formation are obtained with the lowest loading (20 wt%CoHPM) and as a result the highest dispersion of active phase.

Anchu Ashok et al., 2017 [67] studied the decomposition of ethanol for hydrogen production of cobalt nanoparticles synthesized via solution combustion synthesis. Cobalt nanoparticles using cobalt nitrate as a metal precursor in presence of different reducing agents; hydrazine, glycine, urea and citric acid. Thermodynamic results show that the type and amount of fuel influence the adiabatic combustion temperature and the gases released during synthesis process affecting nanoparticle size, porosity and microstructure. The synthesized nanoparticles were activated by passing H_2 at 300°C inside the reaction chamber before being used for studying the

reaction pathway of catalytic dehydrogenation of ethanol. These studies indicate that cobalt catalyst is selective for aldehyde and acetate species along with the formation of H_2, H_2O and CO_2. Production of methane was also observed on cobalt surface at 400°C. The spent catalyst nanoparticles indicate a growth in particle size because of sintering, and carbon formation on the catalyst surface due to coking during ethanol dehydrogenation reaction.

Yasmina H. et al., 2016 [68] used cobalt and mixed iron-cobalt spinel oxides $Co_xFe_{(3-x)}O_4$ supported on silica (IMP-Co_x-500) and their bulk analogues (CP-Co_x-500) were prepared via impregnation and co-precipitation methods respectively and calcined at 500°C. Their catalytic behavior in ethanol combustion were investigated. For ethanol combustion of bulk catalysts, full conversion of ethanol was achieved at 275-350°C. As expected, the activity of the mixed oxides $CoFe_2O_4$ and $FeCo_2O_4$ is generally better than that of the single oxide Co_3O_4. For a conversion below 15%, the three oxides have the same reactivity, in contrast to higher conversion levels, where the reactivity closely depends on the solid composition. Cobalt ferrite exhibits the best activity; a conversion increase from 30 to 100% is obtained via the CP-Co_1-500 sample in the temperature range 250-275°C. The activity of iron cobaltite is intermediary between cobalt ferrite $CoFe_2O_4$ and cobalt oxide Co_3O_4; At 300°C, the conversion reached 90% and 50% on CP-Co_2-500 and CP-Co_3-500 samples respectively, this latter solid achieved a total conversion at 350°C. The catalytic performances of the supported solids are greatly different from that of bulk catalysts. Reactivity is substantially similar, for all the solids, till 30% of conversion. Further than, the conversion reached 96, 77 and 60% at 275°C, for the samples IMP-Co_2-500, IMP-Co_3-500 and IMP-Co_1-500 respectively.

จุฬาลงกรณ์มหาวิทยาลัย
CHULALONGKORN UNIVERSITY

3.4 Dehydrogenation reaction of ethanol

In an inert atmosphere, ethanol can be dehydrogenated to acetaldehyde using a redox catalyst. Moreover, the acidic functionality catalyst leads to ethyl acetate as shown in **Figure 6** [38, 69].

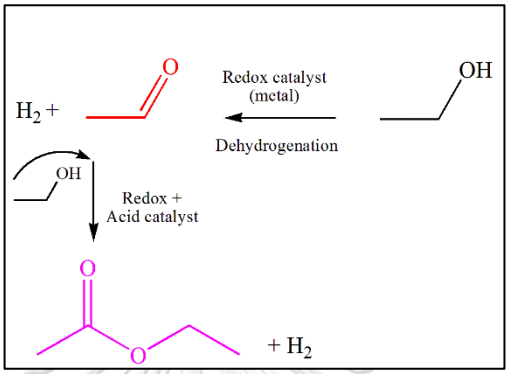

Figure 6 Ethanol conversion to acetaldehyde and ethyl acetate. [rewrite from Gallo et al., [38]]

The ethanol dehydrogenation to acetaldehyde has been studied using varied catalysts. However, this reaction catalyzed by carbon materials have not been studied as widely as with other materials. Thus, Gerald C. et al., 1991 [70] found that carbon molecular sieves (CMS's) are show to be very effective catalysts and catalyst supports for the oxidative dehydrogenation of ethanol. For undoped CMS catalysts, small amounts of products are initially formed, with the major one being ethylene in a N_2 flow 230°C. When the carrier flow is switched to air, 70% of ethanol is converted to acetaldehyde and ethyl acetate (57% and 36% of all products, respectively). For doped CMS catalysts with molybdenum oxide (MoO_3/CMS), is extremely active for dehydrogenation. Essentially 100% of ethanol is converted to acetaldehyde more than 85% at 230 °C.

G. S. Szymanski et al., 1994 [34] investigated catalytic conversion of ethanol on polymeric carbon catalyst and nickel on polymeric carbon catalysts. For nonoxidized activated carbon (C) shows very low catalytic activity in ethanol decomposition. While the activated carbon was impregnated with nickel(II) nitrate hexahydrate (Ni/C) and the

carbon was oxidized with nitric acid follow by impregnated with nickel(II) ions (C-Ni) indicate dominant catalytic activity in the dehydrogenation. For the carbon was oxidized with nitric acid (C-ox) results in higher catalytic activity. At lower temperatures, the dehydrogenation of ethanol dominates, while at higher temperatures dehydration is predominant. An increase of reaction temperature results in a higher dehydrogenation selectivity initially, but at higher temperatures passes through a maximum and then decreases.

F. Carrasco-Marin et al., 1998 [33] examined the dehydrogenation of ethanol on oxidized activated carbon catalysts, were prepared from olive stones and oxidized with $(NH_4)_2S_2O_8$. The unoxidized activated carbons are dehydrogenation catalysts producing acetaldehyde (100%) at very low activity. For the oxidized carbons are able to give both dehydrogenation and dehydration reactions. The conversion increased with the oxidation time, particularly at the beginning of oxidation, because of the formation of the dehydration products.

J. Jasinska et al., 2011 [32] studied activated carbons containing different surface functionalities as catalysts in conversion reactions of ethanol. These carbon materials were prepared from Polish brown coal by chemical activation with KOH and modified by the oxidation with ammonia or chlorine. The main product is acetaldehyde from ethanol dehydrogenation. The carbons modified by Cl_2 show the highest conversion about 75% at reaction temperature of 700 K.

E.A. Tveritinova et al., 2016 [71] studied catalytic conversion of ethanol on carbon nanomaterials. The highest conversion on non-oxidized (CNT), air-oxidized (CNT-AO) and nitric-oxidized (CNT-NO) carbon nanomaterials are 35.8%, 58.8% and 85.0% respectively. The main products of the conversion of ethanol on CNT and CNT-AO catalysts are acetaldehyde. This study found that the selectivity of the formation of acetaldehyde from ethanol on both CNT and CNT-AO catalysts reach 97.0%.

จุฬาลงกรณ์มหาวิทยาลัย
CHULALONGKORN UNIVERSITY

J. Shan et al., 2016 [24] studied selectivity of non-oxidative dehydrogenation of ethanol to acetaldehyde and hydrogen on highly dilute NiCu alloys over silica supported. For $Ni_{0.001}$CuNPs, $Ni_{0.01}$CuNPs and CuNPs catalysts, the formation of CO and CO_2 is negligible up to 350°C, indicating a nearly 100% selectivity of acetaldehyde. But on $Ni_{0.03}$CuNPs, formation of CO is observed at low temperature, which is similar to Ni NPs at temperatures above 300°C.

3.5 Co/AC catalysts

Activated carbon supported cobalt catalysts were studied in many reactions such as Fischer-Tropsch synthesis [72-74], CO oxidation and CO hydrogenation. M. Ferrari et al., 2001 used the activated carbons as supports and investigated the effect of the impregnation order (either cobalt or molybdenum first) and tested in hydrodeoxygenation reactions. Both series of samples exhibit a preferential impregnation of the metal oxides at the exterior of the carbon grains, but CoMo (molybdenum first) is more uniformly distributed than MoCo (cobalt first). When molybdenum is added after cobalt (MoCo), the molybdenum–cobalt interactions cause a thick layer of metal oxide crystals to be formed; it covers the external grain surface and it is only in partial physical contact with the carrier. When cobalt is added after molybdenum (CoMo), it seems to bring about the remobilization and migration of molybdenum to the external part of the grains. Finally it is shown that inorganic impurities, like calcium and iron, which are present in low amounts in the activated carbon can interact with molybdenum and form mixed oxides. For the catalytic activity, MoCo catalysts show lower hydrogenation properties for the conversion of ketonic groups and lower decarboxylation selectivity in the conversion of the ester.

E.A. Sales et al., 2005 [75] used carbon-supported copper catalysts promoted by palladium and cobalt catalysts and tested in the oxidative dehydrogenation of ethanol in the presence of N_2O. All catalysts were active and selectivity of 100% to acetaldehyde coupled with N_2O decomposition in the range of 150–450°C. The Co-

Cu/C and Cu/C catalysts performed the best, with conversions of around 80% at 450°C, either in coupled or separate reactions.

P.R. Shukla et al., 2010 [76] studied oxidation of phenol in aqueous solution on activated carbon supported cobalt catalysts. It was prepared by impregnation of cobalt ion on an activated carbon and used to activate peroxymonosulphate (PMS). It was found that Co_2O_3 was the major form of Co species and was homogeneously distributed on the activated carbon surface. Co/AC exhibited high activity in oxidation of phenol with sulphate radicals and 100% decomposition and 80% TOC removal could be achieved in 60 min at the conditions of 500 ml phenol solution of 25 ppm, 0.1 g catalyst and 1 g peroxymonosulphate. The catalyst also exhibited stable performance after several rounds of regeneration. Several operational parameters such as catalyst and oxidant amount, temperature on the rate of oxidation were found to influence the phenol oxidation.

Z. Zhao et al., 2013 [77] compared to the supported cobalt–cerium oxide catalyst on activated carbons (AC), First fabricated a novel and highly-efficient cobalt–manganese non-precious metal catalyst deposited on modified with unprecedented catalytic activity and extremely wide temperature-operation window for CO complete removal from an H_2-rich stream, which resulted from the strong interaction of finely dispersed cobalt–manganese primarily confirmed by various characterization results. The high catalytic activity and extremely broad temperature-operation window allow the developed catalyst to possess a fascinating perspective for large-scale application in industry.

I. Genova et al., 2014 [78] used high quality micro-mesoporous activated carbon, was prepared from peach shells, for a host matrix of cobalt ferrite nanoparticles. It tested as catalysts for hydrogen production from methanol. Depending on the Co/Fe ratio formation of pure $CoFe_2O_4$ or a mixture of CoO and ferrite phases were observed for carbon supported bi-component materials, while

under the same condition the silica support provides the formation of non-stoichiometric ferrite phase. The catalytic active phase which is formed by the influence of the reaction medium represents a complex mixture of non-changed ferrite, magnetite, Co–Fe alloy and/or Fe_3C in different proportions.

M. Zabihi et al., 2015 [79] used copper and cobalt oxides supported on almond shell derived activated carbon with different loadings were synthesized by sequential and co-deposition–precipitation methods leading to Cu(shell)/Co(core)/AC, Co(shell)/Cu(core)/AC and Cu–Co(mixed)/AC catalysts that were used for catalytic oxidation of gaseous mixtures of toluene and cyclohexane in air. Catalyst efficiency for toluene and cyclohexane oxidation, both separately and in a mixture, was higher over the mixed metal oxides catalysts compared with the core–shell catalysts. An increase in the cobalt loading on the support led to a decrease in the metal oxide crystallite size and a change in the catalyst morphology. The best performance was obtained for the Cu_2–Co_6(mixed)/AC sample (Removal Efficiency >99.9%). For Cu(shell)/Co(core)/AC samples resulted in catalysts with the worst performance for complete oxidation of VOCs. Results indicated a negligible deterrence effect of toluene on cyclohexane oxidation. Furthermore, the addition of water (humid air) decreased the conversion of hydrocarbons.

จุฬาลงกรณ์มหาวิทยาลัย
CHULALONGKORN UNIVERSITY

Y. Zhuang et al., 2015 [80] used mesoporous carbon-supported cobalt (Co-MC) as bifunctional catalysts for application in organic catalytic reactions and degradation of water contaminants is slower. Herein, the catalyst displayed high activity in the selective oxidation of toluene to benzaldehyde, a high selectivity of 92.3%. Co-MC displayed remarkable catalytic activity in degrading dyes relative to the pure metal counterpart. Moreover, the catalyst exhibited excellent reusability. The paper shows the potential of Co-MC as a bifunctional catalyst for both toluene selective oxidation and water contaminant degradation.

W. Zhao et al., 2017 [81] used cobalt-nitrogen-activated carbon as a catalyst for acetylene hydrochlorination reaction, which shows good catalytic performance. The obtained results indicated that Co-N-AC catalyst can significantly improve the adsorption of HCl. And the presence of Co-N_x, which plays a major role in acetylene hydrochlorination reaction.

จุฬาลงกรณ์มหาวิทยาลัย
CHULALONGKORN UNIVERSITY

CHAPTER IV

EXPERIMENTAL

4.1 Preparation of activated carbon derived coffee residue

To study the effect of activation method on carbon material used as catalyst in ethanol dehydrogenation, so the carbon catalysts will be prepared in various activation method.

4.1.1 Chemicals and reagents

1. Sodium bicarbonate ($NaHCO_3$)
2. Zinc chloride ($ZnCl_2$)
3. Distilled water
4. Coffee residues

4.1.2 Experimental procedure

1. Coffee residue as a waste of ground coffee was dried at 110°C for 24 h.
2. The dried coffee residue was mixed with $ZnCl_2$ with a mass ratio of coffee residue to-$ZnCl_2$ as (1:3) and dried in an oven at 110°C for 24 h.
3. The mixed sample was activated under only CO_2, N_2 and N_2 followed by CO_2 atmosphere at 600°C with a heating rate 10°C/min. Once the activation temperature was reached, it was kept for 1 and 4 h before cooling the furnace down to room temperature.
4. The materials were leached out by washing with HCl solution (1%w/v) until neutrality and was several washed with distill water.
5. Finally, the samples were dried at 110°C for 24 h.

4.1.3 The nomenclature of samples

The carbon catalysts were denoted as AC-X

Where AC-A was activated under only CO_2 flow for 4 h.

AC-B was activated under only N_2 flow for 4 h.

AC-C was heated under N_2 and hold under CO_2 for 1 h.

จุฬาลงกรณ์มหาวิทยาลัย
CHULALONGKORN UNIVERSITY

AC-D was heated under N_2 and hold under CO_2 for 4 h.

4.2 Preparation of activated carbon supported cobalt catalyst

4.2.1 Chemicals and regents

1. Activated carbon used as support: activated carbon derived from coffee residue (part 4.1)
2. Cobalt (II) nitrate hexahydrate [$Co(NO_3)_2 \cdot 6H_2O$] as cobalt precursor
3. De-ionized water

4.2.2 Experimental procedure

1. The certain amount of cobalt (4 and 6 wt% loading) was introduced into the de-ionized water which its volume equals to pore volume of catalyst.
2. The aqueous solution of cobalt was slowly impregnated to activated carbons.
3. The catalyst was dried in the oven at 110°C for 24 h.
4. The catalyst was calcined in N_2 at 400°C for 6 h.

4.2.3 The nomenclature of samples

The cobalt catalysts supported on activated carbon were denoted as Y%Co/C,

Where Y is the percentage of % cobalt loading

4.3 Preparation of various metals supported-commercial activated carbon catalysts

จุฬาลงกรณ์มหาวิทยาลัย
Chulalongkorn University

4.3.1 Chemicals and regents

1. Commercial activated carbon used as support
2. Cerium nitrate hexahydrate [$Ce(NO_3)_2 \cdot 6H_2O$] as precursor
3. Cobalt (II) nitrate hexahydrate [$Co(NO_3)_2 \cdot 6H_2O$] as precursor
4. Copper (II) nitrate hemi pentahydrate [$Cu(NO_3)_2 \cdot 2.5H_2O$] as precursor
5. Nickel (II) nitrate hexahydrate [$Ni(NO_3)_2 \cdot 6H_2O$] as precursor
6. De-ionized water

4.3.2 Experimental procedure

1. The certain amount of metals (10 wt% loading) was introduced into the de-ionized water which its volume equals to pore volume of catalyst.

2. The aqueous solution of cobalt was slowly impregnated to activated carbons.

3. The catalyst was dried in the oven at 110°C for 24 h.

4. The catalyst was calcined in N_2 at 400°C for 6 h.

4.3.3 The nomenclature of samples

The metal catalysts supported on activated carbon were denoted as Z/ACC,

Where Z is the metal used as a precursor

4.4 Catalyst characterization

The catalyst was characterized by a variety of techniques as shown below.

4.4.1 Nitrogen adsorption-desorption isotherm

The catalysts approximately 50 mg was measured specific surface area, pore volume and pore diameter by N_2 adsorption-desorption at liquid nitrogen (-196°C) using a Micromeritics ASAP 2000 instrument. The surface area and pore size distribution was calculated by Brunauer-Emmelt-Teller (BET) and BJH method, respectively.

4.4.2 X-ray diffraction (XRD)

X-ray diffraction (XRD) was used to observe the carbon structure of activated carbon and the dispersion of nickel species on carbon material by a SIEMENS D5000 X-ray diffractometer using CuKα radiation with Ni filter in the 2θ range of 10-80 degrees resolution 0.04°.

จุฬาลงกรณ์มหาวิทยาลัย
CHULALONGKORN UNIVERSITY

4.4.3 Thermal Gravimetric analysis (TGA)

Thermal Gravimetric analysis (TGA) was used to study the thermal decomposition of catalyst under the temperature range of room temperature to 1000°C with a heating rate of 10°C/min in nitrogen atmosphere using an STD analyzer model Q600 from TA instrument.

4.4.4 Fourier transforms infrared spectroscopy (FT-IR)

FT-IR analysis was used to determine the functional group as the chemical structure of activated carbon using a Nicolet 6700 FTIR spectrometer.

4.4.5 Scanning Electron Microscopy (SEM) and Energy dispersive X-ray spectroscopy (EDX)

Scanning electron microscopy (SEM) and Energy dispersive X-ray spectroscopy (EDX) were used to determine the morphology and elemental distribution of catalysts. Model of SEM: JEOL mode JSM-5800LV and EDX was perfumed using Link Isis Series 300 program at the Scienctific and Technological Research Equipment Center, Chulalongkorn University (STREC).

4.4.6 CO_2 temperature programed adsorption TPD

The basicity of catalysts was measured by CO_2-TPD using Micromeritics Chemisorb 2750 automated system. The 0.05 g of catalyst sample was packed in the glass sample cell and pretreated at 500°C under helium flow rate 25 cm^3/min for 1 h. The catalyst sample was saturated with CO_2 at ambient temperature. Then, the catalyst surface was physisorbed by the He flow rate 35 cm^3/min for 30 min. After that, the temperature programmed desoption was carried out from 40°C to 550°C at heating rate 10°C/min. the amount of CO_2 in effluent gas was analyzed via thermal conductivity detector (TCD) as a function of temperature.

4.4.7 NH_3 temperature programed adsorption TPD

Temperature-programmed desorption of ammonia (NH_3-TPD) was performed using Micromeritics Chemisorp 2750 automated system (Micromeritics Instrument Corporation, Frankfurt, Germany) to study the acid properties. In the study, 0.05 g of catalyst was packed in a U-tube quartz cell with 0.03 g of quartz wool and pretreated at 500°C under helium flow rate 25 cm^3/min for 1 h. The catalyst sample was saturated with NH_3 at ambient temperature for 30 min. Then, the physisorbed NH_3 on the catalyst surface was removed at a He flow rate of 25 cm^3/min for 15 min. After that, the temperature-programmed desorption was carried out from 40°C to 800°C at a heating rate 10°C/min. The amount of NH_3 in the effluent gas was analyzed via thermal conductivity detector (TCD) as a function of temperature. The total acidity was

calculated from the relation between the TCD results and the temperature, from 40°C to 550°C. After 550°C, the TPD peak was only the decomposition of the catalyst, as proven by the TGA result.

4.4.8 Transmission electron microscopy (TEM)

Transmission electron microscopy (TEM; JEOL JEM-2010; JEOL Solutions for Innovation, Peabody, MA, USA) was used to determine the morphology and size of metal on the catalyst with thermionic electron type LaB_6 as a source, operating at 200 kV.

4.4.9 Inductively coupled plasma mass spectrometer (ICP)

Inductively coupled plasma mass spectrometer (ICP) was used to determine the actual amount of the metals loading.

4.4.10 Temperature-programmed reduction (H_2-TPR)

TPR was used to determine the reducibility of catalysts. The catalyst sample 50 mg was used in the operation and temperature ramping from 35°C to 400°C at 10°C/min. The carrier gas is be 5 % H_2 in Ar. During reduction, a cold trap was placed to before the detector to remove water produced. A thermal conductivity detector (TCD) was measured the amount of hydrogen consumption. The calibration of hydrogen consumption was performed with bulk silver oxide at the same conditions.

จุฬาลงกรณ์มหาวิทยาลัย
Chulalongkorn University

4.5 Measurement of catalytic activity with ethanol dehydrogenation

4.5.1 Chemicals and reagents

1. Absolute ethanol (99.95%)
2. Ultra-high purity grade nitrogen (99.999%)
3. Ultra-high purity grade argon (99.999%)
4. Ultra-high purity grade hydrogen (99.999%)

4.5.2 Instrument and apparatus

The flow diagram of ethanol dehydrogenation reaction system is shown **in Figure 7**. The main system consists of gas controlling system, syringe pump, vaporizer, reactor, electric furnace, temperature controller and gas chromatograph.

(1) Gas controlling system: The flow rate of carrier gas (N_2) is adjusted by mass flow controller. The presser regulator and on-off valve are equipped in this system in order to control gas flow.

(2) Syringe Pump: Liquid ethanol is injected to the vaporizer by syringe pump.

(3) Vaporizer: Liquid ethanol is vaporized in vaporizer at temperature of 120°C.

(4) Reactor: The borosilicate glass tube reactor with inside diameter of 0.7 is used as a reactor. The center of reactor is packed with catalyst on quartz wool layer.

(5) Electric Furnace: the reactor and vaporizer are heated by electric furnace. The temperature of furnace is controlled by temperature controller with the maximum voltage of 220 volt.

(6) Temperature controller: The temperature of electric furnace is set by temperature controller in range between 150°C to 400°C. The temperature controller is connected to variable voltage transformer and thermocouple which attached to the reactor.

(7) Gas Chromatograph (GC): Light hydrocarbon such as ethylene, ethanol, acetaldehyde, etc. are analyzed by a gas chromatograph (Shimadzu GC-14A) equipped with flam ionization detector (FID) and DB-5 capillary column. A Shimadzu GC-8A gas chromatograph equipped with thermal conductivity detector (TCD), molecular sieve 5A and Porapak Q column is used to analyzed carbon dioxide, carbon monoxide and oxygen in the stream. The operating conditions of GC are shown in the **Table 4**.

จุฬาลงกรณ์มหาวิทยาลัย
CHULALONGKORN UNIVERSITY

Table 5 Operating conditions for gas chromatographs.

Gas chromatographs	**Shimadzu GC-8A**		**Shimadzu GC 14B**
Detector	TCD	TCD	FID
Column	Molecular sieve 5A	Porapak Q	DB5
Maximum temperature	350°C	150°C	350°C
Carrier gas	He (99.999%)	He (99.999%)	N_2 (99.999%)
Carrier gas flow	40 cc/min	-	-
Column temperature			
Initial (°C)	60	60	40
Final (°C)	60	60	40
Injection temperature (°C)	100	100	150
Detector temperature (°C)	-	-	150
Current (mA)	80	80	-
Analyzed gas	CO, O_2, N_2	CO_2, CH_4, C_2H_4	Ethanol, acetaldehyde, ethylene, diethyl ether

4.5.3 Ethanol dehydrogenation reaction procedure

Catalytic dehydrogenation reaction of ethanol was performed in the fixed-bed continuous flow reactor 0.05 g of catalyst and 0.01 g of quartz wool bed were packed in the middle of glass tube reactor which located in the electric furnace. Before the reaction was carried out, catalyst was preheated at 200°C for 30 min in N_2 to remove the moisture. For part 4.2 and 4.3, The catalysts were reduced with H_2 at 400°C for 4 h before the catalytic reaction. Ethanol was vaporized at 120°C with N_2 gas (60 ml/min) for dehydrogenation reaction. The gas stream was introduced to the reactor with WHSV of 8.4 h^{-1} and the reaction was carried out at temperature range from 250°C to 400°C under atmospheric pressure. The gaseous products were analyzed by gas

chromatograph with flame ionization detector (FID) and thermal conductivity detector (TCD). The dehydrogenation of ethanol is shown in **Figure 7**.

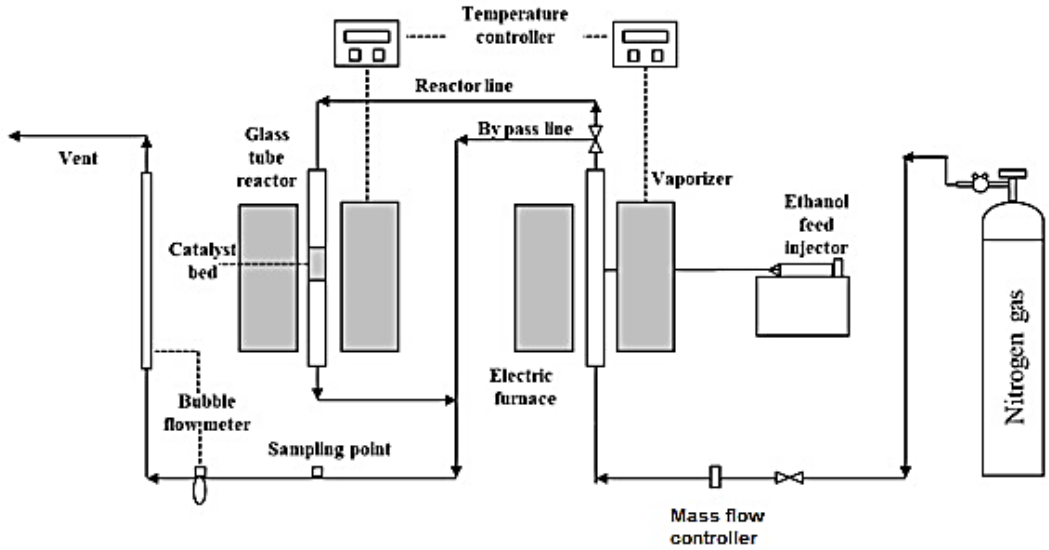

Figure 7 Flow diagram of catalytic dehydrogenation reaction of ethanol.

จุฬาลงกรณ์มหาวิทยาลัย
CHULALONGKORN UNIVERSITY

CHAPTER V
RESULTS AND DISCUSSIONS

This chapter was aimed to investigate the effects of preparation on activated carbons, cobalt loading on activated carbons derived from coffee ground residues and effect of various metals on commercial activated carbons for catalytic dehydrogenation of ethanol to acetaldehyde. This study was divided into three sections. The first section demonstrated the preparation of activated carbon catalysts derived from coffee ground residues with different methods of physical activation and catalytic activity by dehydrogenation of ethanol of all catalysts. In the second part showed the effect of various cobalt metal loading on activated carbons. The result found that 4%wt of cobalt loading, improved to the best of activity of catalyst. For the third part, 10%wt of four metals such as Ce, Co, Cu and Ni load to improving the commercial activated carbons. The results show that Cu metal used to suitable for commercial activated carbon support for ethanol dehydrogenation to acetaldehyde.

5.1 Characteristics of activated carbons prepared by different physical activation and catalytic activity for ethanol dehydrogenation.

5.1.1 Characteristics of synthesized-activated carbons.

Table 5 shows the BET surface areas, pore volume and pore size diameter of activated carbons prepared from $ZnCl_2$ activation observed at different conditions of physical activation. The structural parameters obtained from the N_2 adsorption-desorption are summarized in **Table 5.** Data are tabulated for BET area, total pore volume, micropore volume, average pore width, and the ratio of micropore volume to total pore volume (% microporosity). It is quite evident that the AC-B (chemically activated only) sample exhibited the lowest surface area among other samples. Thus, a subsequent physical activation process was necessary to improve the textural characteristics [8]. Of the two chemically and physically activated samples, AC-C and AC-D exhibited high surface area, but AC-D showed the highest surface area and

micropore volume of all samples. The micropore volume accounts for nearly 100% of the total pore volume of the sample [8].

Table 6 Pore characteristics for activated carbons.

Activated carbons	AC-B	AC-A	AC-C	AC-D
S_{BET} (m^2/g)	797	967	1,045	1,037
V_t (cm^3/g)	0.47	0.59	0.64	0.49
V_{mic} (cm^3/g)	0.36	0.43	0.42	0.49
% V_{mic}	76.7	72.7	65.3	100
D_p (nm)	2.4	2.4	2.4	1.9

S_{BET}, BET surface area; V_t, total pore volume; V_{mic}, micropore volume; $\%V_{mic}$, (V_{mic}/V_t) x 100; Dp, average pore diameter calculated as 4V/A by BET

The most common procedure for determining the structure of porosity and specific surface area of catalysts is the adsorption-desorption of liquid nitrogen at -196°C. **Figure 8** shows the N_2 adsorption-desorption isotherms of the activated carbons derived coffee ground residues prepared by different activation conditions. All catalysts exhibit a combination of Type-I and Type-IV isotherms [82], which usually represent the presence of both microporous initial relative pressure range, displaying that all catalysts present microporous structure. Furthermore, all catalysts also represent similar isotherm with hysteresis loop (between the adsorption and desorption isotherm) at high relative pressure (P/P_o>0.4), indicating the formation of mesoporous structure [83, 84]. Consequently, all catalysts are composed of both microporous and mesoporous structure. Of the two chemically and physically activated samples (AC-C sample) shows the highest nitrogen adsorption capacity, which relates to high pore

volume in **Table 5.** In addition, the activated carbon (AC-D) has a main Type-I isotherm associating with origination of complete micropore structure [85] in **Table 5**.

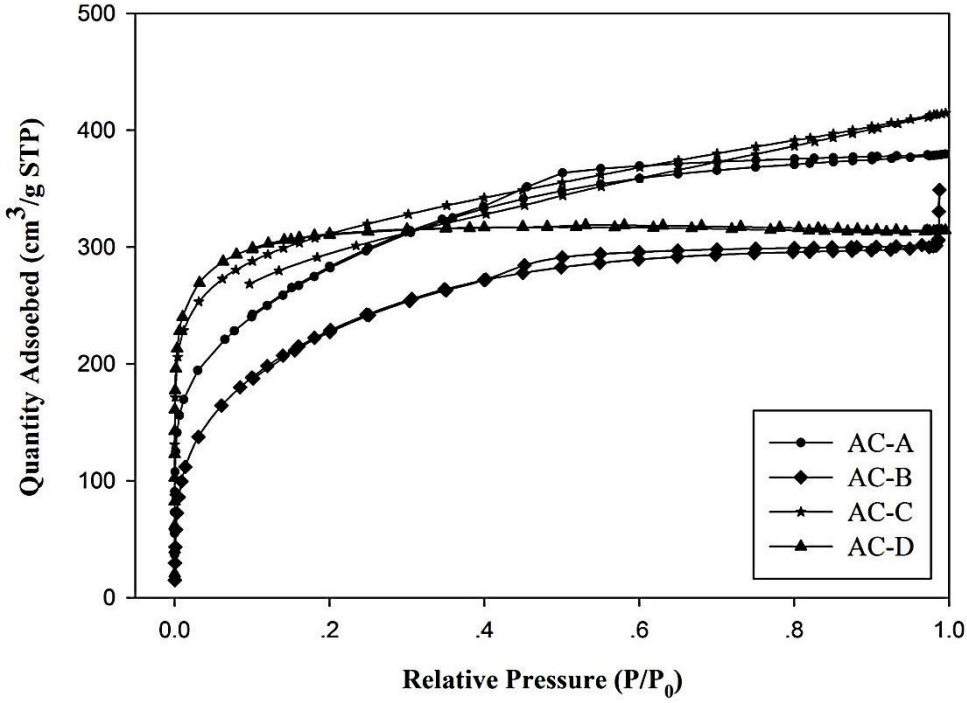

Figure 8 Adsorption-desorption isotherm at -196°C of activated carbons at different activation conditions.

The NH_3-TPD can be used to examine the total acidity of the catalysts as also shown in **Table 6.** The NH_3-TPD profiles are also shown in **Figure 9** indicating that all catalysts mainly contained strong acid. The total acidity of activated carbons, which is in the order from the greatest to the least as following: AC-D > AC-C > AC-B > AC-A > AC-COM. It notices that AC-D sample exhibits the highest total acid density, which is 647 μmol/g. The CO_2-TPD was used to investigate the total basicity of the catalysts. The CO_2-TPD profiles are also shown in **Figure 10** indicating that all catalysts mainly contained strong base. The results as also seen in **Table 6** show that AC-A catalyst has the greatest basicity followed by AC-D, which is shown high value of both acidity and basicity. The order of the total basicity is shown as followed: AC-C > AC-B > AC-COM. The results of catalytic performance of all activated carbon catalysts toward the

จุฬาลงกรณ์มหาวิทยาลัย
CHULALONGKORN UNIVERSITY

dehydrogenation of ethanol under steady-state conditions are presented in **Table 6** and depicted in **Figure 9.**

Table 7 Total acidity and total basicity of activated carbons.

Activated carbons	Total acidity[a] (μmol/g)	Total basicity[b] (μmol/g)
AC-A	450.27	15.01
AC-B	602.15	10.48
AC-C	617.04	11.34
AC-D	646.82	13.70
AC-COM	132.97	7.83

[a] NH_3-TPD, [b] CO_2-TPD, Calculated in temperature. range 40-400°C

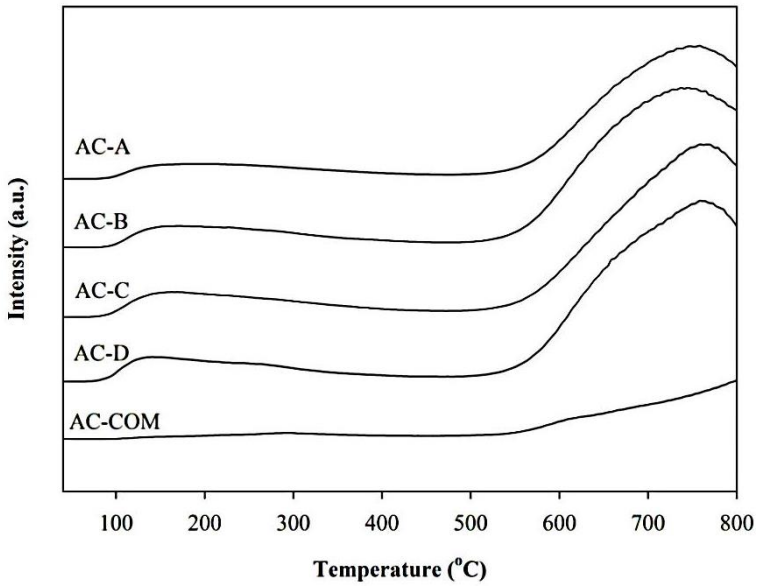

Figure 9. NH_3-TPD profiles of activated carbons..

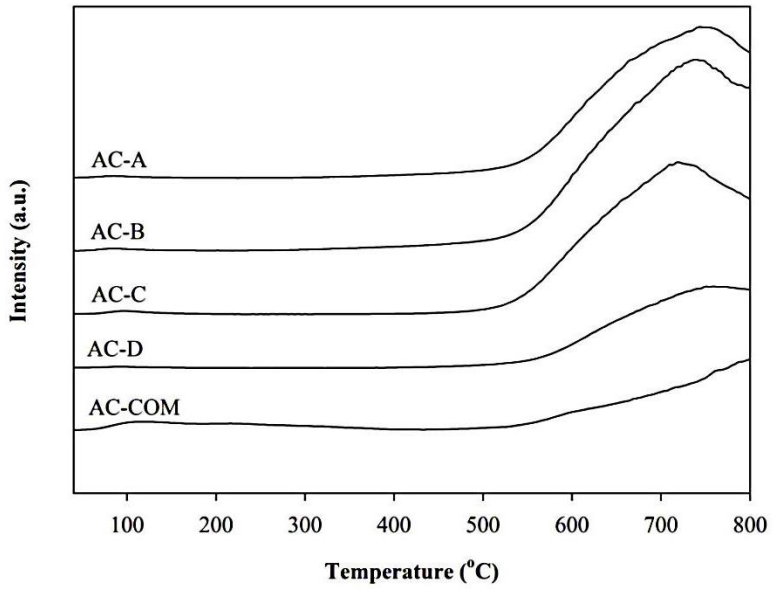

Figure 10 CO_2-TPD profiles of activated carbons.

Figure 11 shows XRD patterns of activated carbon catalysts prepared by various activation methods. In all samples, there are broad diffraction peak around 2θ=22.5°, which can be denoted as amorphous carbon composed of aromatic carbon sheets [32]. In addition, broad diffraction peak around 2θ=45° is defined as graphite structure. The morphologies of activated carbons are shown in **Figure 12.** Considering all activated carbons from chemical activation by $ZnCl_2$, the activation process resulted in a substantial removal of inorganic material that can be seen in the micrographs [6] and all of activated carbons show the same morphology. In addition, it is clearly seen that the peaks located at 2θ = 31-38°, 47°, 56°, 62° and 67-69° were remained. This shows that when larger particles are sieved out, the remaining small particles are the mixture of amorphous and a small amount of graphitize carbon [86].

จุฬาลงกรณ์มหาวิทยาลัย
Chulalongkorn University

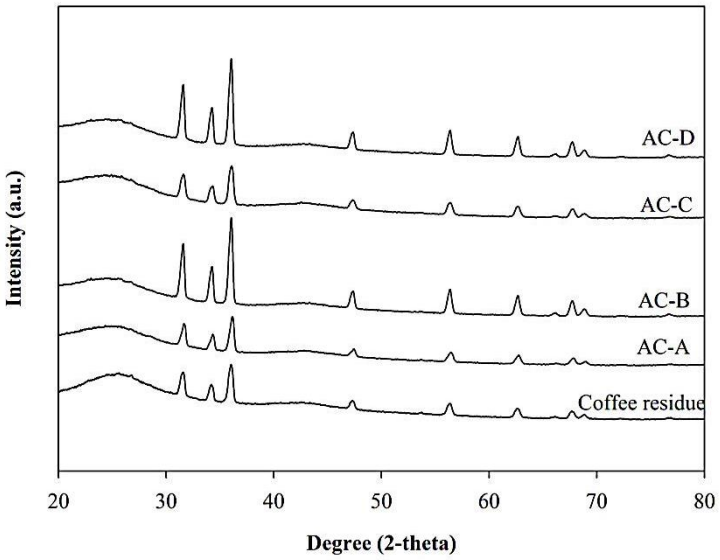

Figure 11 XRD patterns of activated carbons and coffee residue.

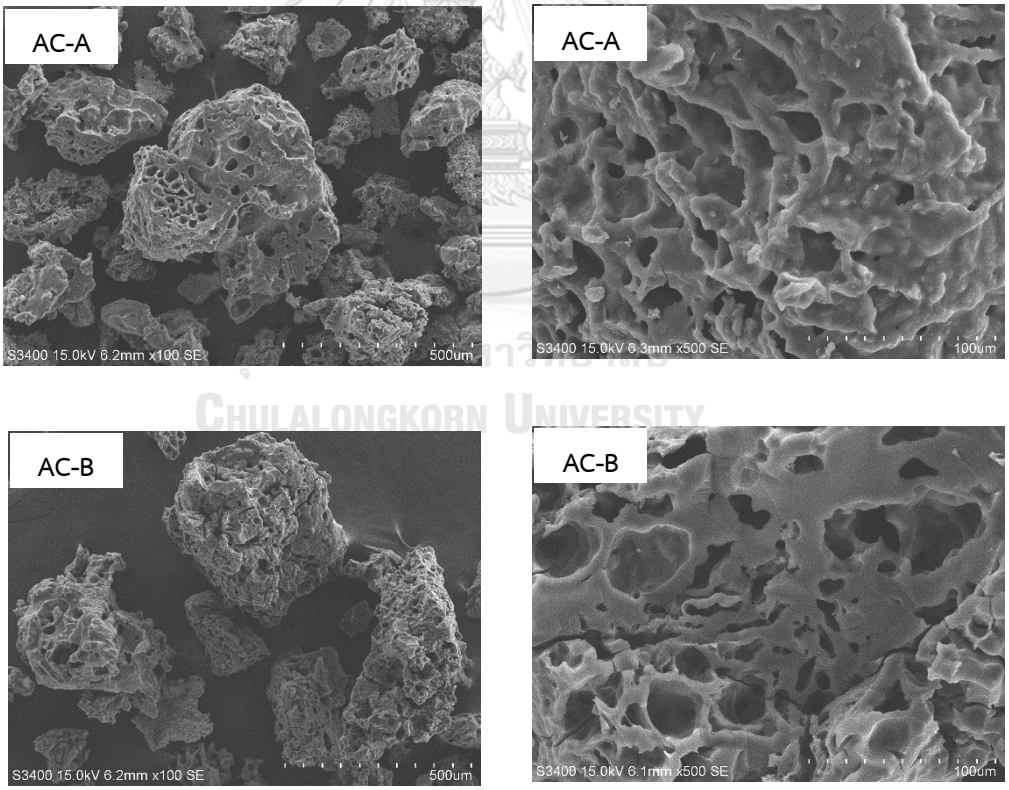

Figure 12 Scanning electron micrographs of activated carbons.

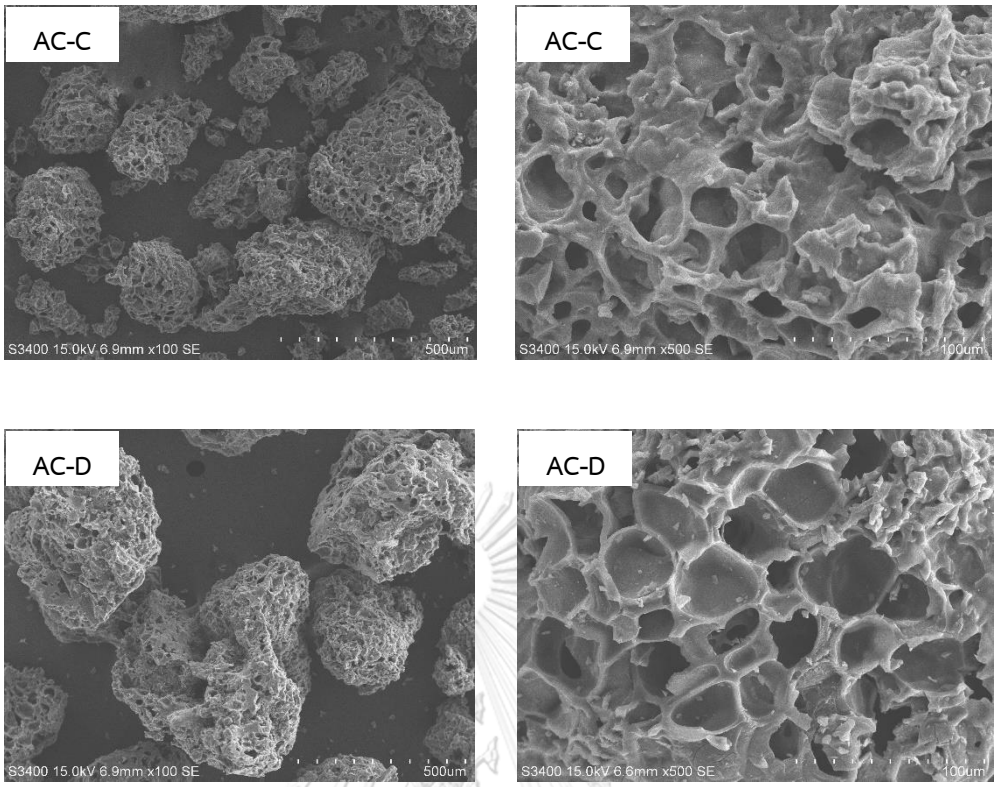

Figure 12 Scanning electron micrographs of activated carbons (continued).

The FT-IR is the common technique to examine the chemical structure of activated carbon as oxygen functional groups. **Figure 13** shows FT-IR spectra of activated carbon derived from coffee found residues with different methods of activations. Details of functional group assignment are illustrated in **Table 7.** All catalysts show band in range of 600-3800 cm^{-1}. The broad band located around 3328 cm^{-1} could be attributed to the O–H stretching vibration of hydroxyl group as alcohols and phenol or/and hydrogen bonded-OH group as water molecule. The band at 2970 cm^{-1} is related to C–H interaction with carbon surface. The sharp bands located at 2361 cm^{-1} are attributed to the C≡C stretching vibration of alkyne group. There is the shape band at 1742 cm^{-1}, which can be denoted as stretching C=O of carbonyl groups. Previously, Shafeeyan et al. [87] claimed that the IR band around 1720-1750 cm^{-1} is ascribed to the C=O stretching of carboxylic acids. The region around 1364 and 1212 cm^{-1} may relate to C–O stretching vibration from ethers [88]. In fact, carboxyl,

จุฬาลงกรณ์มหาวิทยาลัย
Chulalongkorn University

anhydride and lactone are acidic, while phenol, carbonyl, quinine and ether are neutral or weak acid. Consequently, the presence of oxygen surface functional group may be associated with the total acidity. It appears that the result from IR spectra is consistent with the total acid density obtained using NH_3-TPD method [88].

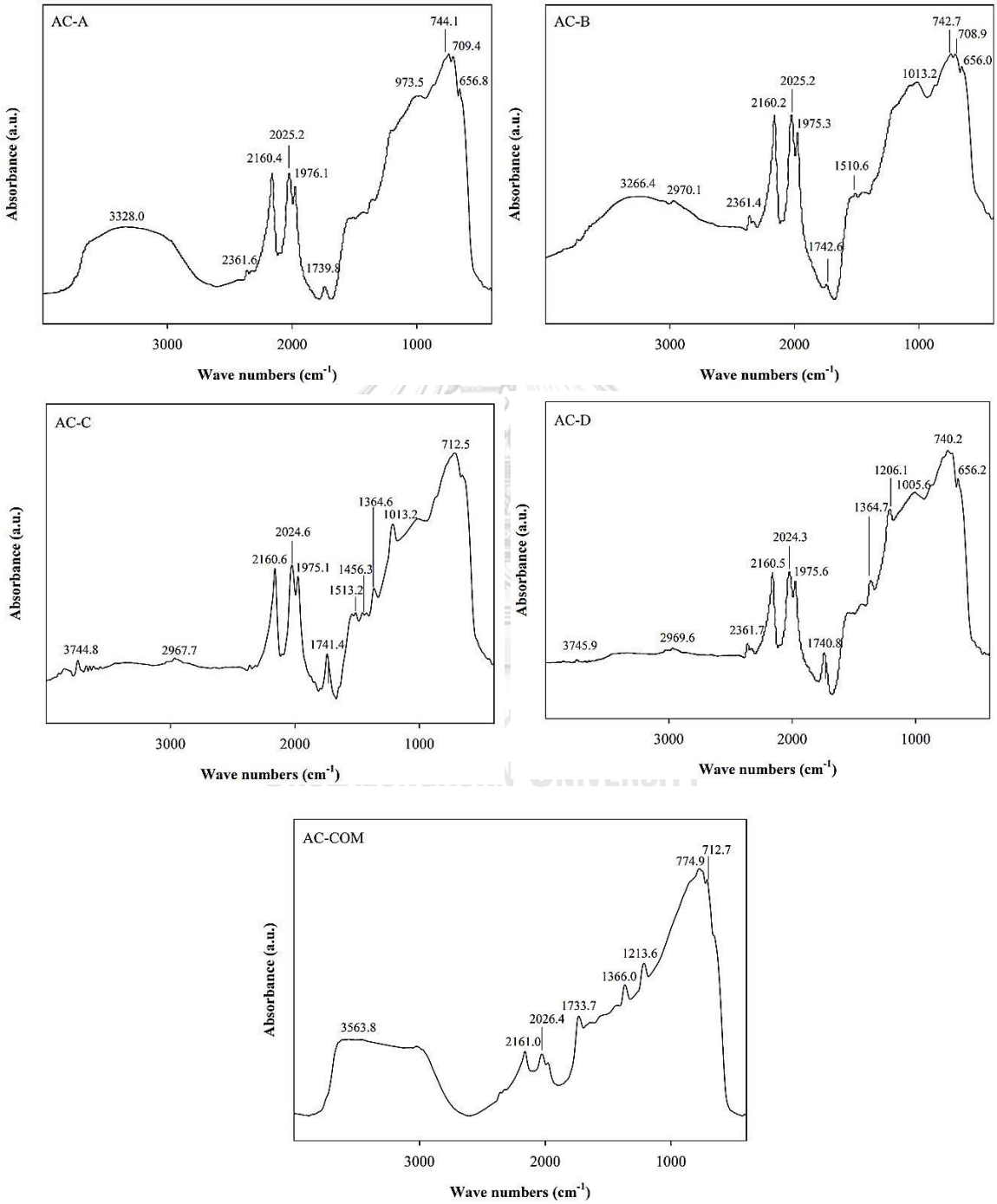

Figure 13 FTIR spectra of activated carbons.

Table 8 Functional group of activated carbons [87, 89-91].

Catalysts	Assignment	Remark	Wave number (cm^{-1})
AC-A	O-H stretching	Hydroxyl group as alcohol/phenol	3328
	C ≡ C	Alkyne groups	2361
	C ≡ C	Alkyne groups	2160
	C=C asymmetric stretch	Alkene groups	2025
	C=C asymmetric stretch	Alkene groups	1976
	C=O stretching	Carboxylic acids	1740
	C-O	Esters, ether or phenol groups	973
	C-H	Benzene derivaties	744
	C-Cl	Alkyl Halide	709
	O-H	Hydroxyl group	657
AC-B	O-H stretching	Ethers	3266
	C-H stretching	With carbon surface	2970
	C ≡ C	Alkyne groups	2361
	C ≡ C	Alkyne groups	2160
	C=C asymmetric stretch	Alkene groups	2025
	C=C asymmetric stretch	Alkene groups	1975
	C=O stretching	Carboxylic acids	1743
	C=C	Aromatics group	1511
	C-O	Esters, ether or phenol groups	1013
	C-H	Benzene derivaties	743

จุฬาลงกรณ์มหาวิทยาลัย
CHULALONGKORN UNIVERSITY

Table 7 Functional group of activated carbons [87, 89-91] (continued).

Catalysts	Assignment	Remark	Wave number (cm^{-1})
AC-B	C-Cl	Alkyl Halide	709
	O-H	Hydroxyl group	656
AC-C	O-H stretching	Hydroxyl group as alcohol	3745
	C-H stretching	With carbon surface	2968
	C ≡ C	Alkyne groups	2161
	C=C asymmetric stretch	Alkene groups	2025
	C=C asymmetric stretch	Alkene groups	1975
	C=O stretching	Carboxylic acids	1741
	C=C	Aromatics group	1513
	C-H	Alkanes, alkyl groups	1456
	C-O	Carboxylate group	1365
	C-O	Esters, ether or phenol groups	1013
	C-Cl	Alkyl Halide	712
AC-D	O-H stretching	Hydroxyl group as alcohol	3746
	C-H stretching	With carbon surface	2970
	C ≡ C	Alkyne groups	2362
	C ≡ C	Alkyne groups	2160
	C=C asymmetric stretch	Alkene groups	2024,1976
	C=C	Carbonyl group	1741
	C-O	Carboxylate group	1365

จุฬาลงกรณ์มหาวิทยาลัย
Chulalongkorn University

Table 7 Functional group of activated carbons [87, 89-91] (continued).

Catalysts	Assignment	Remark	Wave number (cm^{-1})
AC-D	C-O	Esters, ether or phenol groups	1206
	C-O	Esters, ether or phenol groups	1006
	C-H	Benzene derivaties	740
	O-H	Hydroxyl group	656
AC-COM	O-H stretching	Ethers	3564
	C ≡ C	Alkyne groups	2161
	C=C asymmetric stretch	Alkene groups	2026
	C=O stretching	Carboxylic acids	1734
	C-O	Carboxylate group	1366
	C-O	Esters, ether or phenol groups	1214
	C-H	Benzene derivaties	775
	C-Cl	Alkyl Halide	713

The results of thermogravimetric analysis of activated carbons are presented in **Figure 14.** The mass loss during the thermogravimetric analysis can be divided into stages [8] The initial mass loss for temperature up to 200°C can be attributed to moisture elimination. The second stage is found at 200–300 °C range indicating the volatilization of organic materials. The third stage was found in the 300–600 °C range that may be attributed to further thermal decomposition of organic materials. Above 600°C, the mass loss is likely attributed to the reaction between the activating agent

and carbonaceous residue. These results are also in agreement with other researchers [6].

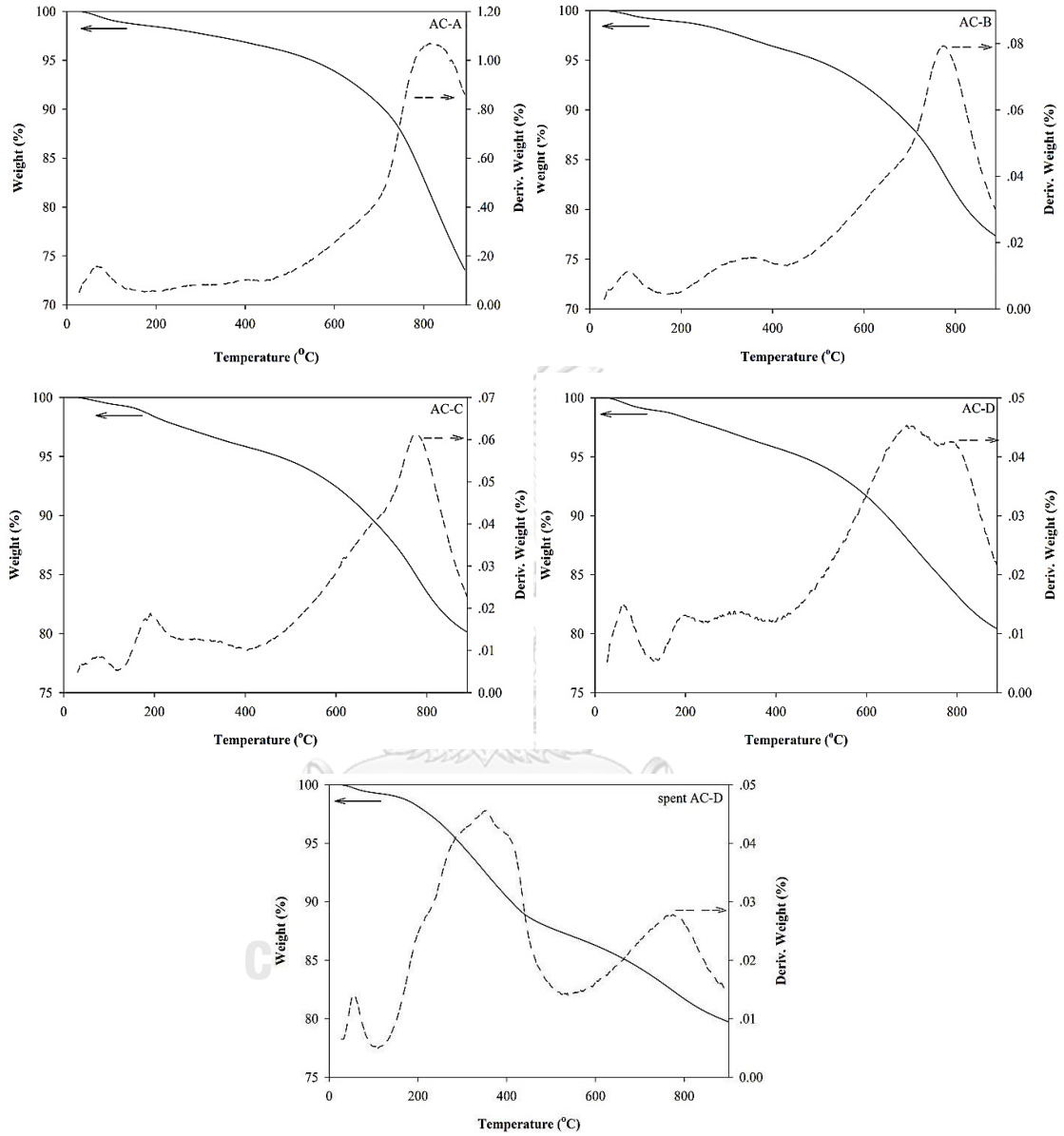

Figure 14 Thermal analysis of fresh activated carbons and spent AC-D catalyst.

5.1.2 Dehydrogenation of ethanol of synthesized-activated carbons

Considering the reaction study, **Figure 15** represents the steady state conversion of ethanol for each temperature on the activated carbon catalysts derived from coffee ground residues with different activation methods. In addition, ethanol conversion and acetaldehyde yield for all catalysts are shown in **Table 8**. As expected, ethanol

conversion increases with increasing the reaction temperature because of its endothermic reaction. According to the literature, ethanol decomposition leads to ethylene and diethyl ether by dehydration process and acetaldehyde by dehydrogenation process. The reaction of dehydrogenation takes place in a simultaneous presence of Lewis base and acid center, while that of dehydration involves only acid center [32]. In order to better understand the dehydrogenation process, the mechanism of ethanol to acetaldehyde by Lewis acid and Lewis base sites on activated carbon catalyst is illustrated in **Figure 16.**

Results of the catalytic reaction test in this study ensured that all activated carbons acted as catalysts of ethanol dehydrogenation, but in different activity. For all temperature (250-400°C), it is obviously seen that the AC-D catalyst shows the highest activity among other catalysts. Especially at temperature of 400°C, the AC-D catalyst shows ethanol conversion about 48%, while other catalysts (AC-A, AC-B and AC-C) display lower ethanol conversion about 26-32%, whereas AC-COM catalyst shows the lowest ethanol conversion only 4%. According to total acidity and total basicity results, it reveals that the AC-D catalyst has the highest total acidity (648 μmol/g) and high basicity (14 μmol/g). Therefore, this confirms that dehydrogenation of ethanol is dependent on both of acidity and basicity. The result agrees with the previous wok of Carrasco-Marin F. et al., [33], who reported that ethanol conversion increased with rise in the total surface acidity and basicity of unoxidised carbon and carbon prepared by oxidizing treatment with $(NH_4)_2S_2O_8$. It should be noted that all synthesized activated carbon catalysts exhibit the selectivity of acetaldehyde more than 96% without significant side reactions. It is also evident from Jasinska et al., [32], who claimed that chlorinated carbon catalysts showed greater domination of the process of dehydrogenation over dehydration than the oxidised carbon samples. In addition, Perez-Cadenas et al., [92] claimed that chlorination leads to increased acidity of Lewis acid centres on the activated carbon, but on the other hand, it reduces acidity of the

จุฬาลงกรณ์มหาวิทยาลัย
CHULALONGKORN UNIVERSITY

Bronsted centres. The comparison of catalytic performance of catalysts in this work and other catalysts is summarized in **Table 9**, which shows that this catalyst is quite promising among other previous catalysts.

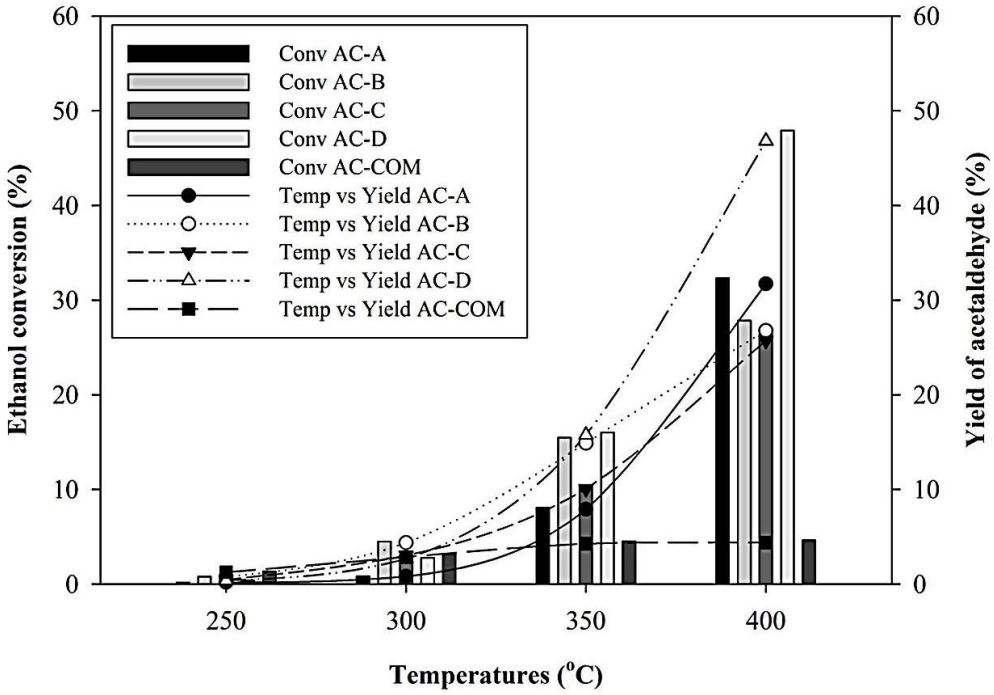

Figure 15 Ethanol conversion and acetaldehyde yield of activated carbon catalysts for ethanol dehydrogenation.

จุฬาลงกรณ์มหาวิทยาลัย
CHULALONGKORN UNIVERSITY

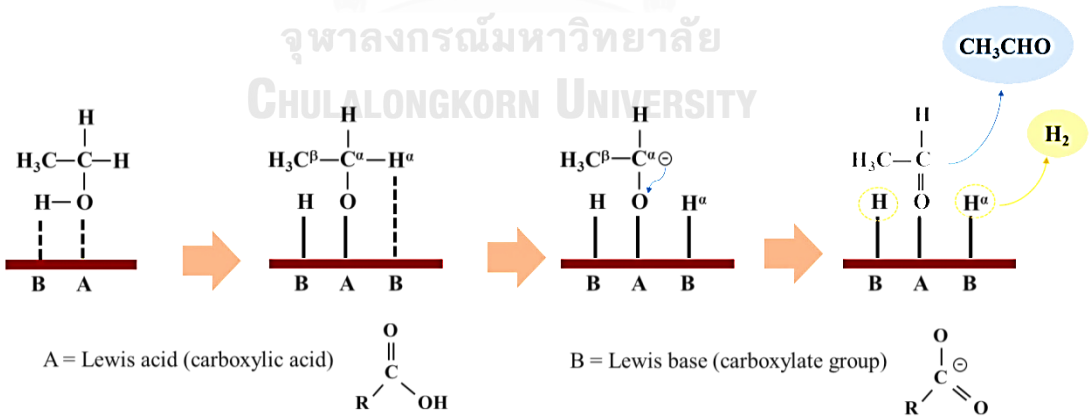

Figure 16 Mechanism of ethanol to acetaldehyde by Lewis acid and Lewis base sites on activated carbon catalyst.

Table 9. Ethanol conversion and acetaldehyde yield for all catalysts.

Samples	Temperatures (°C)	C_2H_5OH conversion (%)	CH_3CHO yield (%)
AC-A	250	0.2	0.2
	300	0.8	0.8
	350	8.1	7.9
	400	32.3	31.7
AC-B	250	0.8	0.8
	300	4.5	4.4
	350	15.5	14.9
	400	27.8	26.8
AC-C	250	0.5	0.5
	300	3.8	3.0
	350	10.4	10.1
	400	26.4	25.7
AC-D	250	0.4	0.4
	300	2.8	2.7
	350	16.0	15.8
	400	47.9	46.8
AC-COM	250	1.3	1.2
	300	3.2	2.9
	350	4.5	4.3
	400	4.6	4.4

Finally, the stability test of the best catalyst (AC-D) under time on stream of 10 h was also performed at the reaction temperature of 400°C. The stability result is shown in **Figure 17**. The ethanol conversion is fairly constant within 8 h of reaction. After 8 h, the ethanol conversion gradually decreased because of perhaps coke formation or pore blockage of the spent catalyst. The morphology of spent AC-D

จุฬาลงกรณ์มหาวิทยาลัย
Chulalongkorn University

catalyst after reaction is shown in **Figure 18.** Some pores of this catalyst were lacerated because of the thermal destruction by long time reaction. In addition, thermal analysis of the spent catalyst was performed as seen in **Figure 14**. The weight loss in other temperature ranges possibly came from desorption of other carbon compounds such as coke deposition and the adsorbed products, which was corresponding to the result of stability test as mentioned above. Moreover, the remained Cl on surface of spent catalyst (0.065 wt%) apparently decreased from fresh catalyst (3.66 wt%) due to the decomposition of HCl from the reaction between $ZnCl_2$ with H_2O [93] relating to TGA result in the decomposition temperature between 200 to 400°C.

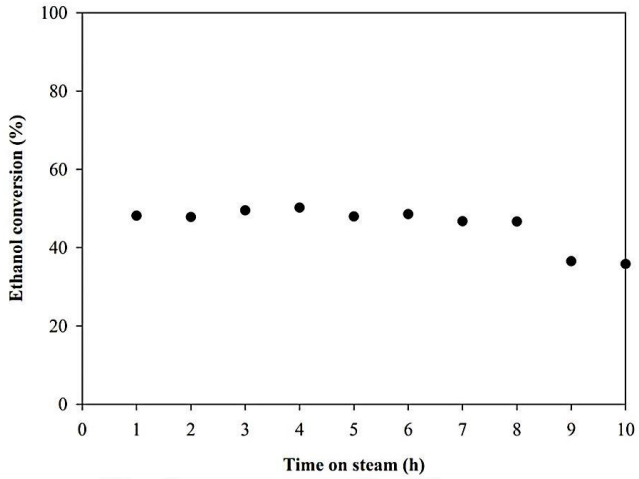

Figure 17 Stability test for AC-D catalyst at reaction temperature of 400°C.

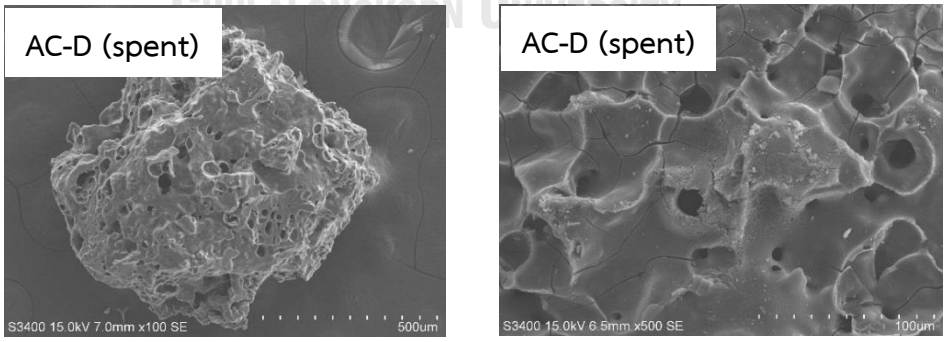

Figure 18 Scanning electron micrographs of spent AC-D catalyst after ethanol dehydrogenation.

Table 10 Comparison of carbon catalysts for ethanol dehydrogenation and their catalytic ability.

Catalysts	Source	Surface area (m^2/g)	Reaction temp(°C)	Ethanol conversion (%)	CH_3CHO yield (%)	Refs
AC-D	Coffee residue	1,037	400	47.9	46.8	This work
K/Cl_2/4h/723K	Polish brown coal	2,374	477	-	75	[32]
AZ46-24	Olive stones	810	180	16.0	3.2	[33]
MoO_3/CMS	Carbon molecular sieve	-	230	100	85	[70]
C-Ni	Polymeric carbon	-	260	-	1	[34]
CNT-AO	Carbon nanomat'l	193	300	58.8	57.0	[87]
50Al/BC-TD	Bacterial cellulose	10.50	400	66.4	8.4	[94]

จุฬาลงกรณ์มหาวิทยาลัย
Chulalongkorn University

5.2 Characteristics and catalytic activity of cobalt metal supported on synthesized activated carbon for ethanol dehydrogenation.

This part describes the characteristic and behavior of cobalt catalyst which supported on activated carbon (AC-D from part 5.1) with various percentage of cobalt loading (4 and 6%wt).

5.2.1 Catalyst Characterization

Table 11 Surface areas and pore characteristics for Co/C catalysts.

Catalysts	C	4%Co/C	6%Co/C
S_{BET} (m^2/g)	1,037	727	683
V_t (cm^3/g)	0.49	0.36	0.35
V_{mic} (cm^3/g)	0.49	0.35	0.33
% V_{mic}	100	98.83	92.70
D_p (nm)	1.87	1.96	2.07

S_{BET}, BET surface area; V_t, total pore volume; V_{mic}, micropore volume; %V_{mic}, (V_{mic}/V_t) x 100; Dp, average pore diameter calculated as 4V/A by BET

จุฬาลงกรณ์มหาวิทยาลัย
CHULALONGKORN UNIVERSITY

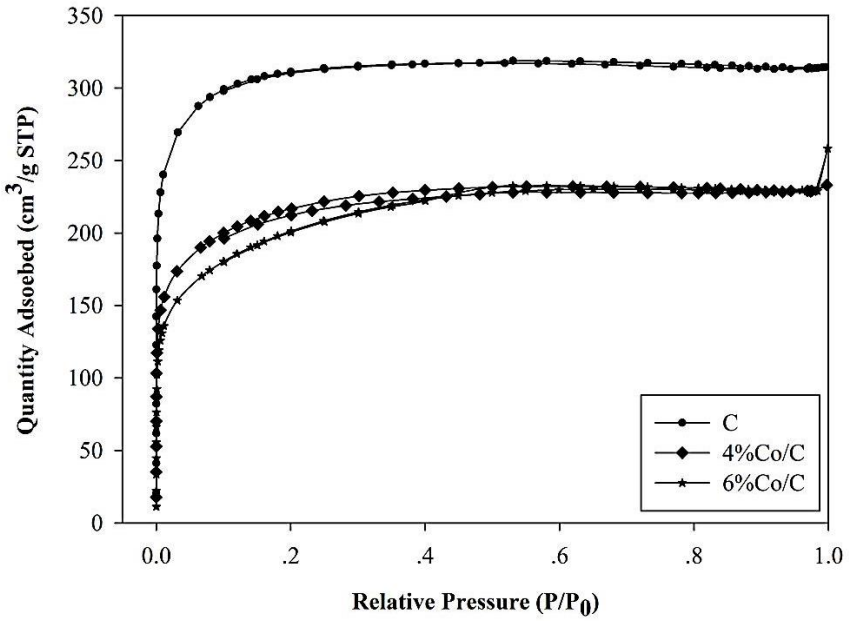

Figure 19 Adsorption-desorption isotherm at -196°C of activated carbon-supported Co catalysts.

Table 10 shows the BET surface areas, pore volume and pore size diameter of Co/C catalysts. Other structural parameters obtained from the N_2 adsorption-desorption are also summarized in **Table 10**. Data are tabulated for BET surface area, total pore volume, micropore volume, average pore width, and the ratio of micropore volume to total pore volume (% microporosity). The C catalyst exhibited the highest BET surface area and total pore volume. When the amount of cobalt metal loading increased, the BET surface area and the total pore volume of catalysts apparently decreased. This indicated that the pore blockage by cobalt clusters evidently occurred.

The characteristics of adsorption-desorption isotherms are effectively used to identify the type of pores characteristics of catalyst samples. The N_2 adsorption-desorption isotherms of all catalysts are shown in **Figure 19.** The isotherms of the activated carbons exhibit a combination of types I (major) and IV (minor) according to the IUPAC [82]. A combination of types I and IV isotherms are usually indicated the presence of both microporous and mesoporous structure. The isotherms display a sharply increase in N_2 adsorption in the initial relative pressure range indicating the

formation of micropores. In addition, the isotherms also appear to contain hysteresis loop at high relative pressure suggesting that the pore structure is partly mesopores. So, the activated carbons with different cobalt loadings have both microporous and mesoporous structures. The adsorption capacity is at a maximum of the C catalyst showing that the pore volume has the maximum amount at this sample. While the C catalyst has 100% of micropore volume and smallest pore size.

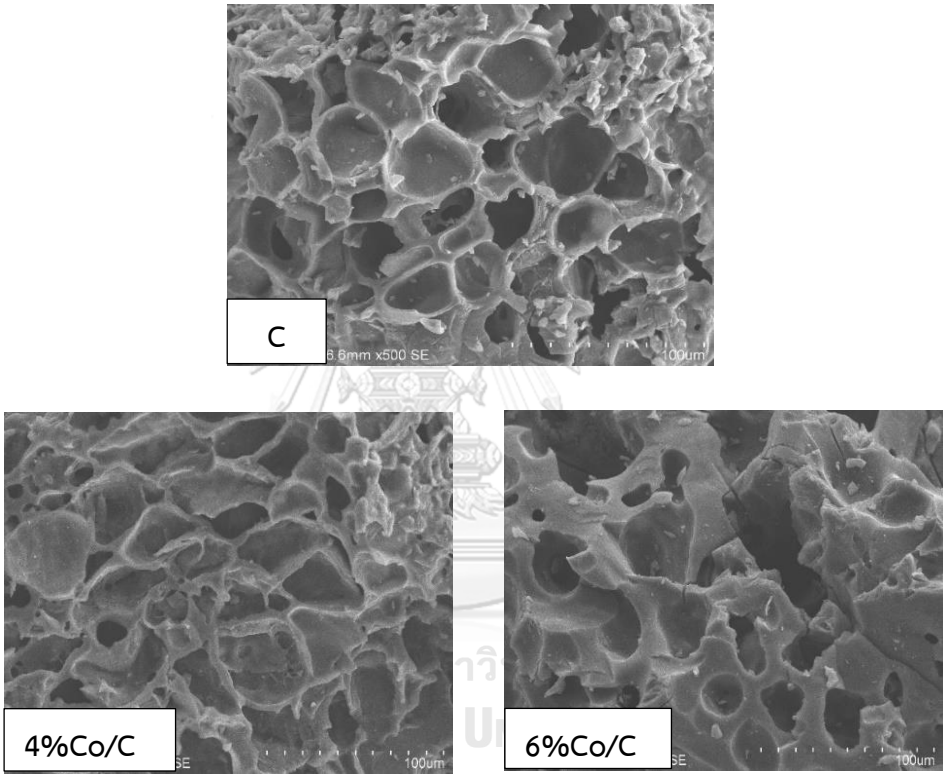

Figure 20 SEM images of activated carbon-supported Co catalysts.

Scanning electron microscopy (SEM) was conducted in order to study the morphologies of the samples. From **Figure 20**, it was found that all catalysts exhibited high porosity. The C and 4%Co/C catalysts have a uniformly porous structure. With 6% of Co impregnated, the agglomeration occured due to cobalt blocked of carbon substrate.

Table 12 Metal content of the carbon-supported Co catalysts.

Activated carbons	% wt Co[*a]	% wt Co[*b]
4% Co/C	4.2	17.06
6% Co/C	6.2	31.38

[*a] by ICP, [*b] by EDX

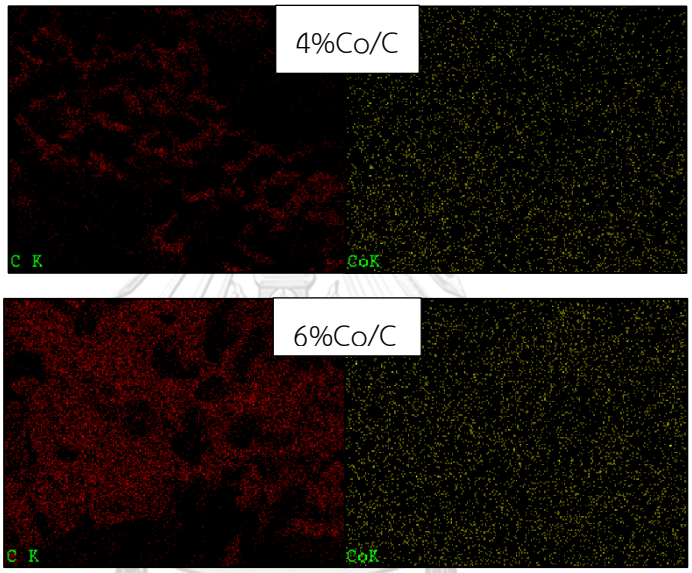

Figure 21 EDX of activated carbon-supported Co catalysts.

จุฬาลงกรณ์มหาวิทยาลัย
CHULALONGKORN UNIVERSITY

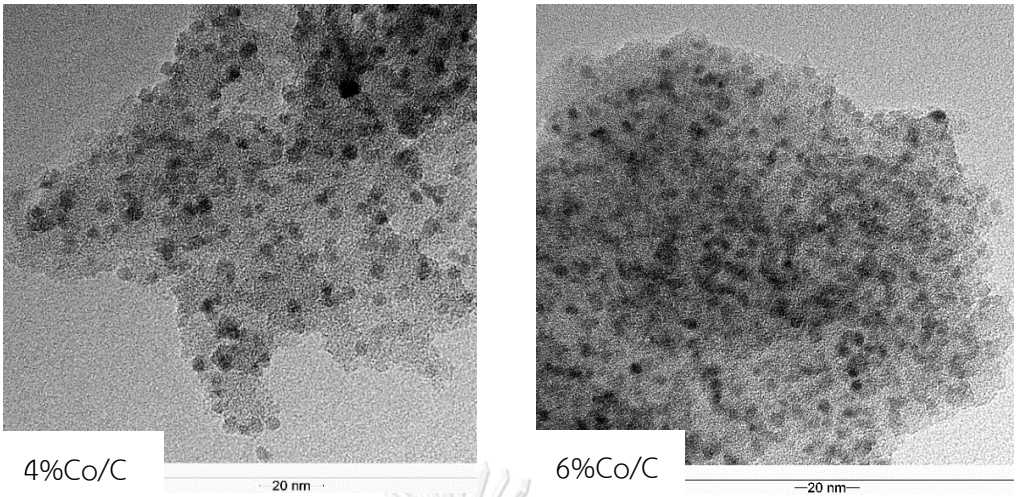

Figure 22 TEM images of activated carbon-supported Co catalysts.

The results of Co content for the catalyst samples are illustrated in **Table 11**. Results found that Co content on surface of catalysts was higher than that in bulk of catalysts. This was probably due to particle size of Co metal is larger than the pore size of catalysts. Energy dispersive X-ray spectroscopy (EDX) was performed in order to study cobalt distribution (as displayed in **Figure 21**). On the right hand side, the yellow dots represent the distribution of cobalt metal. In addition, TEM micrographs of activated carbon-supported Co catalysts are shown in **Figure 22**. For cobalt catalysts, the dark patches represent the cobalt species dispersing on all catalysts. It revealed that with larger amount of Co loading, the Co species started to agglomerate (6%Co/C). Both techniques showed that cobalt species of 6%Co/C were located mostly on the external surface as seen by EDX with some agglomeration.

Table 13 Total acidity and total basicity of carbon-supported Co catalysts.

Activated carbons	Total acidity (μmol/g)	Total basicity (μmol/g)	Acidity/basicity
C	577.43	383.74	1.50
4%Co/C	244.26	161.33	1.51
6%Co/C	213.76	155.03	1.38

*a NH_3-TPD, *b CO_2-TPD, Calculated in temperature. range 40-500°C

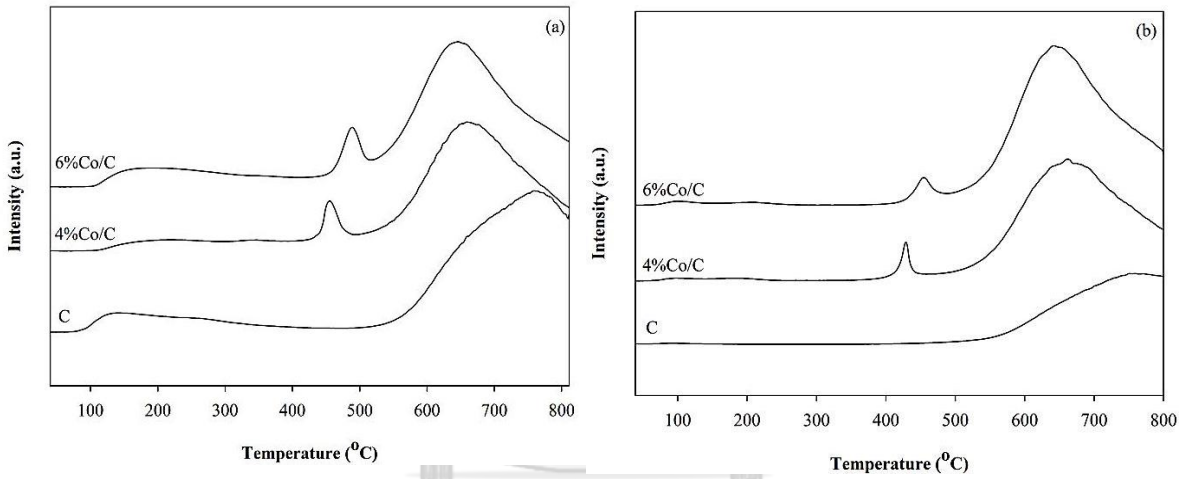

Figure 23 (a) NH_3-TPD profiles and (b) CO_2-TPD profiles.

The NH_3-TPD and the CO_2-TPD can be used to investigate the total acidity and basicity of the catalysts, respectively as also shown in **Table 12**. The NH_3-TPD and CO_2-TPD profiles are also displayed in **Figure 23** (a) and **Figure 23** (b), respectively. It notices that C and 4%Co/C samples show similar total acidity to the total basicity value (ca. 1.50), whereas the 6%Co/C catalyst had lower total acidity to the total basicity value of 1.38.

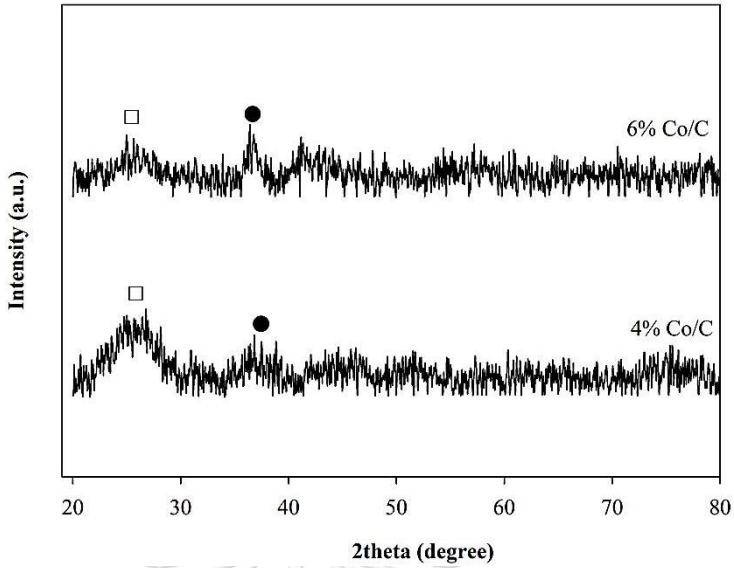

Figure 24 X-ray diffraction patterns of cobalt catalysts. Legend: (□) graphite; (●) Co_3O_4

XRD patterns of the activated carbon-supported Co catalysts are shown in **Figure 24**. There are broad diffraction peak around 2θ=22.5, which can be assigned to the amorphous carbon composed of aromatic carbon sheets [85]. The XRD peak of Co_3O_4 was slightly observed at 36.8°, while the CoO peak at 42.5° was not evidently detected [75]. So, it appears that the 4%Co/C has Co oxide species (Co_3O_4 and CoO) in highly dispersed form.

จุฬาลงกรณ์มหาวิทยาลัย
Chulalongkorn University

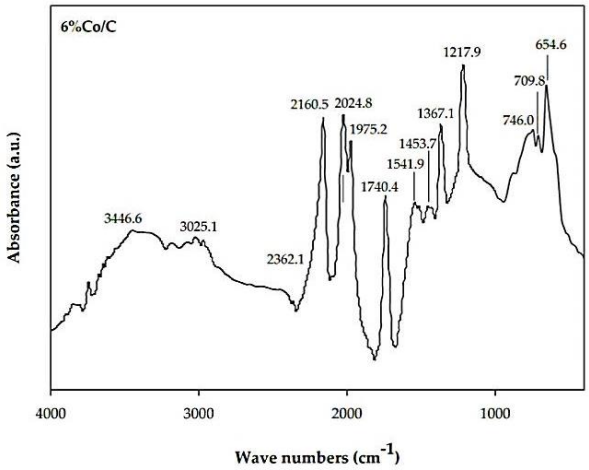

Figure 25 A typical FTIR spectrum of Co/C catalyst.

Table 14 Functional group of activated carbons [87-90].

Catalysts	Assignment	Remark	Wave number (cm^{-1})
All catalysts	C ≡ C	Alkyne groups	2362, 2160
	C=C asymmetric stretch	Alkene groups	2024
	C=C asymmetric stretch	Alkene groups	1975
	C=O stretching	Carboxylic acids	1741
	C-Cl	Alkyl Halide	717
	O-H	Hydroxyl group	654
C	O-H stretching	Hydroxyl group as alcohol	3746
	C-H stretching	Quinones	2970
	C-O or C-OH	Ethers or phenolic groups	1365
	C-O or C-OH	Ethers or phenolic groups	1206
	C-O or C-OH	Ethers or phenolic groups	1006
	C-H	Benzene derivaties	740
4%Co/C	-	Cyclic amides or pyridine-like groups	1510
	C-O or C-OH	Ethers or phenolic groups	1013
6%Co/C	O-H stretching	Hydroxyl group as alcohol	3447
	C-H stretching	Carboxylic acids	3025
	-	Cyclic amides or pyridine-like groups	1542
	-	Nitro groups	1454
	C-O or C-OH	Ethers or phenolic groups	1367
	C-O or C-OH	Ethers or phenolic groups	1218
	γ (C–H) vibration	Benzene derivaties	746

FT-IR spectroscopy is a common technique used to analyze the functional groups in the catalyst samples. **Table 13** and **Figure 25** display FT-IR results of

จุฬาลงกรณ์มหาวิทยาลัย
Chulalongkorn University

catalysts. All catalysts show the visible band in range of 600-3800 cm^{-1}. All catalysts have alkyne, alkene carboxylic and alkyl halide groups which associated with the acid of catalysts. In fact, carboxylic is strong acidic, while phenol, quinone and ether are weak acid [88]. Moreover, alkyl halide is a Lewis acid. In contrast, cyclic amides, pyridine-like groups and nitro groups are basic groups [88]. It appears that the result from FT-IR is consistent with the total acidity and the total basicity obtained using NH_3-TPD and CO_2-TPD.

Thermogravimetric results of all catalysts are presented in **Figure 26**. For both Co/C catalysts, the mass loss during the thermogravimetric analysis can be separated into 3 stages [6]. The initial mass loss for temperature up to 250°C can be attributed to moisture elimination. The second stage is found at 250–400 °C range indicating the decomposition of organic materials that has a great mass loss (~70%). These results are also in agreement with other researchers [6]. While the mass of C catalyst was gradually decreased throughout the range of temperature that has a little mass loss about 20%

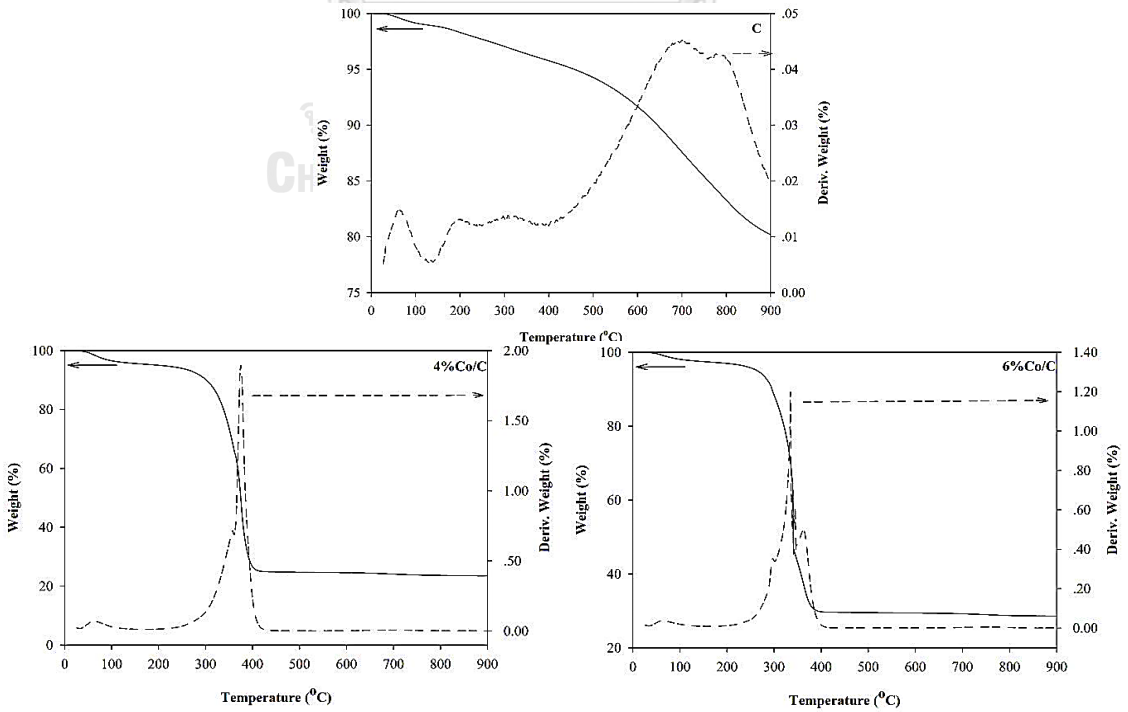

Figure 26 Thermal analysis of all catalysts.

5.2.2 Catalyst Testing

Figure 27 shows the steady-state conversion of ethanol for each temperature on activated carbon and activated carbon-supported Co catalysts. In addition, ethanol conversion and acetaldehyde yield for all catalysts are shown in **Table 14**. As expected, ethanol conversion increases with increasing in reaction temperature because of its endothermic reaction. According to the literature, ethanol decomposition leads to ethylene and diethyl ether by dehydration process and acetaldehyde by dehydrogenation process. The reaction of dehydrogenation takes place in a simultaneous presence of Lewis base and acid sites, while that of dehydration involves only acid sites [32]. Results of the catalytic reaction test in this study ensured that all activated carbons acted as catalysts of ethanol dehydrogenation, but in different activity. For temperature 250-350°C, it is obviously seen that all carbon catalysts show the similar activity. At temperature of 400°C, the C and 4%Co/C catalysts display high ethanol conversion about 48% and 54%, respectively. For the impregnated 6% of Co, the ethanol conversion decreased rapidly about 18%. This may be caused by agglomeration and pore blockage. Based on the reaction test, it was found that all activated carbons exhibited the very high selectivity of acetaldehyde more than 90% during ethanol dehydrogenation. Carrasco-Marin et al., [33] reported that all synthesized activated carbon catalysts exhibit the selectivity of acetaldehyde more than 96% without significant side reactions. It is also evident from Jasinska et al., [32], who claimed that chlorinated carbon catalysts showed greater domination of the process of dehydrogenation over dehydration than the oxidized carbon samples. In addition, Perez-Cadenas et al., [92] claimed that chlorination leads to increased acidity of Lewis acid sites on the activated carbon, but on the other hand, it reduces acidity of the Bronsted sites. Furthermore, our results show that the C and the 4%Co/C have the high total acidity to total basicity. So, it can be active for dehydrogenation of ethanol.

จุฬาลงกรณ์มหาวิทยาลัย
CHULALONGKORN UNIVERSITY

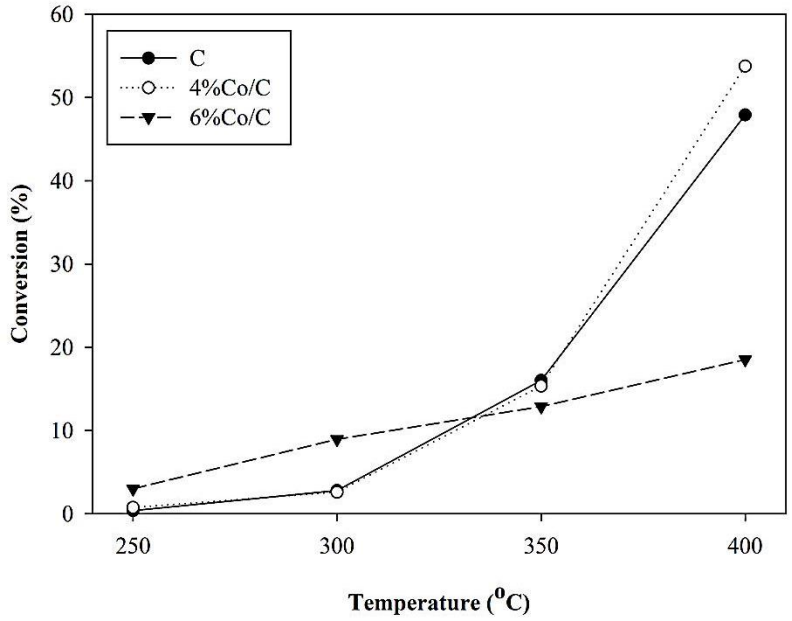

Figure 27 Ethanol conversion of activated carbon-supported Co catalysts.

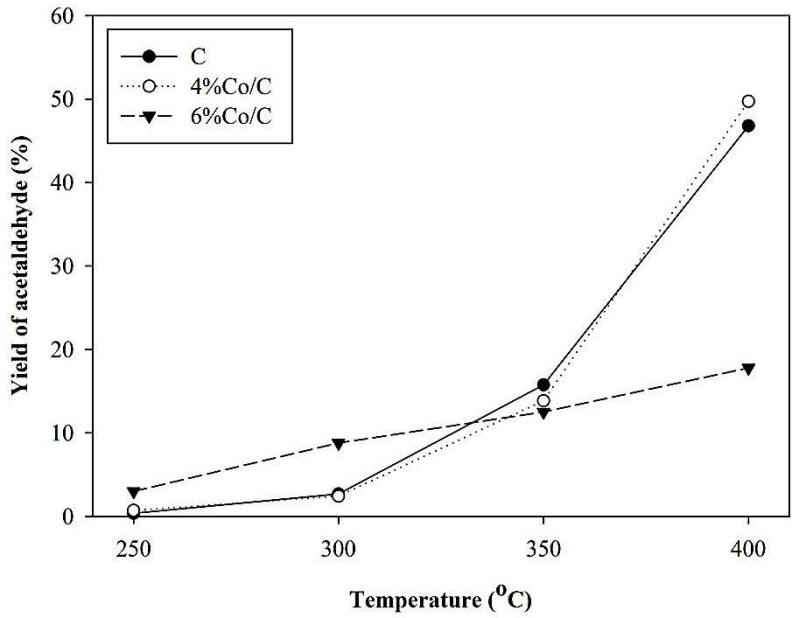

Figure 28 Acetaldehyde yield of activated carbon-supported Co catalysts.

Table 15 Ethanol conversion and acetaldehyde yield for activated carbon-supported Co catalysts.

Samples	Temperatures (°C)	C_2H_5OH conversion (%)	CH_3CHO yield (%)
C	250	0.37	0.36
	300	2.78	2.69
	350	16.02	15.75
	400	47.92	46.80
4%Co/C	250	0.74	0.71
	300	2.59	2.42
	350	15.34	13.84
	400	53.78	49.73
6%Co/C	250	2.99	2.99
	300	8.93	8.78
	350	12.87	12.50
	400	18.51	17.78

The comparison of catalytic performance of activated carbon-supported Co catalysts in this work and Co-promoter on Cu/carbon commercial catalyst was considered [75]. It revealed that the best catalyst in this work had surface area of 727 m^2/g and gained 54% of ethanol conversion with acetaldehyde yield of 50% at 400°C in ethanol dehydrogenation reaction, whereas the bimetallic Co-Cu on carbon catalyst showed surface area 986 m^2/g having ethanol conversion about 77% with 70% yield of acetaldehyde at the same temperature in oxidative ethanol dehydrogenation reaction. Although the catalyst in this work exhibits lower ethanol conversion and acetaldehyde yield, it is still competitive since the dehydrogenation undergoes without the introduction of oxygen.

จุฬาลงกรณ์มหาวิทยาลัย
Chulalongkorn University

5.3 Characteristics and catalytic activity of various metal supported on commercial activated carbon for ethanol dehydrogenation.

5.3.1 Catalysts Characterization

Table 15 shows the structural parameters obtained from the N_2 adsorption-desorption such as BET surface area (S_{BET}), micropore surface area ($S_{micropore}$), external surface area ($S_{external}$), total pore volume, micropore volume and average pore width. The original activated carbon exhibited the highest BET surface area and total pore volume. At 10% loading by various metals, the BET surface area and the total pore volume of catalysts decreased, which is attributed to the pore blockage by metal clusters [95].

Table 16 Surface areas and pore characteristics for activated carbon catalysts.

Catalysts	ACC	Ce/ACC	Co/ACC	Cu/ACC	Ni/ACC
S_{BET} (m^2/g)	852	837	744	823	699
$S_{micropore}$(m^2/g)	310.4	805.5	723.0	779.1	626.8
$S_{external}$ (m^2/g)	541.7	31.8	20.9	43.6	71.7
V_{total} (cm^3/g)	0.86	0.45	0.38	0.44	0.40
V_{mic} (cm^3/g)	0.16	0.38	0.34	0.37	0.31
D_p (nm)	1.4	3.7	3.8	3.9	3.7

S_{BET}, BET surface area; $S_{micropore}$, t-method micropore surface area; $S_{external}$, t-method external surface area; V_{total}, single point adsorption total pore volume; V_{mic}, t-method micropore volume; Dp, average pore diameter adsorption calculated by BJH method

The characteristics of adsorption-desorption isotherms are efficiently used to specify the type of pores characteristics of catalyst samples. The N_2 adsorption desorption isotherms of all catalysts are displayed in **Figure 29**. The isotherms of the activated carbon-supported metal catalysts present a combination of types I (major)

and IV (minor) according to the IUPAC [82]. A combination of types I and IV isotherms are usually denoted the presence of both microporous and mesoporous structure. The isotherms show a sharp increase in N2 adsorption in the initial relative pressure range implying the formation of micropores. Furthermore, the isotherms also appear to contain hysteresis loop at high relative pressure suggesting that the pore structure is partly mesopores. So, the activated carbons with different metals loadings showed the dominant microporous structures. The ACC catalyst exhibited distinct type IV isotherm indicating that mesoporous structure exists. Therefore, addition of metals leads to decrease pore size of catalysts. The adsorption capacity is at a maximum of the ACC catalyst showing that the pore volume has the maximum amount at this sample.

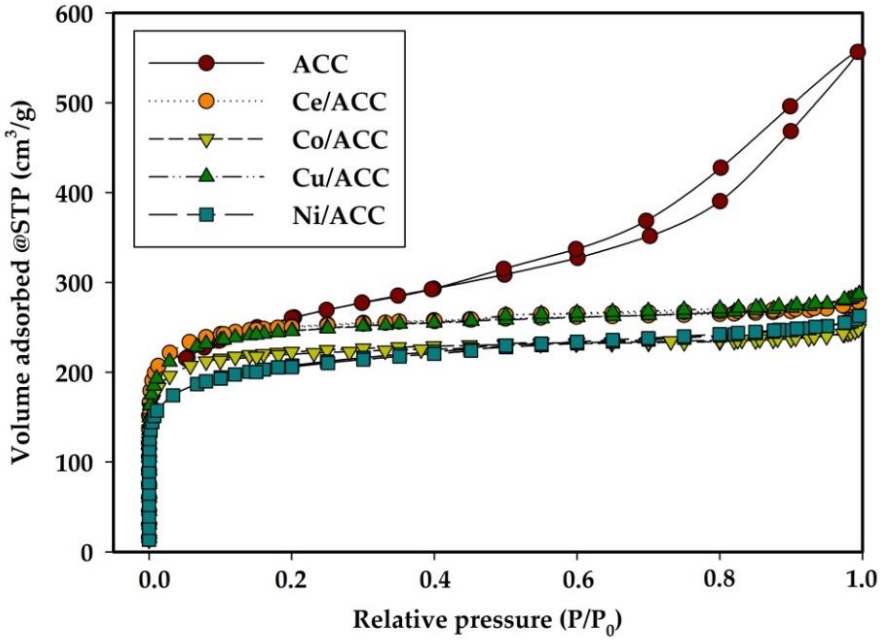

Figure 29

Adsorption-desorption isotherm at -196°C of catalysts.

The results of metal content from ICP technique of the catalyst samples are demonstrated in Table 16. Results shows that metals content in the bulk of catalysts was around 10% by weight As seen by TEM/EDX (Table 19 in Appendix B) result, Cu/ACC sample has the highest amount of metal among other catalysts because the

grids used in measurement is copper. TEM micrographs of activated carbon-supported metal catalysts are shown in Figure 30. The dark patches represent the metal species dispersing on all catalysts. As illustrated, all synthesized catalyst showed a well dispersing of metal.

Table 17 Metal contents of the different commercial activated carbon catalysts.

Activated carbons	% wt metal (ICP)
Ce/ACC	8.8
Co/ACC	8.0
Cu/ACC	7.7
Ni/ACC	11.4

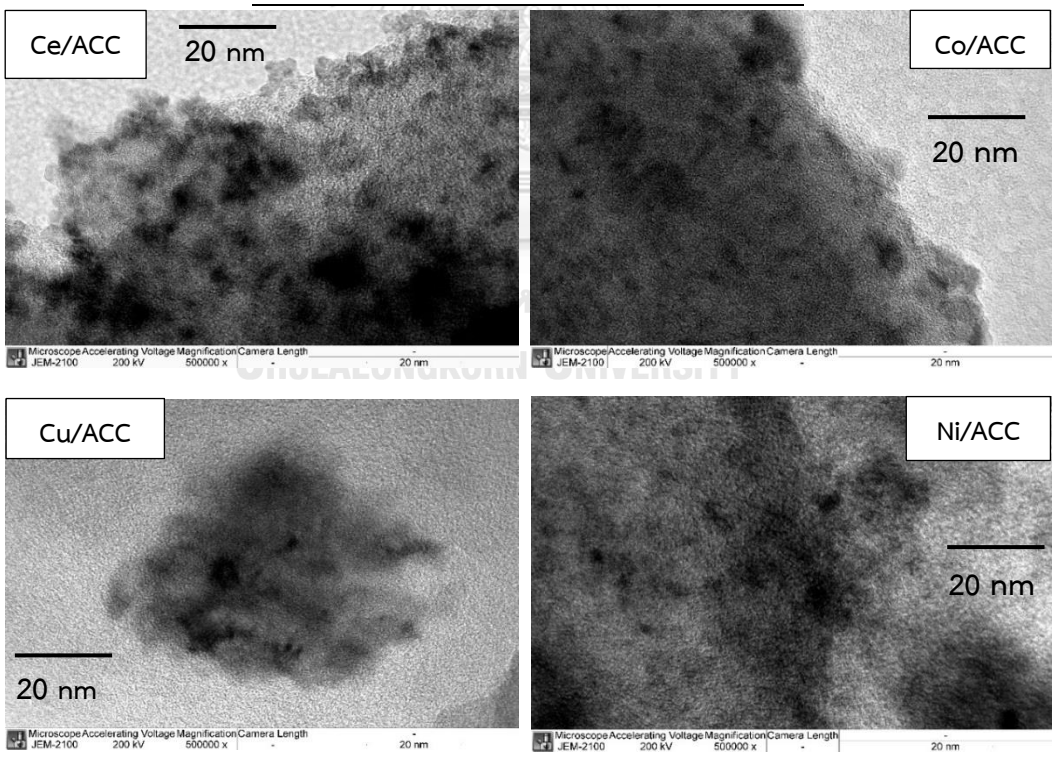

Figure 30 TEM images of activated carbon supported-metal catalysts.

The total surface acidity and the total surface basicity of the samples were measured by NH_3-TPD and CO_2-TPD, respectively. The number of acid site and basic

site on catalysts was calculated under the temperature range of 40°C to 400°C by integration of desorption peaks of ammonia and carbon dioxide according to the Fityk curve fitting method, which are related to the acid sites and basic sites on the catalysts. The typical NH_3-TPD profiles for all activated carbon catalysts are illustrated in **Figure 31** under the temperature range of 40°C to 400°C. The total acidity results are listed in **Table 17**, which is in the order from the greatest to the least as following: Cu/ACC > Co/ACC > Ni/ACC > Ce/ACC > ACC. Thus, the transition metal cations (Lewis acids) apparently results in more active centers [34]. It notices that Cu/ACC catalyst exhibits the highest total acid sites of 549 μmol/g. Moreover, the total basicity results of catalysts as also seen in **Table 17** reveal that Co/ACC catalyst has the greatest basicity followed by Ce/ACC, which is similar to Ni/ACC. The order of the total basicity is shown as followed: Co/ACC > Ce/ACC > Ni/ACC > Cu/ACC > ACC.

Table 18 Total acidity and total basicity of catalysts.

Activated carbons	Total acidity[a] (μmol/g)	Total basicity[b] (μmol/g)
ACC	133	56
Ce/ACC	164	174
Co/ACC	358	319
Cu/ACC	549	90
Ni/ACC	199	158

*a NH_3-TPD, *b CO_2-TPD, Calculated in temperature. range 40-400°C

จุฬาลงกรณ์มหาวิทยาลัย
CHULALONGKORN UNIVERSITY

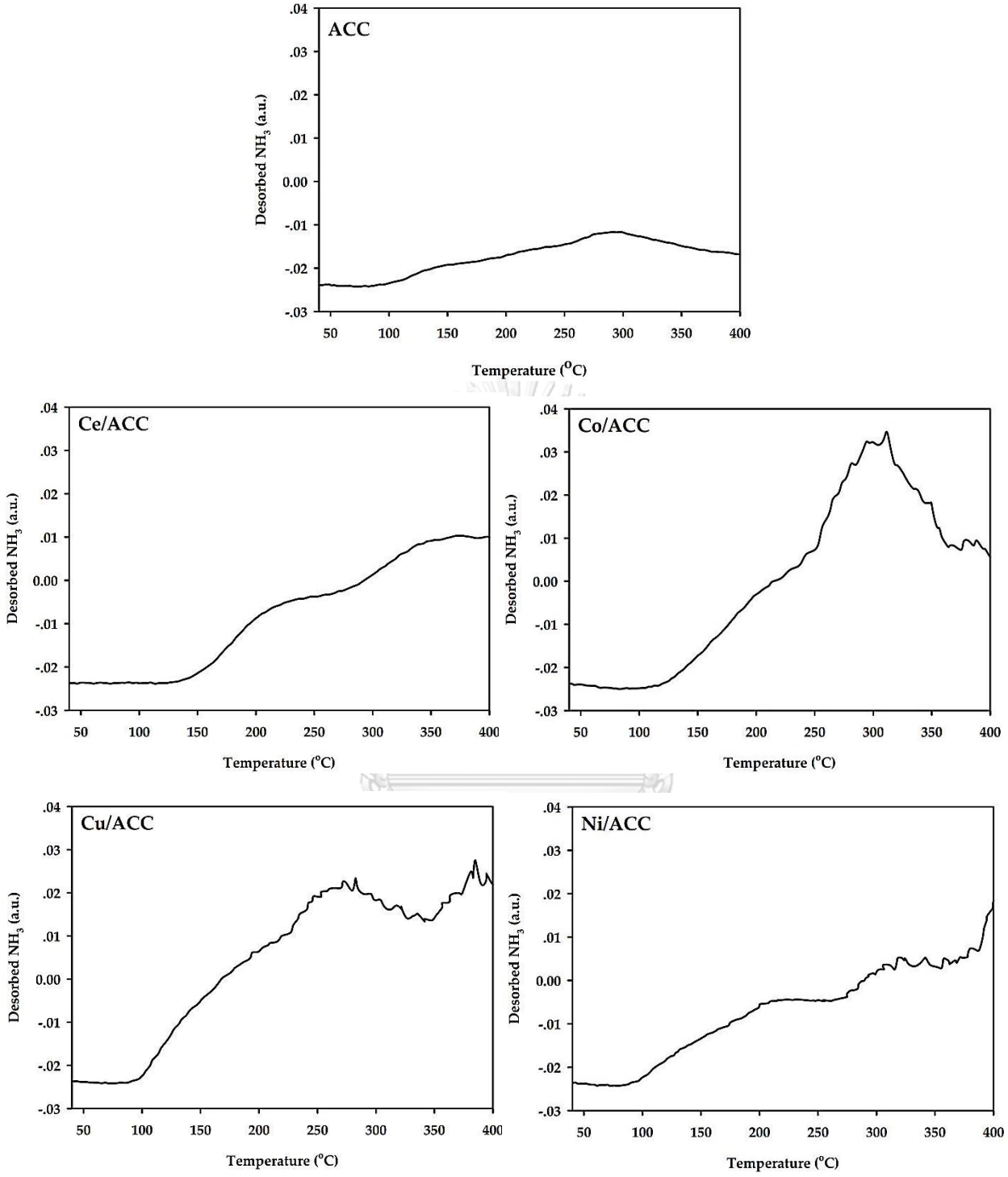

Figure 31 NH_3-TPD profiles of catalysts.

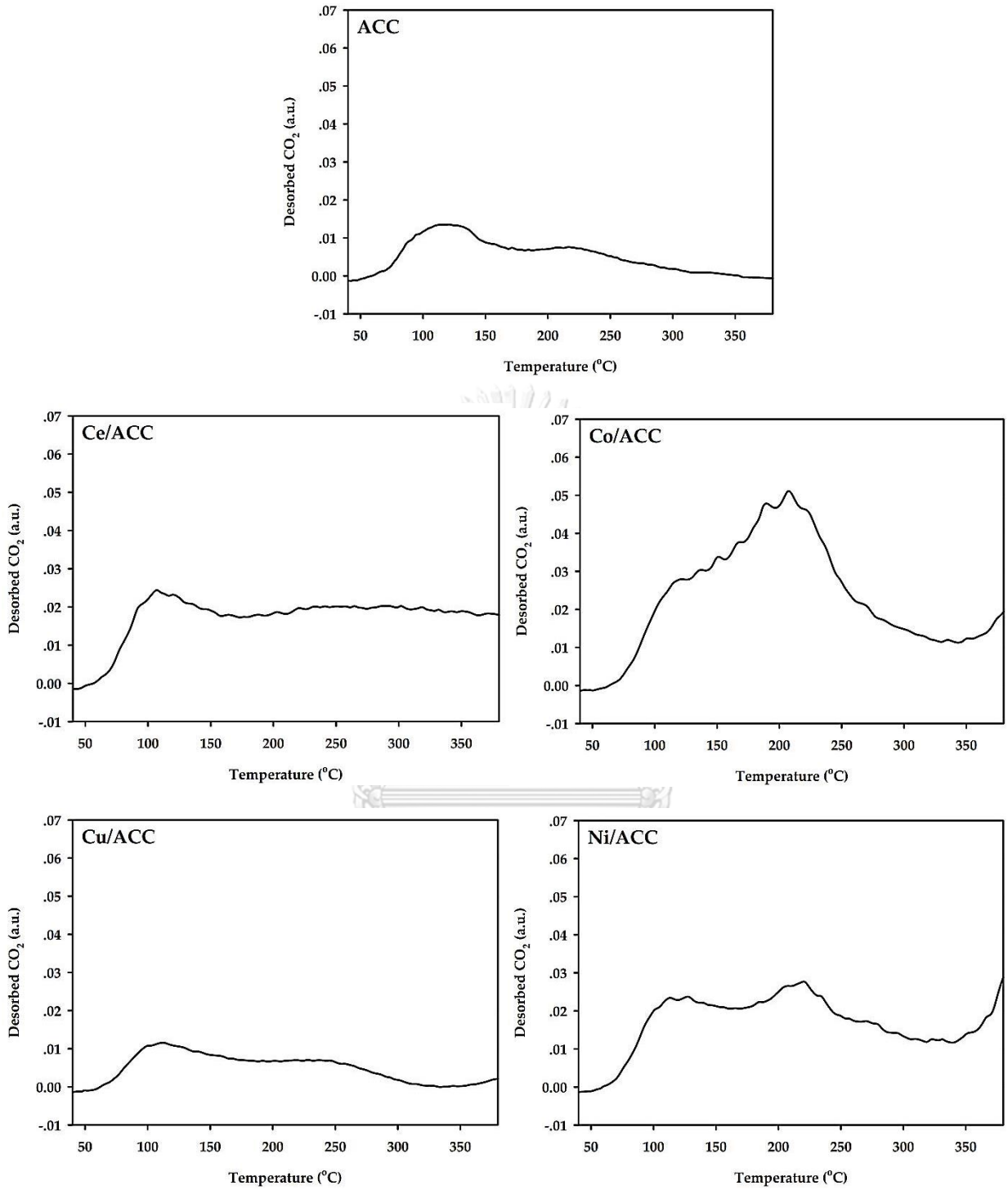

Figure 32 CO_2-TPD profiles of catalysts.

The XRD patterns of metal supported on activated carbon are shown in **Figure 33**. The XRD pattern of ACC sample used as catalyst and support exhibits diffraction peak at 2θ= 26.8°, which can be denoted as graphite structure on activated carbon

[96] and peak at 2θ=45° demonstrate as graphene structure [19]. For ceria catalyst supported on ACC, the CeO_2 peaks evidently show at 2θ=28, 33, 47.5, 56, 69.5 and 77° [97]. Considering nickel catalyst supported on ACC, the NiO peaks display obviously at 2θ=37.3, 43.3, 62.8 and 75.5° [98]. For cobalt catalyst, the XRD peaks of Co_3O_4 and CoO were slightly observed at 36.8 and 42.5°, respectively [99]. In addition, for Cu/ACC, The characteristic peaks of CuO were observed at 35.5, 38.7, 61.6 72.3 and 74.7° [14, 100]. Typically, Cu_2O cubic phase can be observed at 36.4 and 42.3° [13], which were assigned to the Cu^+ species.

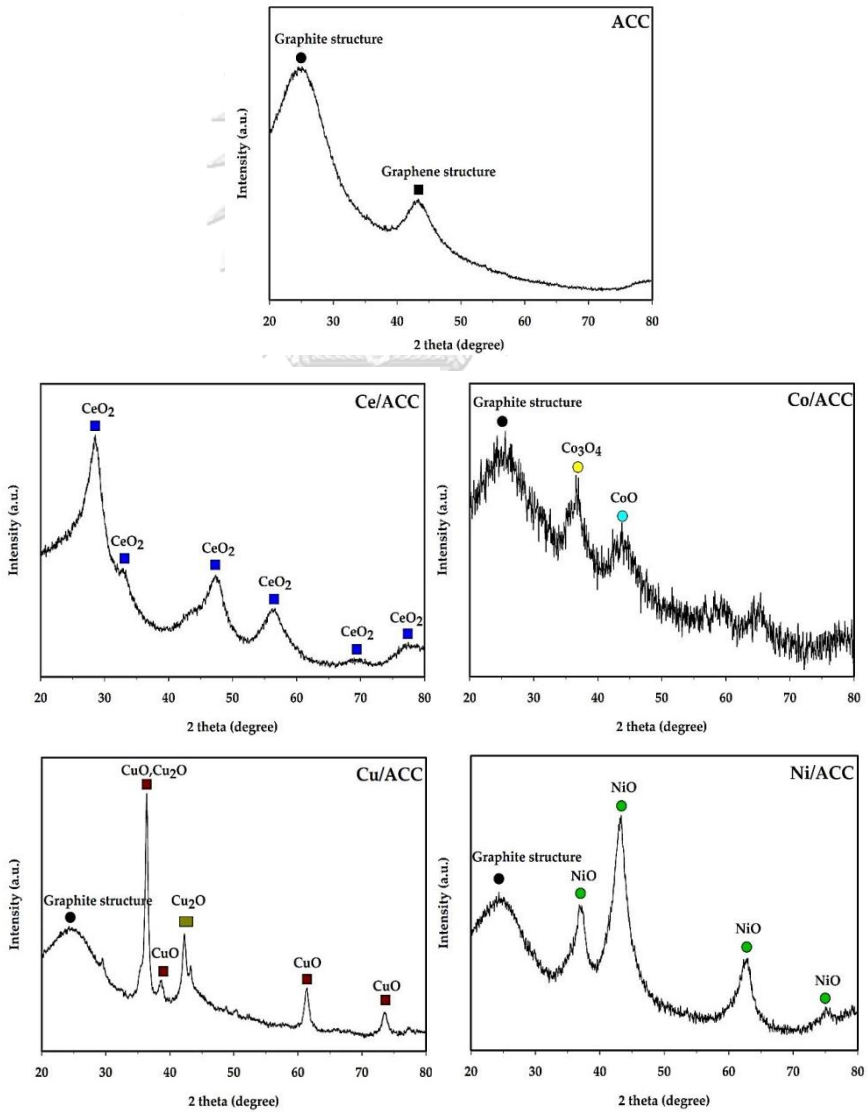

Figure 33 X-ray diffraction patterns of catalysts.

5.3.2 Catalyst Testing

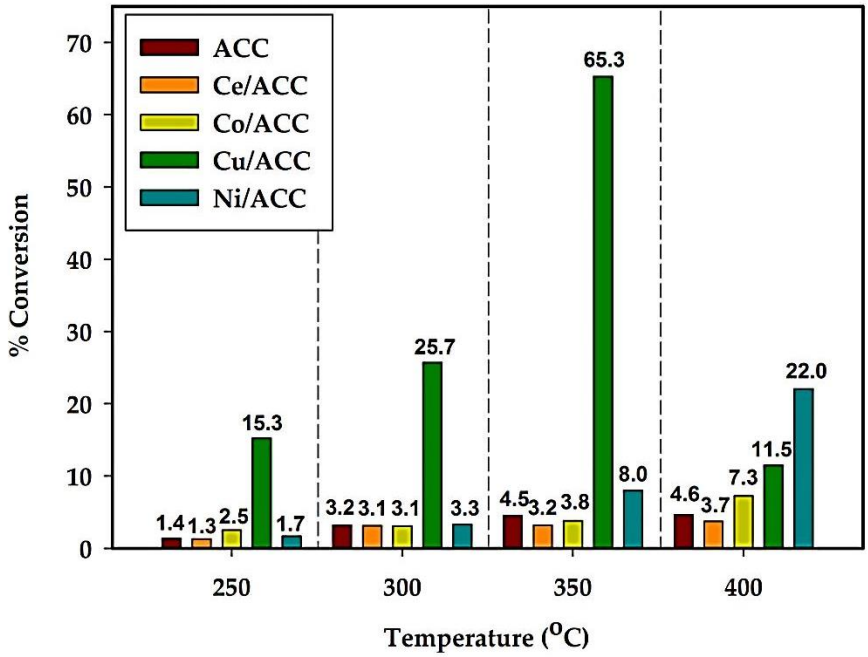

Figure 34 Ethanol conversion of catalysts.

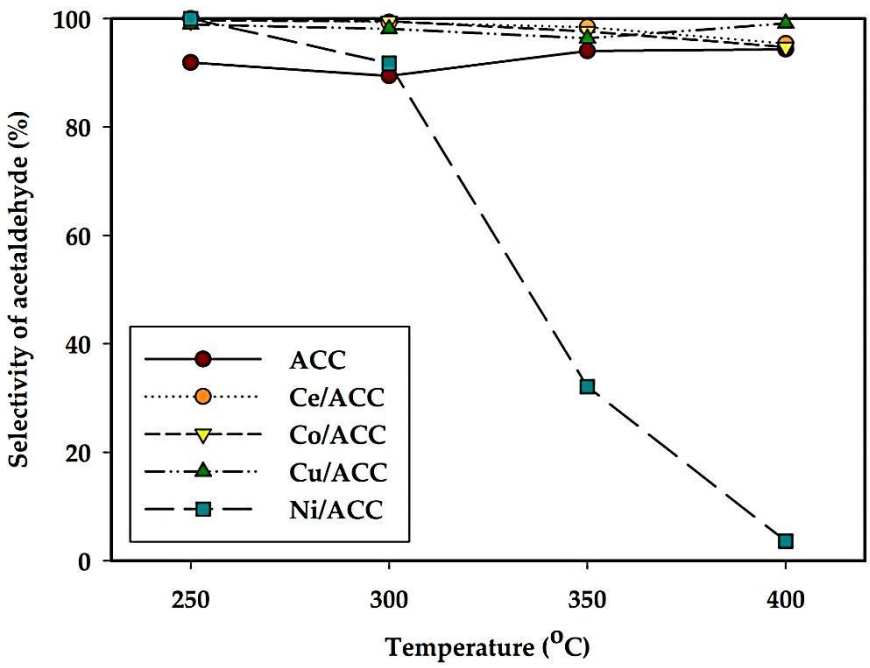

Figure 35 Selectivity of acetaldehyde of catalysts.

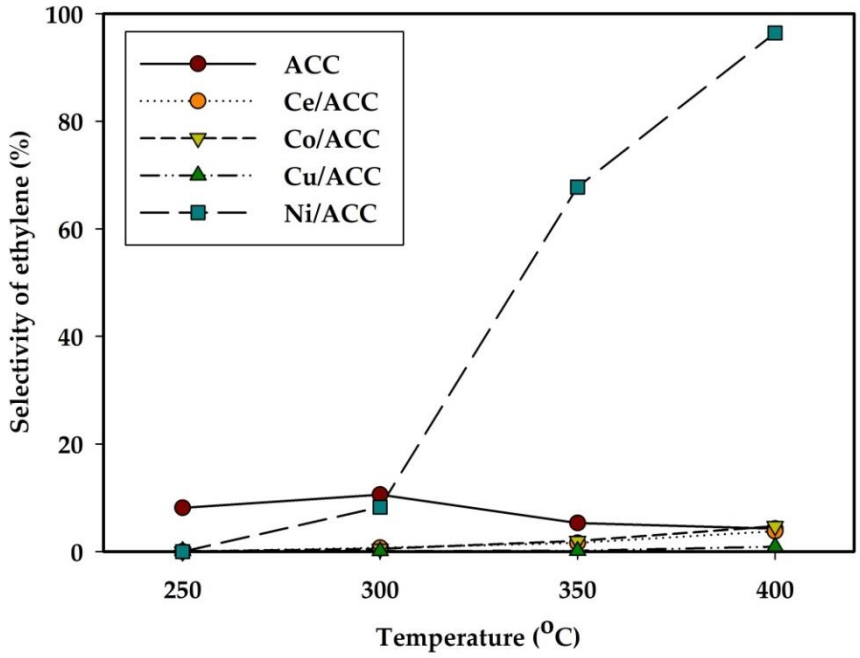

Figure 36 Selectivity of ethylene of catalysts.

Figure 34 shows the catalytic performance of different metals on activated carbon of ethanol dehydrogenation for each temperature. As expected, ethanol conversion increases with increased reaction temperature because of its endothermic reaction, excepting for the Cu/ACC catalyst that shows maximum conversion at temperature of 350°C. For temperature of 250-400°C, both copper and nickel doping on activated carbon evidently improved catalytic performance of these catalysts. Particularly, the Cu/ACC catalyst remarkably exhibited the highest ethanol conversion among other catalysts for all reaction temperatures. Meanwhile, this catalyst showed the highest total acidity as mentioned in **Table 17**. The result correlated with previous studies, they claimed that the dehydrogenation of ethanol favored in Lewis acid sites [32, 33]. The highest ethanol conversion of 65% at 350°C was obtained from Cu/ACC catalyst. Then, the rapid decrease of conversion less than 12% at 400°C was observed due to the agglomeration and pore blockage by coke. The agreement was confirmed by other studies [100-102]. Additionally, the proposed mechanism of catalytic dehydrogenation of this catalyst is shown in **Figure 37** [40, 103]. Volanti et al., [40]

claimed that Cu^+ species were usually over Cu^0 on the metal surface of the Cu/SiO_2 catalyst and the ionic species is more selective to acetaldehyde production. Sato et al., [103] reported in 2013 that ethanol is activated to $CH_3CH_2O^*$ by Cu^+ sites or on the zirconia surface. **Figure 39** (in Appendix B) shows TPR results indicating that bulk CuO (Cu^{2+}) on surface of Cu/ACC catalyst could be reduce to Cu^+ at 160 °C [101], while Cu_2O (Cu^+) was habitually reduced at high temperature around 580-590°C [100]. Therefore, the presence of Cu^+ sites on Cu/ACC can be proven by the formation of acetaldehyde via ethanol dehydrogenation on these sites. From TPR, it should be noted that after reduction at 400°C, some portion of non-reducible CuO still remains based on H_2 consumption. It was found that the cobalt doping only slightly enhanced the activity of catalyst, whereas the cerium doping apparently produced acetaldehyde without a significant improvement of activity. Considering the selectivity of acetaldehyde and ethylene for all catalysts, it is shown in **Figure 35** and **36**, respectively. Results of the catalytic reaction test in this study confirmed that most of activated carbons acted as catalysts of ethanol dehydrogenation to acetaldehyde with the very high selectivity more than 90% as similar to other studies [33]. Only Ni/ACC catalyst shows that the decreased selectivity of acetaldehyde after 300°C but trading by the increased selectivity of ethylene (ca. 100% at 400°C) with increasing reaction temperature [104, 105]. An increase of the reaction temperature also improves the dehydration selectivity. The dehydrogenation selectivity also enlarges initially, but at above temperatures of 573 K passes through a highest selectivity and then decrease [34]. For the ACC sample, Moreover, all catalysts extremely exhibited low selectivity (less than 1%) of diethyl ether and acetic acid (not shown).

จุฬาลงกรณ์มหาวิทยาลัย
CHULALONGKORN UNIVERSITY

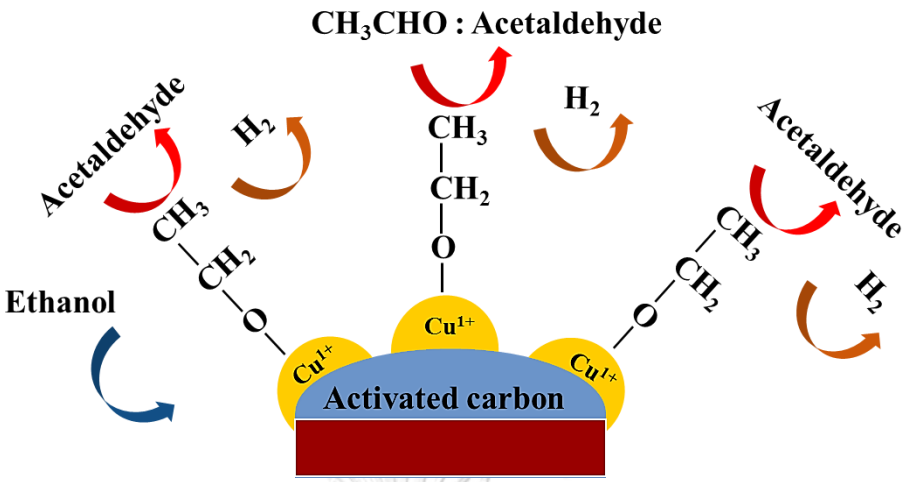

Figure 37 A proposed mechanism for dehydrogenation reaction of ethanol on Cu/ACC catalyst.

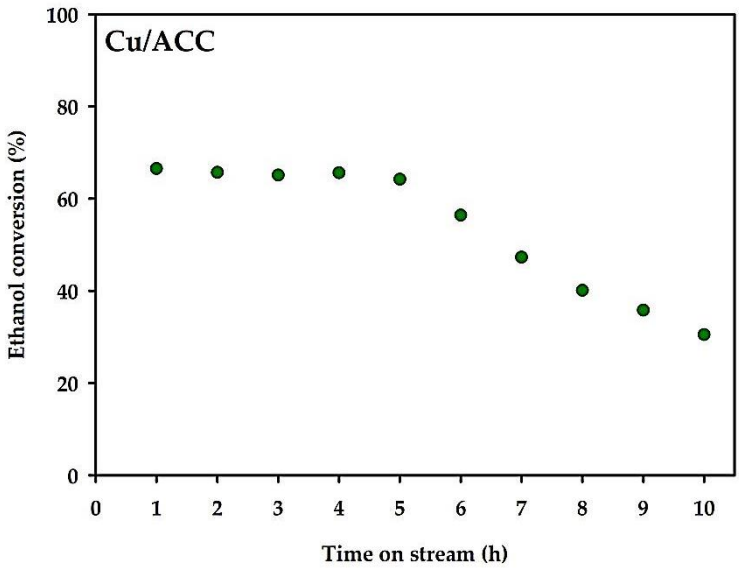

Figure 38 Stability test of Cu/ACC catalyst at 350 °C.

Eventually, the stability test of Cu/ACC catalyst under time on stream of 10 h was carried out at the reaction temperature of 350°C. The stability result is displayed in **Figure 38.** The ethanol conversion is fairly constant within 5 h of reaction. After 5 h, the ethanol conversion continuously decreased because of possible coke formation or pore blockage from the thermal destruction by long time reaction [101, 102].

Table 19 Comparison of metal on commercial activated carbon for ethanol dehydrogenation and their catalytic ability.

Catalysts	Reaction temperature (°C)	Ethanol conversion (%)	Acetaldehyde yield (%)	LHSV [ml/(h.gcat)]	Refs
Cu-CeO_2/AC	250	46	3.3	4	(109)
Co-CeO_2/AC	250	34	2.5	4	(109)
Ni-CeO_2/AC	250	32	1.5	4	(109)
CeO_2/AC	250	3	0.4	4	(109)
4Cu1Ce/AC	250	46	3.6	4	(109)
5%Ni/ACC	250	17	16.1	290	(107)
Cu/ACC	250	15	15.1	290	[this work]

The comparisons of catalytic performance of activated carbon catalysts in this work and other works are summarized in **Table 18**. It appears that, apart from when higher liquid hourly space velocity (LHSV) was carried out, Cu/ACC catalyst was quite promising compared to other previous catalysts.

จุฬาลงกรณ์มหาวิทยาลัย
CHULALONGKORN UNIVERSITY

CHAPTER VI

CONCLUSION AND RECOMMENDATIONS

6.1 Conclusion

In the first part of this work, the preparation of activated carbon catalysts derived from coffee ground residues with different gases and holding times of physical activation. The influence of carbonization on the characteristics of these materials and the catalytic performance of ethanol dehydrogenation range of 250 to 400°C has been examined. It seems that the synthesized activated carbon with chemical activated by $ZnCl_2$ followed by physical activated under carbon dioxide flow at 600 °C for 4 hours (AC-D), exhibited the highest activity with 48% conversion of ethanol and 47% yield of acetaldehyde at 400°C. The activation with $ZnCl_2$ followed by CO_2 at 600°C for 4 h apparently resulted in increased acid and basic sites. The increase in the amount of Lewis acid and basic sites leads to enhance catalytic activity of ethanol dehydrogenation. All activated carbon catalysts in this study show very high selectivity to acetaldehyde (more than 90%), which is quite promising compared to other activated carbon catalysts, which have significant side reactions. In addition, the synthesized activated carbon from coffee ground residues has an acceptable stability showing quite constant ethanol conversion under specified condition.

จุฬาลงกรณ์มหาวิทยาลัย
CHULALONGKORN UNIVERSITY

In the second part, the catalytic performance for ethanol dehydrogenation from the temperature range of 250 to 400°C over 4 and 6%wt cobalt on synthesized activated carbon (from the first part) was investigated. It appears that 4 wt% of Co impregnated on activated carbon, led to improve activity of ethanol dehydrogenation having 54% conversion of ethanol and 50% yield of acetaldehyde at 400°C. This catalyst has the acidity to the basicity similar the activated carbon (~1.50). However, 6% of Co doped on activated carbon caused sample to pore blockage with some

agglomeration. This resulted in a decrease of the acidity to the basicity to 1.38. Therefore, it exhibited low activity of this reaction by 19% of ethanol conversion.

In the third part, the catalytic performance of different metals, including Ce, Co, Cu, and Ni, doped on commercial activated carbon catalyst (ACC) for ethanol dehydrogenation with in a temperature range of 250 to 400°C were examined. It was found that the type of metal has a significant impact on catalytic performance, because it affects the surface acidity. It appears that Cu/ACC catalyst exhibits the highest catalytic activity, at 65.3% ethanol conversion, with an acetaldehyde selectivity of 96.3%, resulting in an acetaldehyde yield of ca. 62.9% at 350°C. This can be attributed to its optimal total acid amount and Cu^{+} species. It should be mentioned that the Ni/ACC catalyst was potentially suitable to produce ethylene via ethanol dehydration at 400°C, giving an ethylene yield of around 21.3%.

6.2 Recommendations

1. In the further study, the IR of pyridine and pyrrole chemisorbed should be used to distinguish types of the acid and basic sites, respectively.

2. To increase the catalytic performance, the effect of copper loading on the catalytic performance should be further investigated other than 10%wt of loading.

3. Deactivation of the catalysts at different reaction temperature should also be investigated in order to improve these catalysts for utilization in industry.

จุฬาลงกรณ์มหาวิทยาลัย
CHULALONGKORN UNIVERSITY

REFERENCES

1. Zhou, M., W. Wang, and M. Chi, *Enhancement on the simultaneous removal of nitrate and organic pollutants from groundwater by a three-dimensional bio-electrochemical reactor.* Bioresour Technol, 2009. **100**(20): p. 4662-4668.
2. Daifullah, A.A.M., B.S. Girgis, and H.M.H. Gad, *Utilization of agro-residues (rice husk) in small waste water treatment plans.* Materials Letters, 2003. **57**(11): p. 1723-1731.
3. Bedia, J., et al., *Pd supported on mesoporous activated carbons with high oxidation resistance as catalysts for toluene oxidation.* Applied Catalysis B: Environmental, 2010. **94**(1-2): p. 8-18.
4. Gu, J.Y., et al., *Control growth of carbon nanofibers on Ni/activated carbon in a fluidized bed reactor.* Microporous and Mesoporous Materials, 2010. **131**(1-3): p. 393-400.
5. Sekirifa, M.L., et al., *Preparation and characterization of an activated carbon from a date stones variety by physical activation with carbon dioxide.* Journal of Analytical and Applied Pyrolysis, 2013. **99**: p. 155-160.
6. Niticharoenwong, B., et al., *Characteristics of Activated Carbons Derived from Deoiled Rice Bran Residues.* Chemical Engineering Communications, 2013. **200**(10): p. 1309-1321.
7. Almansa, C., M. Molina-Sabio, and F. Rodriguez-Reinoso, *Adsorption of methane into $ZnCl_2$-activated carbon derived discs.* Microporous and Mesoporous Materials, 2004. **76**(1-3): p. 185-191.
8. Azevedo, D.C.S., et al., *Microporous activated carbon prepared from coconut shells using chemical activation with zinc chloride.* Microporous and Mesoporous Materials, 2007. **100**(1-3): p. 361-364.
9. Bedia, J., et al., *Ethanol dehydration to ethylene on acid carbon catalysts.* Applied Catalysis B: Environmental, 2011. **103**(3-4): p. 302-310.

จุฬาลงกรณ์มหาวิทยาลัย
Chulalongkorn University

10. Neramittagapong, A., W. Attaphaiboon, and S. Neramittagapong, *Acetaldehyde Production from Ethanol over Ni-Based Catalysts.* Chiang Mai J. Sci., 2008. **35**(1): p. 171-177.

11. *Acetaldehyde Market - Global Industry Analysis, Size, Share, Trends and Forecast 2015 - 2023.* 2015.

12. Xu, J., et al., *Silver/hydroxyapatite foam as a highly selective catalyst for acetaldehyde production via ethanol oxidation.* Catalysis Today, 2016. **276**: p. 19-27.

13. Sato, A.G., et al., *Site-selective ethanol conversion over supported copper catalysts.* Catalysis Communications, 2012. **26**: p. 122-126.

14. Freitas, I.C., et al., *Effect of Cu content on the surface and catalytic properties of Cu/ZrO_2 catalyst for ethanol dehydrogenation.* Journal of Molecular Catalysis A: Chemical, 2014. **381**: p. 26-37.

15. DeWilde, J.F., C.J. Czopinski, and A. Bhan, *Ethanol Dehydration and Dehydrogenation on γ-Al_2O_3: Mechanism of Acetaldehyde Formation.* ACS Catalysis, 2014. **4**(12): p. 4425-4433.

16. Skinner, M.J., et al., *Ethanol dehydration to ethylene in a stratified autothermal millisecond reactor.* ChemSusChem, 2011. **4**(8): p. 1151-6.

17. Autthanit, C. and B. Jongsomjit, *Production of Ethylene through Ethanol Dehydration on SBA-15 Catalysts Synthesized by Sol-gel and One-step Hydrothermal Methods.* J Oleo Sci, 2018. **67**(2): p. 235-243.

18. La-Salvia, N., J.J. Lovon-Quintana, and G.P. Valenca, *Vapor-phase catalytic conversion of ethanol into 1,3-butadiene on Cr-Ba/MCM-41 catalysts.* Brazilian Journal of Chemical Engineering, 2015. **32**(2): p. 489-500.

19. Kamsuwan, T., P. Praserthdam, and B. Jongsomjit, *Diethyl Ether Production during Catalytic Dehydration of Ethanol over Ru- and Pt- modified H-beta Zeolite Catalysts.* J Oleo Sci, 2017. **66**(2): p. 199-207.

20. Almukhlifi, H.A. and R.C. Burns, *Oxidative dehydrogenation of isobutane to isobutene by pyrovanadates, $M_2V_2O_7$, where M(II) = Mn, Co, Ni, Cu and Zn, and*

จุฬาลงกรณ์มหาวิทยาลัย
Chulalongkorn University

Co_2VO_4 and ZnV_2O_4 : The effect of gold nanoparticles. Journal of Molecular Catalysis A: Chemical, 2015. **408**: p. 26-40.

21. Guan, Y. and E.J.M. Hensen, *Ethanol dehydrogenation by gold catalysts: The effect of the gold particle size and the presence of oxygen.* Applied Catalysis A: General, 2009. **361**(1-2): p. 49-56.
22. Lippits, M.J. and B.E. Nieuwenhuys, *Direct conversion of ethanol into ethylene oxide on copper and silver nanoparticles. Effect of addition of CeO_x and Li_2O.* Catalysis Today, 2010. **154**(1-2): p. 127-132.
23. Ochoa-Hernandez, C., et al., *Hydrocarbons production through hydrotreating of methyl esters over Ni and Co supported on SBA-15 and Al-SBA-15.* Catalysis Today, 2013. **210**: p. 81-88.
24. Shan, J., et al., *Selective non-oxidative dehydrogenation of ethanol to acetaldehyde and hydrogen on highly dilute NiCu alloys.* Applied Catalysis B: Environmental, 2017. **205**: p. 541-550.
25. Gao, D., et al., *Coupling reaction between ethanol dehydrogenation and maleic anhydride hydrogenation catalyzed by Cu/Al_2O_3, Cu/ZrO_2, and Cu/ZnO catalysts.* Chemical Engineering Journal, 2013. **233**: p. 349-359.
26. Santacesaria, E., et al., *Ethanol dehydrogenation to ethyl acetate by using copper and copper chromite catalysts.* Chemical Engineering Journal, 2012. **179**: p. 209-220.
27. Hidalgo, J.M., et al., *(V)/Hydrotalcite, $(V)/Al_2O_3$, $(V)/TiO_2$ and (V)/SBA-15 catalysts for the partial oxidation of ethanol to acetaldehyde.* Journal of Molecular Catalysis A: Chemical, 2016. **420**: p. 178-189.
28. Autthanit, C., P. Praserthdam, and B. Jongsomjit, *Oxidative and non-oxidative dehydrogenation of ethanol to acetaldehyde over different VO_x/SBA-15 catalysts.* Journal of Environmental Chemical Engineering, 2018. **6**(5): p. 6516-6529.
29. Israel E. Wachs and R.J. Madix, *The oxidation of methanol on a silver (110) catalyst.* Surface Science, 1978. **76**: p. 531-558.

จุฬาลงกรณ์มหาวิทยาลัย
Chulalongkorn University

30. Lim, S.P., et al., *Silver/titania nanocomposite-modified photoelectrodes for photoelectrocatalytic methanol oxidation.* International Journal of Hydrogen Energy, 2014. **39**(27): p. 14720-14729.

31. Wu, X., et al., *Catalytic upgrading of ethanol to n-butanol over M-CeO_2/AC (M = Cu, Fe, Co, Ni and Pd) catalysts.* Catalysis Communications, 2017. **100**: p. 15-18.

32. Jasinska, J., B. Krzyzynska, and M. Kozlowski, *Influence of activated carbon modifications on their catalytic activity in methanol and ethanol conversion reactions.* Open Chemistry, 2011. **9**(5).

33. Carrasco-Marin, F., A. Mueden, and C. Moreno-Castilla, *Surface-Treated Activated Carbons as Catalysts for the Dehydration and Dehydrogenation Reactions of Ethanol.* J. Phys. Chem. B, 1998. **102**(46): p. 9239-9244.

34. Szymanski, G.S., G. Rychlicki, and A.P. Terzyk, *Catalytic conversion of ethanol on carbon catalysts.* Carbon, 1994. **32**(2): p. 265-271.

35. Eckert, M., et al., *Acetaldehyde*, in *Ullmann's Encyclopedia of Industrial Chemistry*. 2006.

36. *Documentation of the Threshold Limit Values and Biological Exposure Indices, 7th Ed.* 2001.

37. *Data extracted from Gas Data Book, 7th edition.* 2001: p. 443.

38. Gallo, J.M.R., J.M.C. Bueno, and U. Schuchardt, *Catalytic Transformations of Ethanol for Biorefineries.* Journal of the Brazilian Chemical Society, 2014.

39. Janlamool, J. and B. Jongsomjit, *Oxidative dehydrogenation of ethanol over AgLi–Al_2O_3 catalysts containing different phases of alumina.* Catalysis Communications, 2015. **70**: p. 49-52.

40. Volanti, D.P., et al., *Insight into Copper-Based Catalysts: Microwave-Assisted Morphosynthesis, In Situ Reduction Studies, and Dehydrogenation of Ethanol.* ChemCatChem, 2011. **3**: p. 839-843.

41. Ponomarev, D.A. and S.M. Shevchenko, *Hydration of Acetylene: A 125th Anniversary.* Journal of Chemical Education, 2007. **84**(10): p. 1725-1726.

42. Panda, H., *Handbook On Chemical Industries (Alcohol Based).* 2002.

43. Wexler, P., *Encyclopedia of Toxicology 2nd Edition.* 2005.

44. *Chemical Economics Handbook (Acetaldehyde).* 2013.

45. *Chemical Economics Handbook (Acetaldehyde).* 2016.

46. *Global Acetaldehyde Market to Reach 1.2 Million Tons by 2015.* 2011.

47. *Acetaldehyde-Market Analysis, Trends, and Forecasts.*

48. Soderberg, T., *Organic Chemistry With a Biological Emphasis.* 2017.

49. Poreddy, R., C. Engelbrekt, and A. Riisager, *Copper oxide as efficient catalyst for oxidative dehydrogenation of alcohols with air.* Catalysis Science & Technology, 2015. **5**(4): p. 2467-2477.

50. Pansanga, K., et al., *Effect of mixed γ- and χ-crystalline phases in nanocrystalline Al_2O_3 on the dispersion of cobalt on Al_2O_3.* Catalysis Communications, 2008. **9**(2): p. 207-212.

51. Chaitree, W., et al., *Effect of nanocrystalline χ-Al_2O_3 structure on the catalytic behavior of Co/Al_2O_3 in CO hydrogenation.* Catalysis Today, 2011. **164**(1): p. 302-307.

52. Liu, P., et al., *On the metal–support synergy for selective gas-phase ethanol oxidation over $MgCuCr_2O_4$ supported metal nanoparticle catalysts.* Journal of Catalysis, 2015. **331**: p. 138-146.

53. Guo, J. and A.C. Lua, *Microporous activated carbons prepared from palm shell by thermal activation and their application to sulfur dioxide adsorption.* J Colloid Interface Sci, 2002. **251**(2): p. 242-7.

54. Boudrahem, F., F. Aissani-Benissad, and H. Ait-Amar, *Batch sorption dynamics and equilibrium for the removal of lead ions from aqueous phase using activated carbon developed from coffee residue activated with zinc chloride.* J Environ Manage, 2009. **90**(10): p. 3031-9.

55. Boudrahem, F., A. Soualah, and F. Aissani-Benissad, *Pb(II) and Cd(II) Removal from Aqueous Solutions Using Activated Carbon Developed from Coffee Residue Activated with Phosphoric Acid and Zinc Chloride.* Journal of Chemical & Engineering Data, 2011. **56**(5): p. 1946-1955.

56. Goncalves, M., et al., *A friendly environmental material: iron oxide dispersed over activated carbon from coffee husk for organic pollutants removal.* J Environ Manage, 2013. **127**: p. 206-11.

จุฬาลงกรณ์มหาวิทยาลัย
Chulalongkorn University

57. Ngaosuwan, K., J.G. Goodwin, and P. Prasertdham, *A green sulfonated carbon-based catalyst derived from coffee residue for esterification.* Renewable Energy, 2016. **86**: p. 262-269.

58. Laksaci, H., et al., *Synthesis and characterization of microporous activated carbon from coffee grounds using potassium hydroxides.* Journal of Cleaner Production, 2017. **147**: p. 254-262.

59. Sun, S., N. Tsubaki, and K. Fujimoto, *The reaction performances and characterization of Fischer–Tropsch synthesis Co/SiO_2 catalysts prepared from mixed cobalt salts.* Applied Catalysis A: General, 2000. **202**: p. 121-131.

60. Dutta, P., et al., *Characterization of Fischer–Tropsch cobalt-based catalytic systems(Co/SiO_2 and Co/Al_2O_3) by X-ray diffraction and magnetic measurements.* Catalysis Letters, 2004. **98**(4): p. 203-210.

61. Xiong, J., et al., *The formation of Co_2C species in activated carbon supported cobalt-based catalysts and its impact on Fischer–Tropsch reaction.* Catalysis Letters, 2005. **102**(3-4): p. 265-269.

62. Gaudillere, C., et al., *YSZ monoliths promoted with Co as catalysts for the production of H_2 by steam reforming of ethanol.* Applied Catalysis A: General, 2017. **538**: p. 165-173.

63. Jiratova, K., et al., *Cobalt Oxides Supported Over Ceria–Zirconia Coated Cordierite Monoliths as Catalysts for Deep Oxidation of Ethanol and N_2O Decomposition.* Catalysis Letters, 2017. **147**(6): p. 1379-1391.

64. Jiratova, K., et al., *Cobalt oxide catalysts supported on CeO_2–TiO_2 for ethanol oxidation and N_2O decomposition.* Reaction Kinetics, Mechanisms and Catalysis, 2017. **121**(1): p. 121-139.

65. Zhao, G., et al., *Reaction-Induced Self-Assembly of CoO@Cu_2O Nanocomposites In Situ onto SiC-Foam for Gas-Phase Oxidation of Bioethanol to Acetaldehyde.* ChemSusChem, 2017. **10**(7): p. 1380-1384.

66. Popa, A., et al., *Preparation and catalytic properties of cobalt salts of Keggin type heteropolyacids supported on mesoporous silica.* Catalysis Today, 2018. **306**: p. 233-242.

67. Ashok, A., et al., *Study of ethanol dehydrogenation reaction mechanism for hydrogen production on combustion synthesized cobalt catalyst.* International Journal of Hydrogen Energy, 2017. **42**(37): p. 23464-23473.

68. Hammiche-Bellal, Y., et al., *Cobalt and cobalt-iron spinel oxides as bulk and silica supported catalysts in the ethanol combustion reaction.* Journal of Molecular Catalysis A: Chemical, 2017. **426**: p. 97-106.

69. Fleischmann, G., R. Jira, H.M. Bolt, and K. Golka, *Ullmann's Encyclopedia of Industrial Chemistry.* 2002: p. 31-44.

70. Grunewald, G.C. and R.S. Drago, *Carbon Molecular Sieves as Catalysts and Catalyst Supports.* Journal of the American Chemical Society, 1991. **113**: p. 1636-1639.

71. Tveritinova, E.A., et al., *Catalytic conversion of aliphatic alcohols on carbon nanomaterials: The roles of structure and surface functional groups.* Russian Journal of Physical Chemistry A, 2017. **91**(3): p. 448-454.

72. Moreno-Castilla, C. and F. Carrasco-Main, *Cobalt Catalysts supported on Activated Carbons : Preparation and Behaviour in the Hydrogenation of Carbon Oxides* Journal of the Chemical Society, Faraday Transactions 1995. **91**(19): p. 3519-3524.

73. Zaman, M., A. Khodadi, and Y. Mortazavi, *Fischer–Tropsch synthesis over cobalt dispersed on carbon nanotubes-based supports and activated carbon.* Fuel Processing Technology, 2009. **90**(10): p. 1214-1219.

74. Ma, W.-P., Y.-J. Ding, and L.-W. Lin, *Fischer-Tropsch Synthesis over Activated-Carbon-Supported Cobalt Catalysts: Effect of Co Loading and Promoters on Catalyst Performance.* Industrial & Engineering Chemistry Research, 2004. **43**(10): p. 2391-2398.

75. Sales, E.A., et al., *N_2O decomposition coupled with ethanol oxidative dehydrogenation reaction on carbon-supported copper catalysts promoted by palladium and cobalt.* Catalysis Today, 2005. **107-108**: p. 114-119.

76. Shukla, P.R., et al., *Activated carbon supported cobalt catalysts for advanced oxidation of organic contaminants in aqueous solution.* Applied Catalysis B: Environmental, 2010. **100**(3-4): p. 529-534.

จุฬาลงกรณ์มหาวิทยาลัย
Chulalongkorn University

77. Zhao, Z., et al., *Efficient cobalt–manganese oxide catalyst deposited on modified AC with unprecedented catalytic performance in CO preferential oxidation.* Catalysis Communications, 2013. **32**: p. 47-51.

78. Genova, I., et al., *Cobalt ferrite nanoparticles hosted in activated carbon from renewable sources as catalyst for methanol decomposition.* Catalysis Communications, 2014. **55**: p. 43-48.

79. Zabihi, M., F. Khorasheh, and J. Shayegan, *Supported copper and cobalt oxides on activated carbon for simultaneous oxidation of toluene and cyclohexane in air.* RSC Advances, 2015. **5**(7): p. 5107-5122.

80. Zhuang, Y., et al., *Mesoporous carbon-supported cobalt catalyst for selective oxidation of toluene and degradation of water contaminants.* Particuology, 2016. **24**: p. 216-222.

81. Zhao, W., M. Zhu, and B. Dai, *Cobalt-nitrogen-activated carbon as catalyst in acetylene hydrochlorination.* Catalysis Communications, 2017. **98**: p. 22-25.

82. Gregg, S.J., and K.S.W. Sing, *Adsorption. London: Surface Area and Porosity.* 1982.

83. Liou, T.-H., *Evolution of chemistry and morphology during the carbonization and combustion of rice husk.* Carbon, 2004. **42**(4): p. 785-794.

84. Kitano, M., et al., *Preparation of a Sulfonated Porous Carbon Catalyst with High Specific Surface Area.* Catalysis Letters, 2009. **131**(1-2): p. 242-249.

85. Goncalves, M., et al., *Micro Mesoporous Activated Carbon from Coffee Husk as Biomass Waste for Environmental Applications.* Waste and Biomass Valorization, 2012. **4**(2): p. 395-400.

86. Yusof, J.M., et al., *Characterisation of Carbon Particles (CPs) derived from dry milled kenaf biochar.* Journal of Engineering Science and Technology, 2014(10): p. 125-131.

87. Shafeeyan, M.S., et al., *A review on surface modification of activated carbon for carbon dioxide adsorption.* Journal of Analytical and Applied Pyrolysis, 2010. **89**(2): p. 143-151.

88. Tasi, W.T., et al., *Adsorption of acid dye onto activated carbons prepared from agricultural waste bagasse by $ZnCl_2$ activation.* Chemosphere, 2001. **45**: p. 51-58.

89. Lua, A.C. and T. Yang, *Effect of activation temperature on the textural and chemical properties of potassium hydroxide activated carbon prepared from pistachio-nut shell.* J Colloid Interface Sci, 2004. **274**(2): p. 594-601.

90. Vikulov K., S. Coluccia, and G. Martra, *Fourier-transform Infrared Spectroscopic Studies of the Adsorption of Ketene on Silica.* Journal of the Chemical. Society, Faraday Transactions, 1993. **89**(7): p. 1121-1125.

91. *Typical Infrared Absorption Frequencies.*

92. Perez-Cadenas, A.F., F.J. Maldonado-Hodar, and C. Moreno-Castilla, *On the nature of surface acid sites of chlorinated activated carbons.* Carbon, 2003. **41**: p. 473-478.

93. Jones, F., et al., *Thermal Stability of Zinc Compounds.* Energy & Fuels, 2013. **27**(10): p. 5663-5669.

94. Ibnu Abdulwahab, M., et al., *Bacterial Cellulose Supported Alumina Catalyst for Ethanol Dehydration.* Catalysis Letters, 2017. **147**(9): p. 2462-2472.

95. Bekyarova, E. and D. Mehandjiev, *Studies of Ni-Impregnated Active Carbon Part I. Effect of Thermal Treatment on the Texture of Active Carbon and the State of the Active Phase.* Journal of Colloid and Interface Science, 1996. **179**(2): p. 509-516.

96. Sun, G., et al., *Preparation and characterization of graphite nanosheets from detonation technique.* Materials Letters, 2008. **62**(4-5): p. 703-706.

97. Reina, T.R., et al., *WGS and CO-PrOx reactions using gold promoted copper-ceria catalysts: "Bulk CuO CeO_2 vs. CuO CeO_2 /Al_2O_3 with low mixed oxide content".* Applied Catalysis B: Environmental, 2016. **197**: p. 62-72.

98. Grzechowiak, J.R., I. Szyszka, and A. Masalska, *Effect of TiO_2 content and method of titania–silica preparation on the nature of oxidic nickel phases and their activity in aromatic hydrogenation.* Catalysis Today, 2008. **137**(2-4): p. 433-438.

จุฬาลงกรณ์มหาวิทยาลัย
CHULALONGKORN UNIVERSITY

99. Qiu, B., et al., *Fabrication of Co_3O_4 nanoparticles in thin porous carbon shells from metal–organic frameworks for enhanced electrochemical performance.* RSC Advances, 2017. **7**(22): p. 13340-13346.

100. Goodarznia, S. and K.J. Smith, *The effect of Cu loading on the formation of methyl formate and C_2-oxygenates from CH_3OH and CO over K- or Cs-promoted Cu-MgO catalysts.* Journal of Molecular Catalysis A: Chemical, 2012. **353-354**: p. 58-66.

101. Church, J.M. and H.K. Joshi, *Acetaldehyde by Dehydrogenation of Ethyl Alcohol.* Industrial and Engineering Chemistry, 1951. **43**(8): p. 1804-1811.

102. Kassim, M.A., *The transport process in the catalytic dehydrogenation of ethyl alcohol.* Advancement in Science and Technology Research, 2015. **2**(2): p. 19-41.

103. Sato, A.G., et al., *Effect of the ZrO_2 phase on the structure and behavior of supported Cu catalysts for ethanol conversion.* Journal of Catalysis, 2013. **307**: p. 1-17.

104. Chatchawanrat, S., *Dehydrogenation of Ethanol to Acetaldehyde over Activated Carbon Catalysts.* 2013.

105. El-Molla, S.A., G.A. El-Shobaky, and S.A. Sayed Ahmed, *Catalytic Promotion of Activated carbon by Treatment with Some Transition Metal Cations.* Chinese Journal of Catalysis, 2007. **28**(7): p. 611-616.

จุฬาลงกรณ์มหาวิทยาลัย
CHULALONGKORN UNIVERSITY

จุฬาลงกรณ์มหาวิทยาลัย
Chulalongkorn University

APENDIX A

CALCULATION FOR CATALYST PREPARATION

Calculation for preparation of cobalt catalyst supported on activated carbon by the incipient impregnation method

Example for 4%Co/C catalyst (part 4.2)

Based on 1.00 g of catalyst used, the composition of catalyst will be as follow:

Cobalt	=	0.04 g		
A synthesized activated carbon	=	1.00 - 0.04	=	0.96 g

Cobalt 0.02 g was prepared from Cobalt (II) nitrate hexahydrate

(formula: $Co(NO_3)_2 \cdot 6H_2O$)

$$\text{Cobalt (II) nitrate hexahydrate required} = \frac{\text{MW of } Co(NO_3)_2 \cdot 6H_2O \times \text{cobalt required}}{\text{MW of Co}}$$

Where Molecular weight of $Co(NO_3)_2 \cdot 6H_2O$ = 291.03 g/mol and

Atomic weight of Co = 58.93 g/mol

จุฬาลงกรณ์มหาวิทยาลัย
CHULALONGKORN UNIVERSITY

$$\text{So, Cobalt (II) nitrate hexahydrate required} = \frac{291.03 \times 0.04}{58.93}$$

$$= 0.1975 \text{ g}$$

<u>Example</u> for Ce/ACC catalyst (part 4.3)

Based on 1.00 g of catalyst used, the composition of catalyst will be as follow:

Cerium	=	0.10 g		
A commercial activated carbon	=	1.00 - 0.10	=	0.90 g

Cerium 0.10 g was prepared from Cerium (III) nitrate hexahydrate

(formula: $Ce(NO_3)_2 \cdot 6H_2O$)

$$\text{Cerium (III) nitrate hexahydrate required} = \frac{\text{MW of } Ce(NO_3)_2 \cdot 6H_2O \times \text{cerium required}}{\text{MW of Ce}}$$

Where Molecular weight of $Ce(NO_3)_2 \cdot 6H_2O$ = 434.22 g/mol and

Atomic weight of Ce = 140.12 g/mol

$$\text{So, Cerium (III) nitrate hexahydrate required} = \frac{434.22 \times 0.10}{140.12}$$

$$= 0.3099 \text{ g}$$

จุฬาลงกรณ์มหาวิทยาลัย
CHULALONGKORN UNIVERSITY

APPENDIX B

THE AMOUNT OF METAL AND THE TEMPERATURE OF REDUCTION OF CATALYSTS

The amount of metal near the surface of different commercial activated carbon catalysts can be determined quantitatively. The results are summarized in **Table 19.**

Table 20 Metal content of the different commercial activated carbon catalysts**.**

Activated carbons	% wt metal[*a]	% wt metal[*b]
Ce/ACC	28.9	7.37
Co/ACC	26.7	6.73
Cu/ACC	27.4	13.23
Ni/ACC	20.8	7.89

[*a] by EDX from SEM

[*b] by EDX from TEM

จุฬาลงกรณ์มหาวิทยาลัย
CHULALONGKORN UNIVERSITY

The temperature of reduction of different metal catalysts is shown in **Figure 39.**

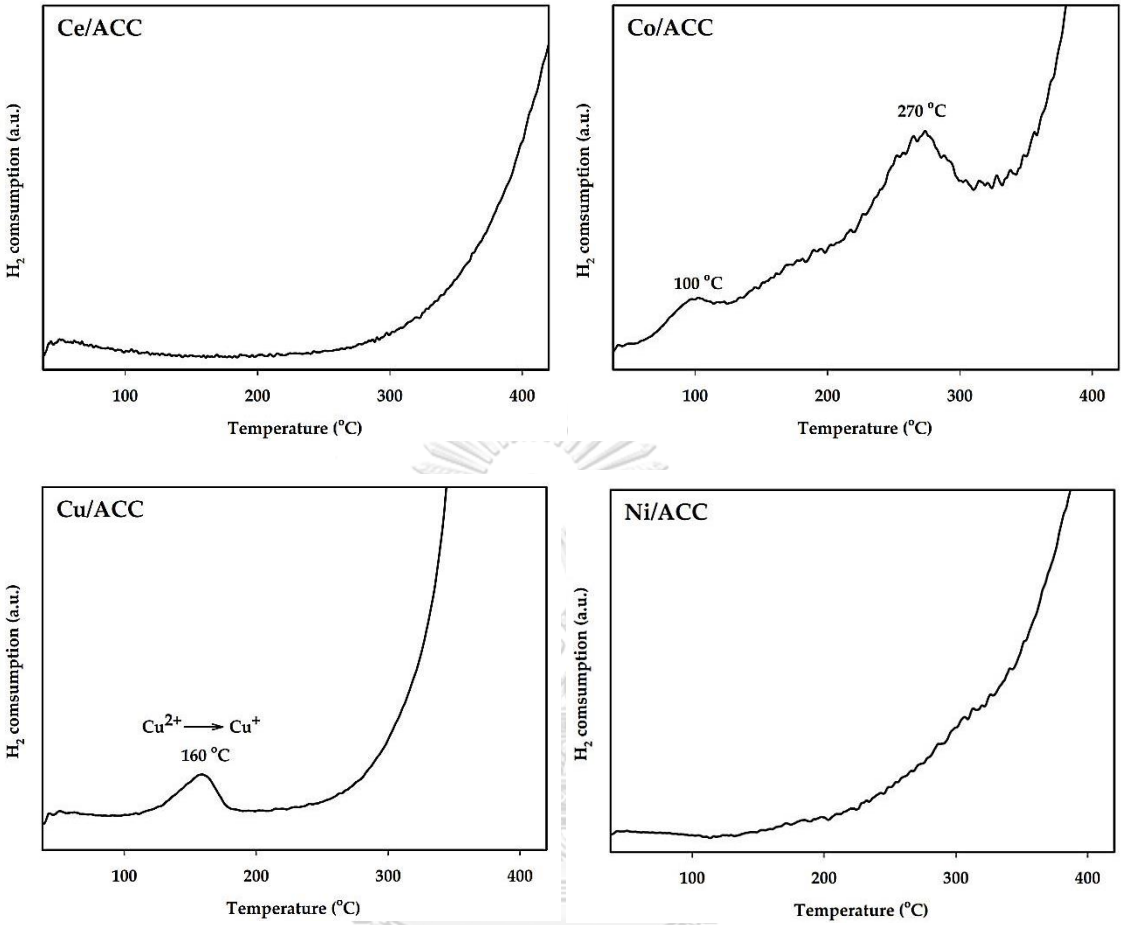

Figure 39 TPR profiles of activated carbon-supported metal catalysts.

CHULALONGKORN UNIVERSITY

APPENDIX C
CALIBRATION CURVES

To ensure the analysis of products, prior to the measurement, the calibration of GC was performed by calibrating the GC-FID and GC-TCD with certified pure gas of ethanol, ethylene, diethyl ether, acetaldehyde, carbon monoxide (CO) and carbon dioxide (CO_2) of the desired concentrations using an internal standard technique. Duplicate injections of each standard were made and the average value was used for the calibration graph of each reactant and product. Then, the ethanol conversion and the selectivity of ethylene, diethyl ether, acetaldehyde, carbon monoxide (CO) and carbon dioxide (CO_2) were calculated.

The retention time of the each component in the chromatogram that showed in **Table 20.**

Table 21 The retention time of the each component in the chromatogram.

Reactant/Products	Retention time (min)
Ethanol	4.6
Ethylene	4.1
Diethyl ether	4.9
Acetaldehyde	4.4

จุฬาลงกรณ์มหาวิทยาลัย
CHULALONGKORN UNIVERSITY

The calibration curves of the main reagent including ethanol, diethyl ether, ethylene and acetaldehyde are illustrated in **Figure 40-43** as follows;

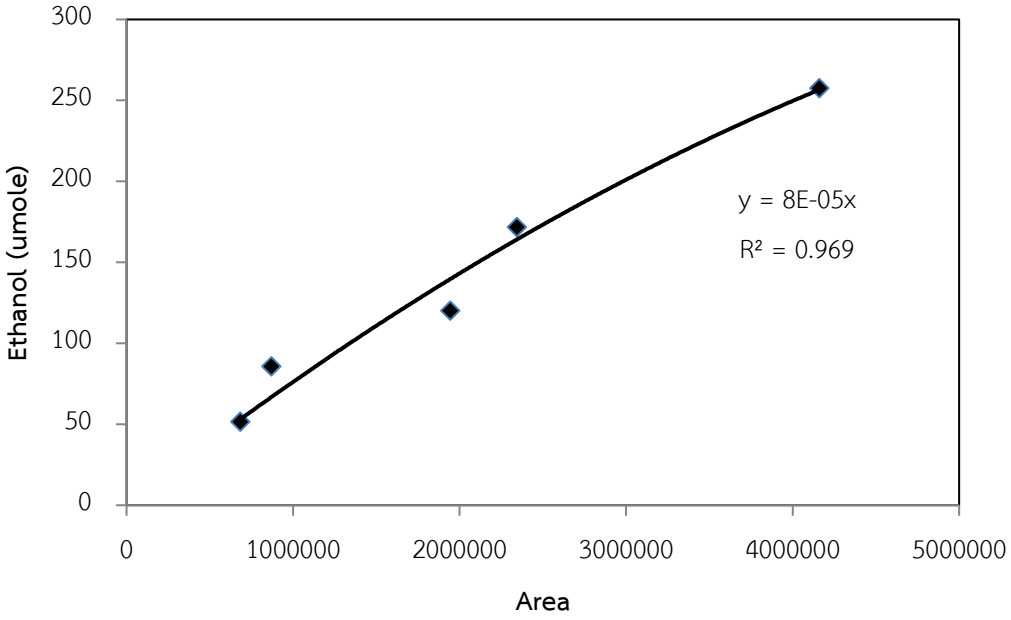

Figure 40 The calibration curve of ethanol.

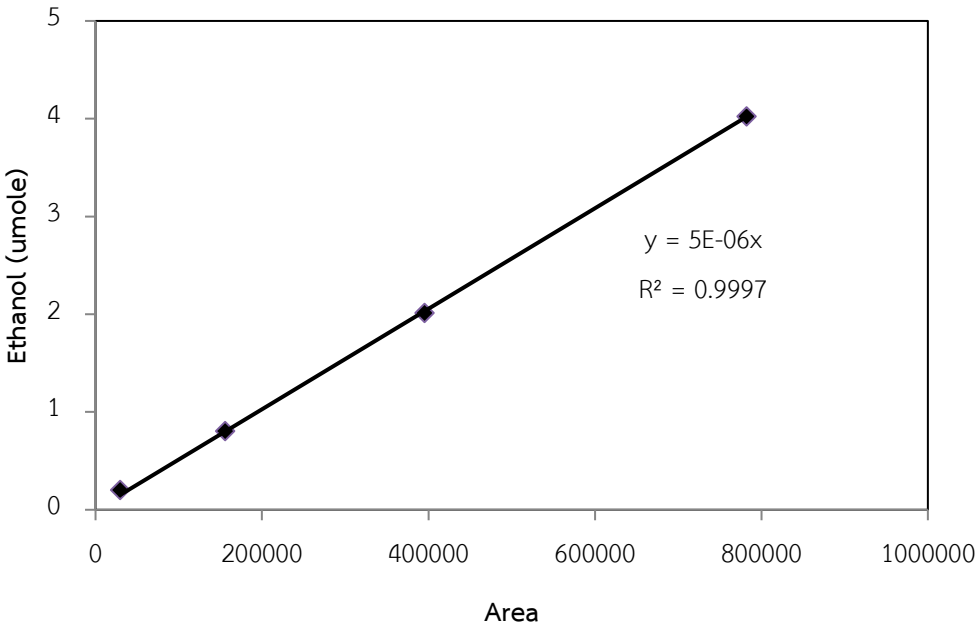

Figure 41 The calibration curve of ethylene.

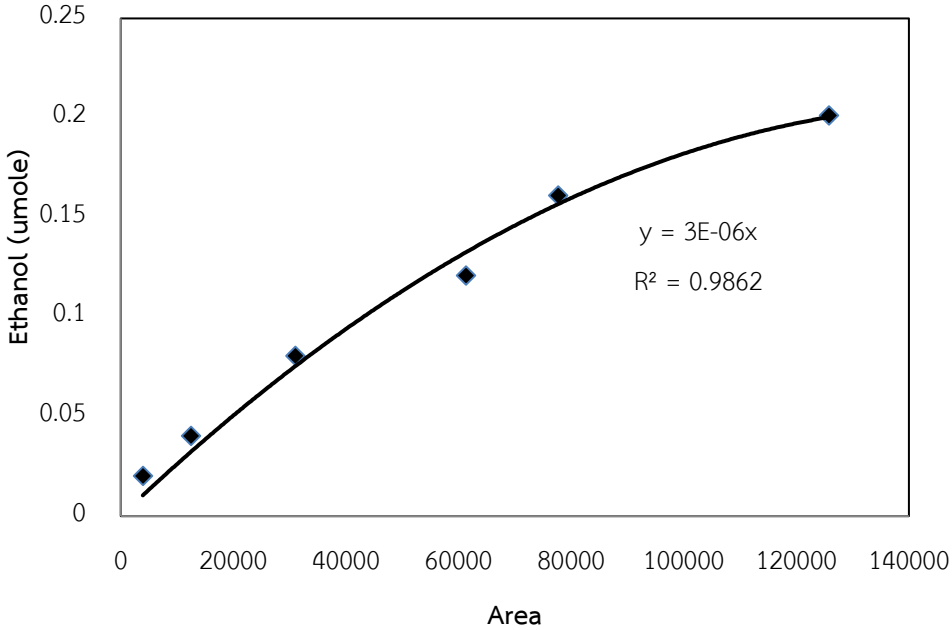

Figure 42 The calibration curve of diethyl ether.

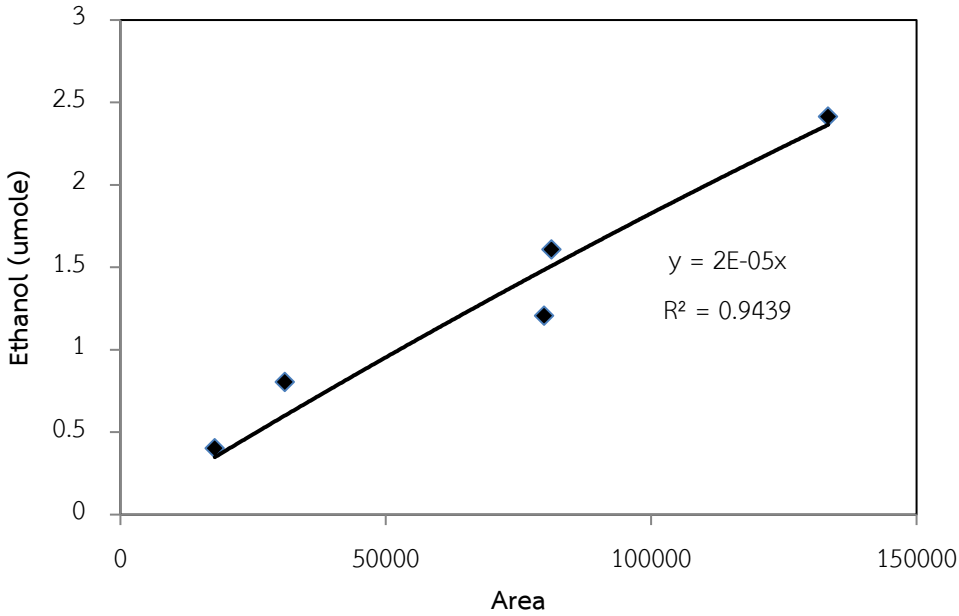

Figure 43 The calibration curve of acetaldehyde.

APPENDIX D
CALCULATION OF REACTANT CONVERSION, PRODUCT SELECTIVITY AND PRODUCT YIELD

The conversion of reactant and selectivity of products exhibited the performance of catalyst. Then, there were used demonstrated the catalytic activity for dehydration, non-oxidative dehydrogenation and oxidative dehydrogenation of ethanol.

Ethanol conversion (Reactant)

The conversion of ethanol is defined as mole of ethanol converted with respect to ethanol in feed;

Ethanol conversion (%) =

$$\frac{[\text{mole of ethanol in feed} - \text{mole of ethanol in product}]}{\text{mole of ethanol in feed}} \times 100$$

Product selectivity

The selectivity towards each product is defined as moles of product formed with respect to total moles of products;

$$\text{Product selectivity (\%)} = \frac{\text{Moles of each product}}{\text{Total moles of product}} \times 100$$

Product yield

Product yield (%) = Reactant conversion × Selectivity of each product

VITA

NAME	Jeerati Ob-eye
DATE OF BIRTH	19 February 1987
PLACE OF BIRTH	Phetchaboon
INSTITUTIONS ATTENDED	Master of Engineering in Chemical Engineering, Chulalongkorn University
HOME ADDRESS	270 Moo4 Tadang Nongphai Phetchaboon 67140
PUBLICATION	1.Jeerati Ob-eye, Piyasan Prasertham and Bunjerd Jongsomjit. Ethanol dehydrogenation to acetaldehyde over activated carbons-derived from coffee residue. Journal of Bulletin of Chemical Reaction Engineering & Catalysis, 2019, doi : 10.9767/bcrec.0.0.3335.xxx-xxx. (in press) 2.Jeerati Ob-eye and Bunjerd Jongsomjit. Dehydrogenation of ethanol to acetaldehyde over Co/C catalysts. (Engineering Journal revised) 3.Jeerati Ob-eye, Piyasan Praserthdam and Bunjerd Jongsomjit. Dehydrogenation of Ethanol to Acetaldehyde over Different Metals Supported on Carbon Catalysts. Catalysts, 9(1), 66, 2019, doi:10.3390/catal9010066.

จุฬาลงกรณ์มหาวิทยาลัย
CHULALONGKORN UNIVERSITY